

Development of a stiffness-modifiable composite

Production of a first prototype using electrocoating of carbon fibres to modify the interface behaviour and mechanical characterisation

by

Joraine Rössler

Technical report no 138/2014

at the Department of Materials and Manufacturing Technology
Chalmers University of Technology
Gothenburg, Sweden

Master's thesis in the Master Degree Programme "Materials Engineering"

Performed at: Swerea SICOMP AB
Composite Structures
SE - 431 22 Mölndal

Supervisor: Leif Asp, Head of Research
Swerea SICOMP AB
SE - 431 22 Mölndal

Co-Supervisor: Angelika Bachinger, Research Engineer
Swerea SICOMP AB
SE - 431 22 Mölndal

Examiner: Mikael Rigdahl, Professor
Department of Materials and Manufacturing Technology
Chalmers University of Technology
SE - 412 96 Gothenburg

Development of a stiffness-modifiable composite

Production of a first prototype using electrocoating of carbon fibres to modify the interface behaviour and mechanical characterisation

Joraine Rössler

© JORAINÉ RÖSSLER, 2014.

Technical report no 138/2014

Department of Material and Manufacturing Technology

Chalmers University of Technology

SE - 412 96 Göteborg

Telephone + 46 (0)31-772 1000

In cooperation with:

Swerea SICOMP AB

Box 271

SE - 941 26 Piteå

Telephone + 46 (0)911-74400

Cover:

Fibres that exhibit a continuous coating appear rainbow-coloured under the microscope (for more information see chapter 4.2 on page 30).

[Chalmers Reproservice]

Gothenburg, Sweden 2014

Development of a stiffness-modifiable composite

Production of a first prototype using electrocoating of carbon fibres to modify the interface behaviour and mechanical characterisation

JORAINE RÖSSLER

Department of Material and Manufacturing Technology

Chalmers University of Technology

Abstract

Within the European project ENLIGHT – Enhanced Lightweight Design – the presented thesis covers the development of a prototype for a stiffness-variable composite that will be integrated into a car hood to enhance traffic safety. To protect pedestrians the material can in case of a crash be activated to reduce its stiffness and hence allow large deflections upon impact. For the realization of this material a thermoplastic interphase is introduced through electrocoating between a thermoset matrix and the carbon fibre reinforcement.

Different parameters such as monomer concentration, potential or current density and the coating speed are varied and experiments are performed to identify the electrochemical coating mechanism. The results are evaluated using optical microscopy, weight measurements, thermogravimetric analysis and scanning electron microscopy. Furthermore, the fibres are characterized by tensile testing and resistivity measurements. A completely covering coating that exhibits a cauliflower-like appearance with a thickness of approximately 0.1 μm can be achieved through continuous coating even if variations in the coating thickness occur. Investigations on the mechanism indicate a combination of anionic and radical polymerization.

The composite is manufactured by vacuum-bagging and an even wetting of the coated fibres is found to be difficult. Two different epoxy-systems are investigated and the composites are characterized by optical microscopy, three-point-bending measurements and DMTA. The three-point-bending tests are performed under the application of a current through the specimens to verify that the material can be activated by the application of current. Composites containing coated fibres show a decrease in stiffness of up to 72% while composites containing sized fibres show a maximum decrease of 50%. It is indicated that a variation of the epoxy system and the introduced temperature allows to tailor the stiffness-reducing properties.

Keywords: smart materials, traffic safety, electropolymerization

Table of Contents

Acknowledgements	iv
List of Publications.....	v
List of Abbreviations.....	vi
1 Introduction	1
1.1 Context and problem description	1
1.2 Aim and objectives.....	3
1.3 Thesis outline	3
2 Theoretical Background	4
2.1 Smart materials.....	5
2.1.1 Definitions.....	5
2.1.2 Applications and materials developed.....	5
2.1.3 Tridech's approach: Composite with active stiffness control	6
2.2 Electrocoating.....	8
2.2.1 Cyclic voltammetry	10
2.2.2 Batch electrocoating.....	10
2.2.3 Continuous coating.....	11
2.2.4 Mechanism	12
3 Experimental	15
3.1 Materials.....	15
3.2 Electrocoating.....	15
3.2.1 Cyclic voltammetry	17
3.2.2 Batch electrocoating.....	18
3.2.3 Continuous electrocoating.....	18
3.2.4 Mechanism	18
3.3 Characterisation of coated fibres.....	19
3.3.1 Optical microscopy	19
3.3.2 TGA and weight measurement.....	19
3.3.3 SEM.....	20
3.3.4 Tensile testing	20
3.3.5 Resistivity.....	21
3.4 Manufacturing of composites.....	21
3.5 Mechanical characterisation of composites.....	23
3.5.1 Three-point bending	23
3.5.2 DMTA.....	23
4 Results	25
4.1 Electrocoating.....	25

4.1.1	Cyclic voltammetry	25
4.1.2	Batch electrocoating	27
4.1.3	Continuous electrocoating	28
4.1.4	Mechanism	28
4.2	Characterisation of coated fibres	30
4.2.1	Optical microscopy	32
4.2.2	TGA and weight measurement	38
4.2.1	SEM	40
4.2.2	Tensile testing	44
4.2.3	Resistivity	44
4.3	Manufacturing of composites	44
4.4	Electrical properties	47
4.5	Mechanical characterisation of composites	49
4.5.1	Three-point bending	49
4.5.2	DMTA	51
5	Discussion	52
5.1	Characterisation of coating quality	53
5.1.1	Cyclic voltammetry	53
5.1.2	Batch electrocoating	53
5.1.3	Continuous coating	56
5.1.4	Mechanism	56
5.2	Characterisation of fibres	57
5.2.1	Tensile testing	57
5.2.2	Resistivity	58
5.3	Manufacturing of composites	58
5.4	Electrical properties	59
5.5	Mechanical characterisation of composites	60
5.5.1	Three-point bending	60
5.5.2	DMTA	61
5.6	Scale-up possibilities for industrial application	61
6	Conclusions and Outlook	63
6.1	Further experiments	64
7	References	65
8	Appendix	70
8.1	Information from (Tridech 2010)	71

Acknowledgements

This thesis was performed at Swerea SICOMP AB in Mölndal. I would therefore thank SICOMP for giving me the opportunity to be part of an international research project.

Special thanks goes to my co-supervisor Angelika Bachinger, who took the challenge with supervising her first master's thesis. In my opinion, it has been a great success and I appreciate the great support given and all feedback. Many thanks as well to my supervisor Leif Asp who always gave new inputs. Thanks to my examiner Mikael Rigdahl who kept an eye on the administrative regulations. Special thanks to Peter Hellström and Erik Marklund in Mölndal, Simon Leijonmarck in Stockholm, Runar Långström and Fredrik Ahlqvist in Piteå and Ruth Ariño in Göteborg, whose help in the lab and beyond made this work possible.

I would also like to thank my family and friends for their support throughout my studies. It has been an exciting journey and I am happy to conclude this chapter of life with the present thesis.

Joraine Rössler, Göteborg, 26.09.2014

List of Publications

Bachinger A, Marklund E, Rössler J, Hellström P, Asp LE (2014): **Stiffness-modifiable composite for pedestrian protection.** *ECCM16 – 16th European Conference on Composite Materials*, Seville, Spain, 22-26 June 2014.

List of Abbreviations

AFM	Atomic force microscopy
AN	Acrylonitrile
CFRP	Carbon fibre reinforced polymer
CA	Chronoamperometry
CE	Counter electrode
CP	Chronopotentiometry
CV	Cyclic voltammetry
DMF	N,N-Dimethylformamide
DMTA	Dynamic mechanical thermal analysis
DPPH	Diphenylpicrylhydrazyl
EDS	Energy-dispersive X-ray spectroscopy
EV	Electric vehicle
MEHQ	Monomethyl ester hydroquinone
MMA	Methyl methacrylate
PAAm	Polyacrylamide
PAN	Polyacrylonitrile
PMMA	Polymethyl methacrylate
RMS	Root mean surface roughness
SEM	Scanning electron microscopy
SMA	Shape memory alloy
SMP	Shape memory polymer
TGA	Thermogravimetric analysis
XPS	X-ray photoelectron spectroscopy
WE	Working electrode

1 Introduction

1.1 Context and problem description

The present thesis is part of the European project ENLIGHT – Enhanced Lightweight Design – where materials, production and design solutions for future electric vehicles (EVs) are developed. The aim of the project is to advance materials for innovative lightweight solutions through research for medium production volumes. However, weight reduction is not the only aspect that is addressed in this project: To increase the acceptance of electric vehicles among customers it is also important to meet the demands regarding efficiency, comfort and safety. (ENLIGHT Consortium 2014) The material developed in this thesis is considered in ENLIGHT due to its potential to improve traffic safety.

Considering traffic safety, car-to-pedestrian accidents are of particular interest for researchers and engineers as they have a higher fatality rate than other accident types only involving cars. (Oh, Kang, and Kim 2008) Furthermore, different studies show that the head is among the body regions most commonly injured during those accidents. (Carter, Neal-Sturgess, and Hardy 2008; Fredriksson and Rosén 2012; Huang and Yang 2010) In the case of accidents involving child pedestrians the head impact location is most likely on the hood. (Yao, Yang, and Otte 2007) To reduce the severity of head injuries during head-to-hood impact, different countermeasures can be considered. In general, these countermeasures are divided into active (pre-crash) or passive (in-crash) systems, which can be combined in an integrated system. (Fredriksson and Rosén 2012) Passive solutions include structural modifications such as extra space under the hood or the use of energy-absorbing materials while active solutions consist of hood lift systems or airbags. (Fredriksson and Rosén 2012; Huang and Yang 2010; Oh, Kang, and Kim 2008; Yao, Yang, and Otte 2007) Fredriksson and Rosén (2012) state that an integrated system including both solutions shows the highest potential to reduce head injuries. However, they also state that the exact distribution of injuries depends on the type of car. To evaluate different car types according to their performance for pedestrian protection, Euro NCAP – the European New Car Assessment Programme – includes a series of tests simulating crash situations (Figure 1, Euro NCAP 2014). The results of these tests are included in the safety rating of each car and a detailed map of different areas of the car front can be assessed (examples are shown in Figure 1).

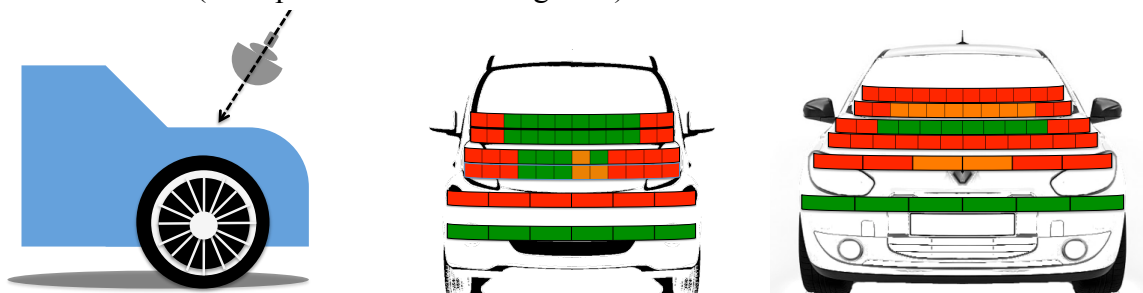


Figure 1 Example for crash impact with the head on the hood (left). Zones of different protection for pedestrians: good (green), adequate (yellow) and marginal (red) measured by Euro NCAP (middle, right). The models shown are Mitsubishi i-MiEV (middle) and Renault Fluence ZE (right). (Redrawn from (Euro NCAP 2014))

Due to the absence of a combustion engine in future electric vehicles, a larger deflection of the hood upon impact can be allowed. Hence, in this thesis a material will be realized that can be activated in case of a crash to reduce its stiffness and hence allow large deflections upon impact. Such material will be achieved by introducing a thermoplastic interphase between a thermoset matrix and the carbon fibre reinforcement. Electrocoating has been used extensively to increase the interfacial adhesion between carbon fibres and polymer matrix. Through the variation of parameters like the current density or the monomer concentration, the thickness of the coating and the availability of functional groups can be controlled which in the best case leads to a uniform, covalently bond layer. (Saraç, Bismarck, and Springer 2006) In the present thesis the coating is furthermore used to allow stiffness-reduction by softening the interphase through heating the thermoplastic coating above its glass transition temperature. The increased temperature will be achieved through heating by applying an electrical current through the carbon fibres. Thus, the designed material will account for an active countermeasure.

1.2 Aim and objectives

The aim of this thesis is to produce a first prototype of the described stiffness-variable composite. To achieve this, two subsidiary aims can be formulated. First, the optimization of the coating process for the continuous production of the fibres that can be scaled for industrial implementation will be achieved by:

- Definition of process parameters that lead to a continuous polymer layer covering the entire fibre surface.
- Optimize coating speed to balance the need for an even coating and a fast process to achieve profitable production rates.
- Reduction of the electrical current required during the coating process to reduce the danger for electricity-related accidents, allow for better control of the electrocoating process (reducing side reactions) and reduce the required energy.
- Minimize the use of harmful substances.
- Set up experiments that can help to identify the electrochemical coating mechanism.

The second aim regards the production of a composite that changes stiffness upon application of electrical current. To achieve this, the following objectives were formulated:

- Find process parameters for vacuum infusion of the coated fibres that allow an even distribution of the fibres within the matrix and complete impregnation of the fibres to minimize the pore volume.
- Characterisation of the mechanical properties of the produced composites under the influence of increased temperature by application of electrical current or voltage.

1.3 Thesis outline

To enable the reader to gain a deeper understanding of the main experimental techniques used and to follow later discussions this thesis starts with a theoretical background dealing with smart materials and presenting the coating process in detail. In the experimental section all experiments and characterisation methods regarding fibre coating, manufacturing of composites and mechanical characterisation of the stiffness-modifiable composite are described. Chapter 4 presents the obtained results according to the structure in the experimental section. However, in chapter 5 (discussion) observations from different characterisation techniques are discussed in relation to each other. This is necessary to get a holistic view over the outcome of the different techniques. The conclusions presented in chapter 6 will consider both the scientific perspective as well as possible industrial implementation. The thesis will be wrapped up with an outlook on future research possibilities. Furthermore, the last chapter will discuss open issues, as well as possible publications with regard to the results presented in this thesis. For the sake of readability all results are presented as clear and compacted as possible.

2 Theoretical Background

2.1 Smart materials

The material developed in this project can be denoted as a smart material. In the following chapters the term “smart material” is clarified. Examples for different smart materials that are already used or might be applicable for the automotive industry are presented. Last, one specific approach is described in detail as in the present work this approach was used as a guidance to develop and optimize the material presented.

2.1.1 Definitions

Michaud (2004) gives a very thorough description of smart materials or structures in the introduction of his article on shape memory alloy composites. He concludes with a definition for a smart material:

“A structural material that inherently contains actuating, sensing and controlling capabilities built into its microstructure. A smart structure or system is thus an assembly, which presents the previously mentioned characteristics through the combination of various materials.”

Smart materials or structures, which can also be called intelligent materials or adaptive materials, thus represent a subgroup of functional materials as they exhibit additional functions such as the ability to sense and respond to external stimuli and change properties depending on these stimuli. These materials evolved as a consequence of the general demands - especially for composite materials - to offer high specific properties and at the same time increase the flexibility and functionality of the material, while keeping production costs low. Smart materials are therefore optimized towards a goal that is dictated by the future application. It is furthermore important to mention that external forces of all kind of origins such as mechanical, thermal, electrical or magnetic can stimulate the response of the material. (Michaud 2004) Chopra (2002) uses the term smart structure and, in contrast to Michaud (2004), defines this as a set of four elements. First, sensors to register an input, then control strategies and power conditioning electronics to secondly analyse the input and thirdly process a signal that is given to the forth element, the actuators, to perform the system response. Thus, a smart structure can react to changes of the environment either in the form of external factors such as applied loads or internal ones such as damage of the structure. (Chopra 2002) The latter definition distinguishes structurally between different parts of a smart material. However, also in this case all elements are combined to one entity as Chopra (2002) presents an active fibre composite as an example.

2.1.2 Applications and materials developed

Smart structures are developed for a variety of applications in a wide range of fields including the automotive industry to actively control vibration, shape change, stress distribution and noise and could in consequence enhance the overall performance of a system. Different smart

materials can serve as actuators or sensors for example piezoelectric materials, shape memory alloys or materials that change properties on electric or magnetic impulses. (Chopra 2002)

The term shape memory alloy (SMA) denotes a metal, which can return to an initial shape after an applied deformation upon the influence of temperature. SMAs can be used as actuators and sensors and are often combined with other structural or functional materials to form so called hybrids. These hybrids offer specific properties: They can be self-strengthening, damage resistant and highly damping. SMA fibres can be used as reinforcement in polymer composites. Simulations suggest that these fibres can be used to actively alter static and dynamic properties such as damping, shape or stiffness. (Yang 2000) However, Michaud (2004) comes to the conclusion that both SMAs as well as composites containing SMA can only be identified as a smart material in a restricted sense. For example, even though these materials exhibit the ability to sense temperature and strain and react in actuating, their sensing capability and therefore their field of application is often limited. Further drawbacks are the challenges in manufacturing which cannot yet be adjusted to industrial production volumes. (Michaud 2004)

Smart materials that are investigated for use in automotive structures comprise piezoelectric ceramics for vibration and thus noise control of the roof-panel (Manz and Breitbach 2001), SMAs for composite automotive body parts (Michaud 2004) as well as magnetoactive elastomer composites for active stiffness and vibration control (Farshad and Benine 2004). Possible areas of use for smart materials within automobiles are listed by Peelamedu, Naganathan, and Buckley (1999) and include among others engine mounts to reduce vibration and noise, shape control to control the aerodynamics of the car body or smart bumpers to improve crashworthiness.

One general aim is to define and optimize modelling techniques to determine the behaviour of smart structures, as experiments for more complex structures are not suitable (Manz and Breitbach 2001). This includes the modelling of induced stresses created by manufacturing and complex load cases (Michaud 2004).

2.1.3 Tridech's approach: Composite with active stiffness control^a

Tridech's and Maples' (Tridech and Maples 2013; Tridech 2010) aim was to develop a composite material with controllable stiffness primarily for the use within the aerospace industry in the form of morphing skins. For their composite, they continuously coated carbon fibres with polyacrylamide (PAAm) and polymethyl methacrylate (PMMA) and then manufactured carbon-fibre reinforced composites with epoxy as a matrix (Figure 2). Upon application of an electrical current through the carbon fibre reinforcement, the thermoplastic interphase is heated above its glass transition temperature and softens. Hence, the load transfer between the matrix and the fibres is reduced and therefore the stiffness for the material decreases. Additionally, the original stiffness can be restored in heating the composite without any loading condition and cooling it to room temperature.

^a Details of the continuous coating process can be found in chapter 2.2.3 as the present part is mainly focusing on the composite itself and its behaviour.

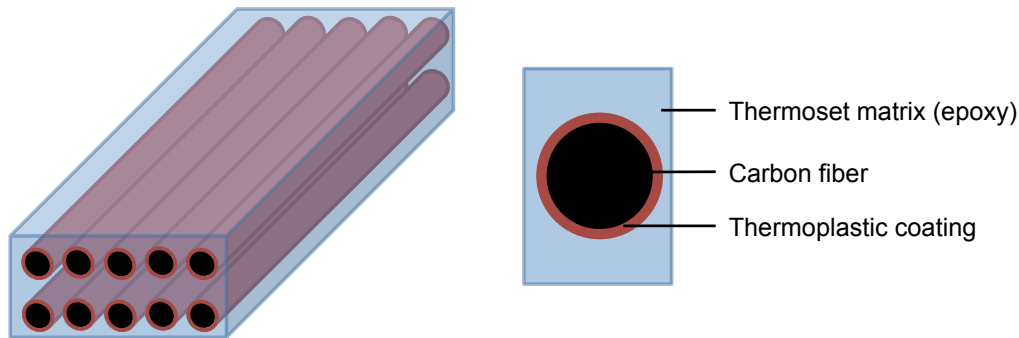


Figure 2 Schematic composition of a composite with active stiffness control proposed by (Tridech and Maples 2013). The fibres (black) have a thermoplastic coating (red), which acts as an interphase between carbon fibres and a thermoset matrix (blue).

Tridech and Maples (2013) and Tridech (2010) characterized the produced composites using DMTA for the determination of viscoelastic properties and three-point bending for flexural properties both at room temperature and at elevated temperatures up to 140°C. The heating of the composites in case of the three-point bending tests was either conducted in an environmental chamber where the whole composite was heated or by applying a current to the carbon fibres (Figure 3). Their results show a drop in flexural stiffness of 46% and 78% for 110°C and 130°C for the composites containing PAAM coated fibres and of 13% and 39% for 110°C and 130°C for the composites containing PMMA coated fibres when the material was heated in an environmental chamber. No decrease was observed for the composites containing uncoated fibres. When heated to the respective temperatures by directly applying a current to the carbon fibres a decrease of the flexural modulus by 88% and 86% for PAAM and 51% and 41% for PMMA was observed. Exact values for the flexural modulus and the flexural strength as well as the voltage and currents applied can be seen in the appendix (8.1, Table 12). Furthermore, to increase the temperature of their specimens (40 mm x 10 mm x 2 mm) to 110°C and 130°C a current of 0.6 A and 0.7 A and a potential of 15 V and 20 V were applied which corresponds to a resistance of 25 and 28.6 Ω , respectively. (Tridech and Maples 2013; Tridech 2010)

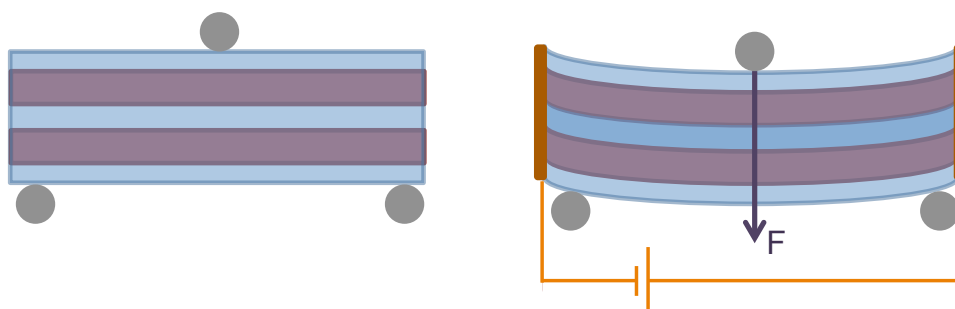


Figure 3 Schematic behaviour of a composite with active stiffness control according to (Tridech and Maples 2013). The coating softens upon an electrical impulse, the fibres are able to glide within the matrix and the stiffness of the composite decreases.

Table 1 Results of the three-point bending test from (Tridech and Maples 2013) and (Tridech 2010) including applied voltages and currents for applying heating directly through the carbon fibres (RT = room temperature).

composite components	flexural strength [MPa]	environmental chamber			applied current			
		Flexural modulus [GPa]						
		RT	110°C	130°C	RT	110°C	130°C	RT
unsized carbon fibres	420 ± 25	62 ± 7	63 ± 8	63 ± 9	60 ± 12	58 ± 9	62 ± 11	60 ± 8
PAAm electrocoated carbon fibres	136 ± 21	69 ± 8	37 ± 8	15 ± 3	65 ± 8	8 ± 5	10 ± 5	67 ± 13
PMMA electrocoated carbon fibres	354 ± 28	90 ± 7	78 ± 14	55 ± 16	84 ± 8	44 ± 5	53 ± 4	88 ± 6

2.2 Electrocoating

Electropolymerization, which also falls under the term electrocoating, describes an electrochemical process where monomers are polymerized in solution on the surface of an electrode or in the vicinity of it. The electrode on which the polymerization occurs or through which the polymerization is initiated is called the working electrode (WE) whereas the other electrode is called counter electrode (CE). Within an electrochemical cell both electrodes are immersed into an electrolyte, which can contain salt, solvent and the monomer. A current is then applied between the two electrodes so that the electrolyte becomes polarized and the coating reaction takes place (see Figure 4). (Gabriel, Jérôme, and Jérôme 2010; Jérôme 2012) As in this two-electrode system the potential is measured against the counter electrode it varies with the flow of current that is passing through the cell, a three-electrode system is often used. In such system, the potential can be adequately controlled between the working and the reference electrode. As a pseudo-reference electrode platinum wire is preferred as it showed good performance in various electrochemical systems that can be aqueous or non-aqueous (Kasem and Jones 2008). Furthermore, conventional reference electrodes are not suitable when a complete water-free environment is required and they can be destroyed in non-aqueous systems. The electrocoating process can further be executed using a constant current, chronopotentiometry (CP), or a constant potential, chronoamperometry (CA). However, the latter process is often preferred, as CP can lead to unexpected side reactions. (Mertens et al. 1996)

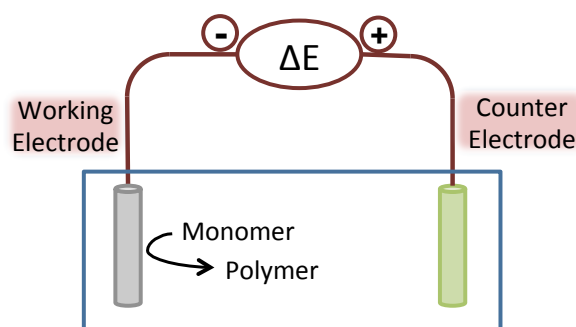


Figure 4 Schematic drawing of an two-electrode electrochemical cell used for electrocoating. In the case of carbon fibres the working electrode represents the cathode where the monomer in solution is polymerized.

While the initiation mechanism at the cathode can be anionic or radical, a current flow can only be detected for anionic initiation (see 2.2.1, (Bureau et al. 1997)). The propagation of the polymerization can also be anionic or radical, depending on the constituents of the electrochemical cell and the conditions for polymerization for example ambient or inert conditions or the ratio of monomer to electrolyte (Gabriel, Jérôme, and Jérôme 2010; Jérôme 2012).

The process that leads to the initial bonding of the polymer to the electrode concerned in this thesis is called cathodic electropolymerization. To simplify the description in the following text the term electrocoating will be used. To refer to different possible interactions of the polymer with the surface, three main types have been identified: The first type describes monomers that are covalently bound to the surface of the electrode and polymerization proceeds from the surface. No polymers are built in solution or no interaction between grafted chains and polymers formed in solution is observed. This type is called “grafting”. (Figure 5a) The second type describes the entanglement of grafted polymers and polymer chains formed in solution. This phenomenon is referred to as “entangled grafting”. (Figure 5b) The third possibility is physical adsorption of polymers formed in solution. Therefore, this configuration is called “physisorption” (Figure 5c).

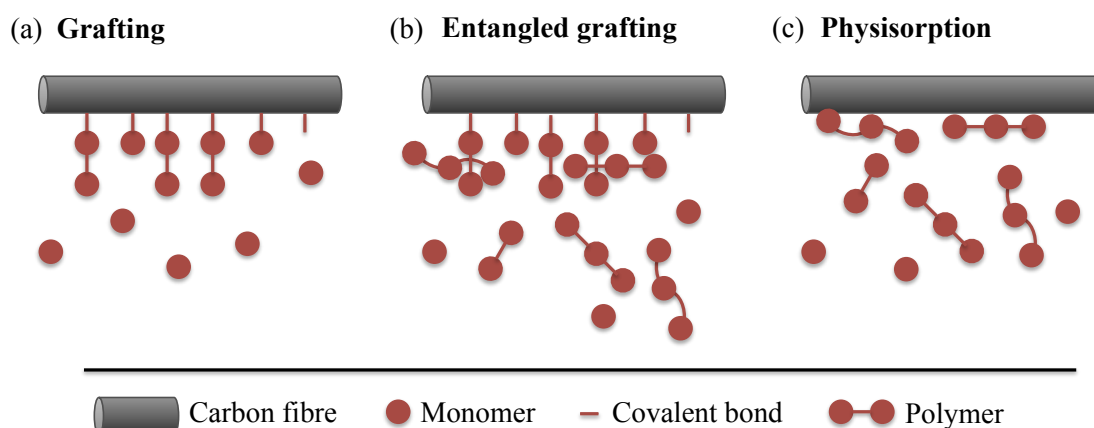


Figure 5 Schema of the three possible interactions of the polymer with the surface for an electrocoating. Monomers are covalently bond to the surface of the electrode and chains grow from the surface. (a) The same as in (a) but additionally polymers are formed in solution. These polymers can then be entangled with the polymer chains growing from the surface. (b) It is also possible that polymerization only takes place in solution and the chains are physisorbed to the surface. (c)

2.2.1 Cyclic voltammetry

Cyclic voltammetry (CV) describes a linear sweep in a defined range of potentials. The resulting current is measured relative to the applied potential. The most important parameter for these experiments is the scan rate, which is usually expressed in mV/s. In the field of electropolymerization, cyclic voltammetry is widely used to identify the reduction potential of the monomer. (Jérôme 2012; Leijonmarck et al. 2013) This method can, however, also be used for the coating process itself. (Saraç, Evans, et al. 2004)

It is described by Gabriel, Jérôme, and Jérôme (2010) and Jérôme (2012) that two peaks are visible during voltammetry of acrylic monomers: A rather weak signal is identified at a low cathodic potential, which is referred to as the grafting peak and a more intensive signal is observed at a lower cathodic potential. The authors refer to the latter as diffusion peak. (Figure 6) It is explained that a passivation of the cathode is achieved at the potential of the first signal by chemisorption of the polymer. If the potential is further decreased the grafted chains are released from the electrode surface and polymerize further in solution, which is observed at the second signal (Mertens et al. 1996). However, according to Bureau (1999) observed signals in the voltammogram are not necessarily related to these specific reactions and various explanations for signals are possible. According to him the grafting peak cannot be assigned to a passivation but can also express the depletion of the monomer through polymerization. The second peak would then be assigned to polymerization caused by diffusion of left monomers.

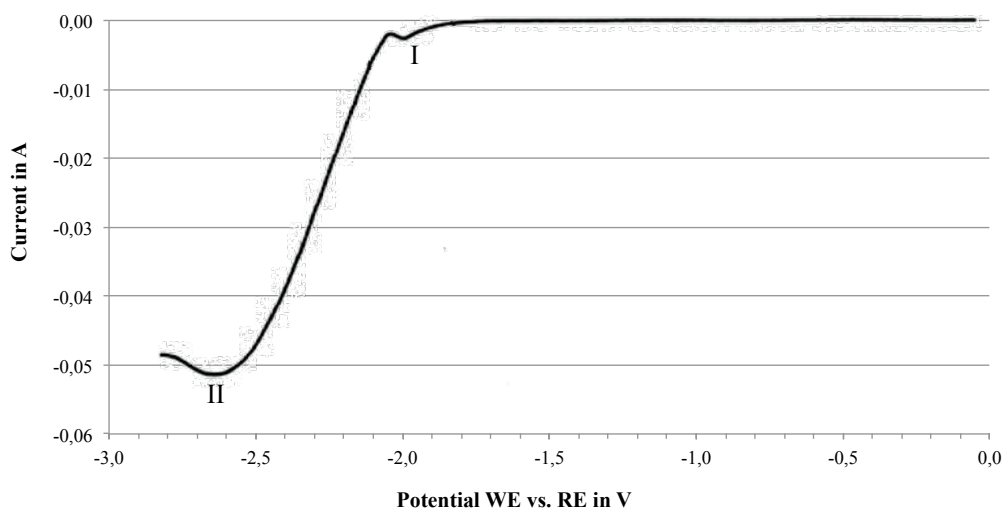


Figure 6 Sketch of a possible voltammogram from a linear potential sweep that has been observed in a similar way by Jérôme (2012). Two peaks are visible: The grafting peak (I) and the diffusion peak (II).

2.2.2 Batch electrocoating

The batch electrocoating of carbon fibres has been studied with various polymers for use in high performance composites (Bismarck et al. 2005; Kumru et al. 2001) or novel micro batteries (Leijonmarck et al. 2013). Bismarck et al. (2005) successfully electrodeposited MMA on carbon fibres using different MMA concentrations in DMF containing either NaNO_3 or LiClO_4 as a salt, depending on the monomer concentration. A constant current density of 1.56 mA/cm^2 was applied for all experiments. The two-electrode electrochemical

cell consisted of a one-compartment glass cell with a stainless steel counter electrode. The electrolyte was not stirred during the coating process. The coated carbon fibres were washed thoroughly with distilled acetone and water, and dried overnight at 1 mbar and 50°C. The surface morphology and composition of the coated fibres were studied using SEM, EDS and XPS. While low monomer concentrations and the use of NaNO₃ led to poor coating, high monomer concentrations showed a high degree of grafting and an increased coating thickness. The fibre diameter was estimated from SEM-images and through a laser diffraction method. For molar concentrations of 7.7 M and 11 M of MMA the coating thickness, eq. the difference in diameter, was 1.76 µm and 0.61 µm respectively (Bismarck et al. 2005). Tridech (2010) used a three-electrode electrochemical cell for the batch electrocoating of MMA on carbon fibres. The electrolyte contained the monomer, DMF as a solvent and LiClO₄ as a salt. He studied the fibre morphology, composition and thermal behaviour of the MMA coating using SEM, Wilhelmy-technique, XPS and TGA. The coating thickness determined by SEM was 0.1 µm and 0.05 µm for weight measurements. From the Wilhelmy measurements the increase in fibre diameter was 0.2 µm. From TGA a coating content of 2 %wt was registered, which would correspond to a coating thickness of approximately 0.05 µm. The SEM images revealed that the fibre was partly covered by a powder-like coating.

2.2.3 Continuous coating

The continuous coating of carbon fibres through electropolymerization is mentioned in some patents concerning the general application of electrocoating (Mertens, Martinot, and Jerome 2001; Naarmann 1988). In these patents, the authors include the continuous process as a general possibility for the described processes. However, a review of the open literature resulted in only one publication on continuous electrocoating of carbon fibres (Tridech and Maples 2013). This journal paper is based on a previous doctoral thesis (Tridech 2010). The parameters applied in the experiments described therein are summarized in Table 2.

Table 2 Experimental parameters for the continuous coating of carbon fibres. (Tridech and Maples 2013; Tridech 2010)

Coating speed [mm/s]	Current density* [mA/cm ²]	Monomer used	Monomer conc. [mol/l]	Solvent used	Salt used	Bath temp. [°C]
1.9	2.38	MMA and AAm	1.5	DMF	LiClO ₄	65

* calculated from the given current of 1.2 A and the length of the steel tube of 20 cm

Tridech and Maples (2013) studied the fibre morphology, composition and thermal behaviour of the PAAm coating using SEM, the Wilhelmy-technique, XPS and TGA. Using a continuous electrocoating process, a coating with a droplet-chain like appearance was achieved. The overall weight gain through the coating determined by TGA was 4%, which they claimed to agree with the analysed coating thickness of 0,2 µm (increase of fibre diameter from 7,3 ± 0.1 µm to 7,5 ± 0.1 µm) from the Wilhelmy-technique. For the PMMA coating, Tridech (2010) presented results from weight measurements, TGA, SEM and the Wilhelmy-technique. The coating thickness showed a wide variation over the different

analysis techniques, ranging from 0.1 μm (from TGA) to 0.8 μm (from SEM; detailed information is presented in 8.1, Table 12). SEM images revealed a smooth, wavy coating.

2.2.4 Mechanism

Various publications can be found summarizing the general mechanism involved in electropolymerization of acrylics and specifying experiments to identify the mechanism.

Two review articles (Gabriel, Jérôme, and Jérôme 2010; Jérôme 2012) mention a series of experiments that have been performed to distinguish between anionic or radical polymerization mechanism. The following experiments are mentioned:

- (i) addition of radical scavenger DPPH
 - No end-capping of the PAN chains was observed, would be observed in the case of a radical mechanism
- (ii) copolymerization of AN with either ϵ -caprolactone, a monomer leading to anionic copolymerization, or vinyl acetate, a monomer that polymerizes radically
 - None of the monomers could be detected in the electrical double layer of the cathode
- (iii) addition of potential radical transfer agent CDCl_3
 - End-capping of the PAN chains by $-\text{D}$ rather than $-\text{CCl}_3$, which suggests anionic propagation
- (iv) substitution of MMA for AN and analysis through TGA
 - TGA profile depends on polymerization mechanism and the observed one-step degradation profile hints towards an anionic mechanism

From all the experiments the authors conclude that the mechanism active in the electrografting of AN is anionic. However, not all of these experiments could be found in the mentioned references (Baute et al. 1998, Phd thesis Baute - chapter 5, Bureau et al. 1997, Mertens et al. 1996) or other open literature and the drawn conclusions could only partly be retraced:

- (i) (Mertens et al. 1996) (Bureau et al. 1997)
- (ii) ϵ -caprolactone is mentioned in (Mertens et al. 1996) but not vinyl acetate, thus for the second no article was found
- (iii) probably in (Poleunis et al. 1998), but not accessible
- (iv) not found, (Holland and Hay 2002) did not observe a general difference in the degradation profile of anionic and radical polymerised PMMA

Based on the above mentioned experiments, Mertens et al. (1996) propose that two different mechanisms are active as two distinct peaks are observed during voltammetry. From the experiments with DPPH and ϵ -caprolactone they come to the conclusion that a radical mechanism is active at the first peak. However, one year later Bureau et al. (1997) publish a comprehensive comment on the article of Mertens et al. (1996), where they question the

previous conclusions as a radical mechanism would not involve charge transfer and thus not be detected as current. They state that only an anionic mechanism can explain the observed current flow and claim the need for more experiments.

While early follow-up articles of Mertens et al. (1996) still emphasize the theory of a radical mechanism (Baute et al. 1998; Calberg et al. 1997) the previously mentioned overviews both come to the conclusion that the electrografting of AN is based on an anionic mechanism (Gabriel, Jérôme, and Jérôme 2010; Jérôme 2012). This mechanism is in more detail explained in another overview article of Palacin et al. (2004). Here the reaction starts with the reduction of the monomer close to the surface of the electrode that gives a radical anion. This then binds to the cathode resulting in a metastable grafted anion (Figure 7a). After that two reactions are possible. The first reaction would be that the anion becomes ejected from the electrode surface and forms a free radical anion in solution. This highly reactive anion soon connects to another radical anion to form a dimer and starts polymerization of free chains in solution (Figure 7b). However, the second and desired reaction would be that the grafted anion reacts with another monomer in solution to grow a polymer chain from the electrode surface (Figure 7c). Going back to the possible interactions of the polymer with the surface (see Figure 5) the polymerization of free chains in solution can in combination with surface-grafted chains lead to entangled chains on the surface of the electrode. At elevated temperatures it is further likely that radical polymerization spontaneously takes place in the solution without the initiation of the electron transfer. These chains could contribute to the entangled grafting on the surface. Moreover, even if radical polymerization cannot explain the detected charge transfer, it cannot be excluded that it proceeds parallel to anionic polymerization.

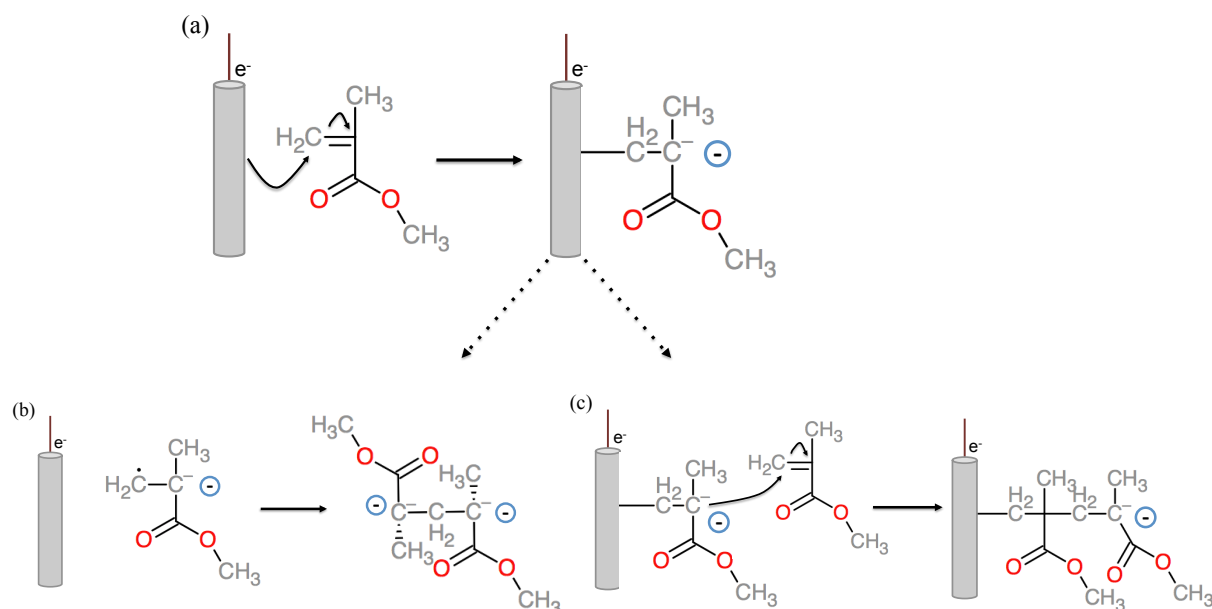


Figure 7 Possible mechanisms for the electropolymerization on the surface of the carbon fibres. To initiate the reaction a MMA monomer becomes reduced by the introduced electrons. A radical anion is produced which binds to the cathode. (a) This grafted anion can either be expelled from the surface to form a free radical anion in solution and further be combined with another radical to build a dimer (b) or it can react with another MMA monomer to form a polymer chain that is grafted onto the surface (c). (chemical structures drawn using the 2D Sketcher from ChemDoodle®, oriented on (Palacin et al. 2004))

To ensure safety during storage most MMA solutions contain inhibitors that stop the formation of radicals and therefore any possibility for polymerization until the inhibitor is consumed. The most common inhibitor to stabilize MMA is monomethyl ester hydroquinone (MEHQ). (Rasmussen 2002)

3 Experimental

3.1 Materials

The following chemicals were used for the electrocoating experiments and are further on only mentioned in form of their abbreviation. Materials used to produce the composites are separately listed in chapter 3.4.

HexTow[®] AS4D carbon fibres from Hexcel without sizing (12K, LOT: 4513-7C, USA PAN 4, DOFF: 04), methyl methacrylate (MMA) from Sigma-Aldrich (contains ≤ 30 ppm MEHQ as inhibitor, 99%, liquid), N,N-Dimethylformamide (DMF) from Sigma-Aldrich (anhydrous, 99.8%, liquid), lithium perchlorate (LiClO_4) from Sigma-Aldrich (≥ 98.0 %, powder) and aluminium oxide from Sigma-Aldrich (activated, basic, powder) were used as received (if not stated differently).

3.2 Electrocoating

The experimental parameters for the electrocoating experiments are summarized in Table 3. For all electrocoating experiments conducted under ambient conditions the experimental set-up presented in Figure 8 was used. The carbon fibres were led over a metal tube before they were inserted into a stainless steel tube that served as the counter electrode. The steel tube was immersed in an electrolyte consisting of the monomer, a salt and a solvent for both the salt and the monomer. The used monomer was MMA and the solvent was DMF. The concentration of MMA in DMF was varied between 5M and 10M as seen from Table 3. The salt (LiClO_4) concentration was kept constant at 0.4M. The metal tube at the beginning connected the fibres to the power supply (Gamry Instruments, Reference 3000), so that they were used as the working electrode. A platinum wire was introduced into the electrolyte to serve as a pseudo-reference electrode. At the end, the fibres were pulled out of the electrolyte, led over a series of electrically isolating spools and wound up on a final reel. During all experiments the temperature was tracked using a thermometer that was inserted beside the reference electrode. The temperature was kept between 56°C and 65°C and a slight increase of temperature was observed during the experiments, especially for experiments at high current densities.

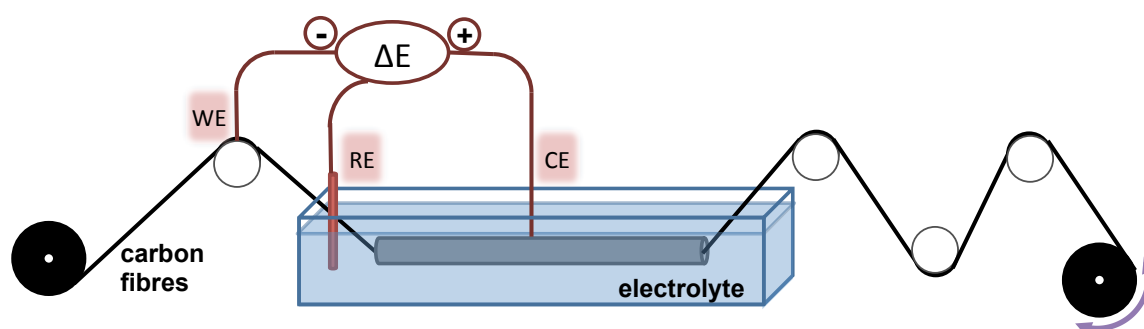


Figure 8 Experimental set-up for the electrocoating process. Carbon fibres are led through a tube in a bath of electrolyte containing monomer, salt and solvent and can be wound up at the end. For the electrocoating the carbon fibres are designated as the working electrode (WE), a stainless steel tube is the counter electrode (CE) and a platinum wire is used as a pseudo-reference electrode (RE). Both, batch electropolymerization as well as continuous coating have been performed using this set-up under ambient conditions.

Table 3 Overview of all coating experiments conducted including specific parameters. (CV – cyclic voltammetry, CA – chronoamperometry, CP – chronopotentiometry, B – beginning of experimental series, E – end of experimental series, RT – room temperature)

Exp.	Treatment	MMA [mol l ⁻¹]	Scan rate [mV/s]	Current density [mA/cm ²]	Potential [V]	Fibre speed [mm/s]	Notes
V1	CV	10	20	-			B, 1 st sweep
V2	CV	10	20	-			B, 2 nd sweep
V3	CA	10	-	-	-1.4		
V4	CP	10	-	0.40			
V5	CP	10	-	0.79			
V6	CA	10	-	-	-1.8		
U1	CV	5	20	-			B, 1 st sweep
U2	CV	5	20	-			B, 2 nd sweep
U3	CA	5	-	-	-1.6		
U4	CA	5	-	-	-2.2		
U5	CP	5	-	0.79			
U6	CP	5	-	1.19			
U7	CP	5	-	1.58			
U8	CP	5	-	1.19		3.4	cont.
T1	CV	5	25	-			B, 1 st sweep
T2	CV	5	25	-			B, 2 nd sweep
T3	CV	5	5	-			
T4	CP	5	-	0.40			
T5	CP	5	-	1.58			
T6	CA	5	-	-	-2		
T7	CP	5	-	0.40			
T8	CP	5	-	1.58			
S1	CV	7	20	-			B, 1 st sweep
S2	CV	7	20	-			B, 2 nd sweep
S3	CA	7	-	-	-5		
S4	CP	7	-	0.79			
S5	CP	7	-	1.19			
S6	CA	7	-	-	-5		
S7	CP	7	-	0.79		3.4	cont.
R	CP	5	-	1.19		3.4	
Q	CP	5	-	1.19		3.4	cont.
P	CP	5	-	1.19		3.4	
O1	CV	5	20	-			
O1_2	CV	5	20	-			
O2	CA	5	-	-	-1.3		
O3	CP	5	-	0.79			
O4	CP	5	-	1.19			removed MEHQ
O5	CP	5	-	1.58			
O6	CV	5	20	-			
O7	CA	5	-	-	-0.9		
O8	CV	5	-	-			
N	CP	5	-	1.19		3.4	
M	CP	5	-	1.19		3.4	cont.
L	CP	5	-	1.19		4.2	
K1	CV	5	20	-			
K2	CV	5	20	-			
K3	CP	5	-	0.79			
K4	CP	5	-	1.19			
K5	CP	5	-	1.58			1.1M H ₂ O
K6	CP	5	-	0.79			
K7	CP	5	-	1.19			
K8	CV	5	20	-			

J1	CV	5	20	-		
J2	CA	5	-	-	-1.3	
J3	CV	5	20	-		
J4	CV	5	20	-		
J5	CP	5	-	0.79		RT
J6	CP	5	-	1.19		(~23°C)
J7	CP	5	-	1.58		
J8	CV	5	20	-		
J9	CV	5	20	-		
J10	CA	5	-	-	-0.7	
J11	CP	5	-	1.58		

For control tests under inert conditions the experimental set-up was different and can be seen schematically in Figure 9. Carbon fibre tows served both as working and counter electrode. A glass fibre mesh (1080 style E-glass fabric, 23% void area) was used as a separator for the two fibre tows. Fibres and mesh were embedded into a Teflon fixture and placed in a petri dish. The electrolyte consisting of monomer MMA, solvent DMF and 0.25 M salt (LiClO_4) was poured onto this setting until everything was covered. The coating fibre length was approximately 25 mm and a lithium metal reference electrode was positioned inside the electrolyte. For the coating experiment the rig was placed inside a glove box and set under argon atmosphere with a maximum moisture and oxygen gas content of 1 ppm each. Cyclic voltammetry and batch electrocoating were done with a Solatron SI 1287 potentiostat controlled digitally by Corrware 3.2 at a temperature of 62°C.

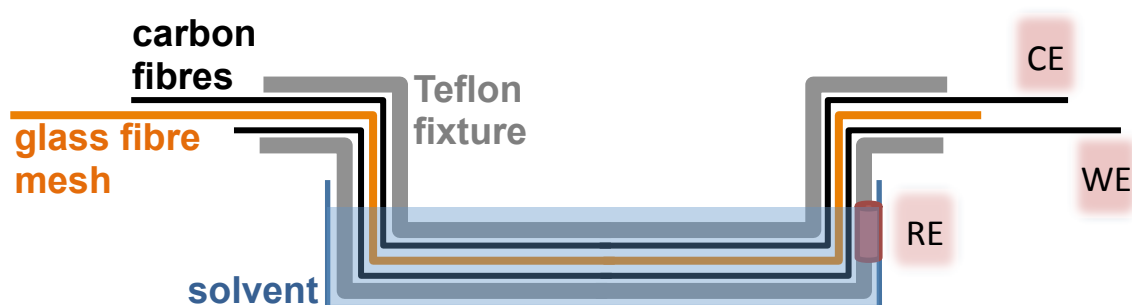


Figure 9 Schematic set-up for the coating experiment under inert conditions. The solvent was filled into a small petri dish. Carbon fibres, which represented both the working electrode and the counter electrode, were fixed in a Teflon frame, separated by a glass fibre mesh and submerged into the solvent. (redrawn from (Leijonmarck et al. 2013))

3.2.1 Cyclic voltammetry

At the beginning of each experimental series a linear potential sweep between 0.1 and -5 V was performed to identify the specific reduction potential of the monomer. Furthermore, sweeps were done in between experiments or at the end of a series to observe changes (see Table 3). In some cases the sweep was performed in two cycles to observe differences caused by a coating. All sweeps were conducted at a scan rate of 20 mV/s. The experiments performed under inert conditions depict an exception as different scan rates were tested. It was assumed that the exclusion of water would assure the occurrence of peaks. In fact, a variation of scan rate had in earlier experiments led to more distinct peaks.

3.2.2 Batch electrocoating

Batch electrocoating was performed at varying current densities (see Table 3) and the reaction time for each experiment was 70s. The coating was performed both at constant potential and at constant current. The potential was chosen according to peaks that could be observed in the voltammograms from the linear potential sweeps. The range of current densities tested was set in accordance to literature (see 2.2.2) and included 0.4, 0.79, 1.19 and 1.58 mA/cm². The electrolyte for every series of batch electrocoating experiments was inserted at the beginning and was used until the end. Only MMA was added in between experiments if necessary to compensate for evaporation. After electrocoating the fibre tows were cut to the length of the steel tube, washed with DMF and dried under reduced pressure at 80°C overnight.

3.2.3 Continuous electrocoating

Continuous electrocoating was performed at a current density of 1.19 mA/cm². To keep control over the experimental parameters the continuous coating process was interrupted in intervals of about 1200 s to slue the basin and add MMA if necessary to compensate for evaporation. This procedure also ensured increased mixing of the solution within the tube. The fibre-pulling speed was controlled through a power supply (8717 from mascot) in terms of volt, which only allowed for a coarse adjustment of the speed. Therefore, a fibre-pulling speed range is given. The first experiments were performed at a fibre-pulling speed of 2.9 to 3.4 mm/s, which was later increased to 3.5 to 4.2 mm/s. Due to polymerization in solution, the viscosity of the electrolyte increased over time. The electrolyte was therefore renewed in intervals of about 3600 s. For the exchange of the solution the tube was removed from the basin while flushing out possible residues inside of the tube. The coating process continued until the desired length of coated fibre was reached.

The washing process for continuous coating differed from the washing process described above for batch coating. The fibres were wound on a spool at the end of the set-up. Therefore, they had to be unwound again and led through a solution of pure DMF for a first washing step. The length of the basin containing the solution was the same as for the coating process and the speed of the fibres was maximum 8.8 mm/s. The fibres were wound around a glass beaker in layers and the beaker holding the coated fibres was then placed in DMF. This washing step was conducted under magnetic stirring over night at an elevated temperature of 55°C. The beaker with the wound fibres was then removed from the DMF solution and dried in the same way as described for the batch electrocoating.

3.2.4 Mechanism

To determine the polymerization mechanism four different experiments were set up. All experiments included voltammetry, coating at constant potential and coating at constant current. A summary of all parameters can be seen in Table 3. All samples were washed and dried as described for the batch electrocoating (3.2.2). The following experiments were performed:

Removal of inhibitor

The inhibitor was removed by passing the liquid MMA through a column containing activated aluminium oxide. The inhibitor-free MMA was then used in a 5 M MMA solution with 0.4 M LiClO₄ and DMF and the electrocoating was performed as described in section 3.2.2.

Addition of water

1.1M distilled water was added to a 5 M MMA, 0.4 M LiClO₄ and DMF solution and the electrocoating was performed as described in section 3.2.2.

Room temperature

The coating was conducted without any heating in a 5 M MMA, 0.4 M LiClO₄ and DMF solution. The temperature was observed at the beginning of every experiment. The experiment was otherwise performed as described in section 3.2.2.

Ultrasonication and bending

Some already coated, washed and dried fibres were placed in a small container and again immersed in DMF. The container was then put into an ultrasonication bath for three minutes (Transsonic T700, Elma; Frequency: 35 kHz). The fibres were dried as described above.

A 7M MMA continuously coated sample (S7) was analysed using optical microscopy before and after it had been vigorously bent in all directions.

3.3 Characterisation of coated fibres

3.3.1 Optical microscopy

Optical microscopy was performed on a BH-2 microscope from Olympus with the camera system Color View and the software ANALYSIS from Soft imaging system GmbH was used. This method was applied to analyse the uniformity of the coating over a large part of the sample. Depending on the appearance of the overall fibre surfaces, the coatings were classified according to the system shown in Table 4.

Table 4 Classification to grade the quality of the coating observed by optical microscopy.

Mark	Description
a	Nearly no coating observed
b	Discontinuous coating covering a small portion of the fibre surface
c	Coating covering a considerable portion of the fibre surface or continuous film on some fibres
d	Continuous film covering complete fibre surface

3.3.2 TGA and weight measurement

The thermogravimetric measurements under air were performed on a TGA/DSC 1 STAR[®] System from Mettler Toledo. A short section of a fibre tow was wound on a pincette so that it was possible to fit it into a 70 µl aluminium oxide crucible. The fibres were then pressed into place using a plastic stick. The sample weights varied between 7 and 18 mg. After insertion the temperature was linearly increased from 50°C to 800°C at a rate of 10°C/min and the

sample weight was monitored. As a result the onset temperature of the degradation of the carbon fibres was determined. Furthermore, the step of the mass change in percentage was measured for the degradation of the polymer coating. This was set to be between 160°C and 350°C to exclude any influence of remaining DMF as DMF evaporates at 153°C. The coating thickness was calculated from the mass loss assuming complete coverage of the fibres with an even cylindrical coating.

Additionally, for some of the coating experiments the weight of 10 cm long fibre tows was determined with a micro-balance and compared against a non-treated fibre tow. From this, the mass change and furthermore the coating thickness were calculated.

3.3.3 SEM

To study the morphology of the coating, scanning electron microscopy was applied. Different systems have been used and are presented in Table 5. The fibres were used without any further treatment (e.g. sputtering).

Table 5 Scanning electron microscopes used for the qualitative analysis of the coating.

Device	University/company	City	Acceleration voltage [kV]	Notes
Hitachi S-4800	Royal Institute of Technology (KTH)	Stockholm	1	
Zeiss DSM 940A	Chalmers University of Technology	Gothenburg	5	
Hitachi TM3000	SiCOMP	Gothenburg	5	Table Top

3.3.4 Tensile testing

Tensile testing of single fibres was performed on a Vibrodyn in combination with a Vibroskop (Lenzing Technik Instruments). The test followed the ASTM standard C1557 – 03 (2913) as far as possible and all changes are listed below. Both coated and uncoated fibres were tested and the number of samples was 20 fibres each. Prior to testing, a fibre was randomly chosen and carefully separated from the fibre tow. The linear density (titer) for each fibre was determined using the Vibroskop, which allowed the estimation of the cross-sectional area. For the non-coated fibres a constant cross-sectional area of $d = 6.7 \mu\text{m}$ was assumed. The fibre was then mounted directly into the grips with the help of a small weight of 70 mg to align the fibre axially in the moving direction of the test machine. The specimen gauge length was 25 mm and the test was conducted at a crosshead speed of 1 mm/min. The load cell used had a capacity of 0 – 500 cN. After the test the Vibrodyn displayed linear density in dtex, tenacity in cN/tex, elongation in %, force to failure in cN, Young's modulus in cN/tex and the work in cN.cm. This data was used as given and Young's modulus as well as the tenacity, which equals the fibre strength, were calculated in GPa and MPa respectively. No system compliance could be determined, because the raw data of the testing machine was not accessible and the modulus values were given directly.

3.3.5 Resistivity

To identify the resistivity of the treated (continuous coating, N) and non-treated fibres the resistance of a fibre tow with a length of 105 mm was measured. To achieve this, the fibres were prepared in the following way: Silver paint was applied to the end of the fibre tow so that all fibres could be contacted. After drying another layer of the silver paint was applied and the ends were wrapped in aluminium foil. The resistance was measured by clamping the wrapped ends and applying a certain voltage. The voltage was set to 1 V at the beginning of the test and was later increased to 3 V. During the test, voltage, current and the temperature at the middle of the fibre tow were recorded. To calculate the electrical resistivity the following equations were used:

$$R_f = \frac{U}{I}$$

where R_f is the resistance of the fibres in Ω , U is the potential in V and I is the current in A, and

$$\rho_f = R_f \cdot \frac{A_f}{l}$$

where ρ_f denotes the electrical resistivity in Ωm , A_f is the area of all fibre diameters in m^2 and l is the distance between the electrodes along the fibre tow in m.

3.4 Manufacturing of composites

As a manufacturing method for the composites vacuum-bagging was chosen because it allows the production of smaller custom-made plates at a low cost. The fibres were automatically aligned on a wound preform with 3 mm bandwidth and eight layers in total. The set-up for the vacuum-bagging can be seen in Figure 10. Firstly the plate with the wounded fibres was wrapped into the peel ply. Additionally, this fabric served as the flow media to enable an even infusion. The plate was then placed on the vacuum-bag rig and the spiral tubing was placed so that the resin would be injected in the 90° fibre direction. The spiral tubing was connected to the inlet tube for the resin. On the other end a tube was connected to the resin trap and the vacuum pump. To provide a uniform pressure a piece of breather fabric was placed between the vacuum line and the composite. The vacuum bag was attached using sealant tape around the rig and folds were integrated at the edges of the carbon fibre plate to assure a flat distribution of the vacuum bag on top of the composite. Before infusion it was secured that the vacuum bag was sealed completely. The process parameters for infusion and curing are presented in Table 6.

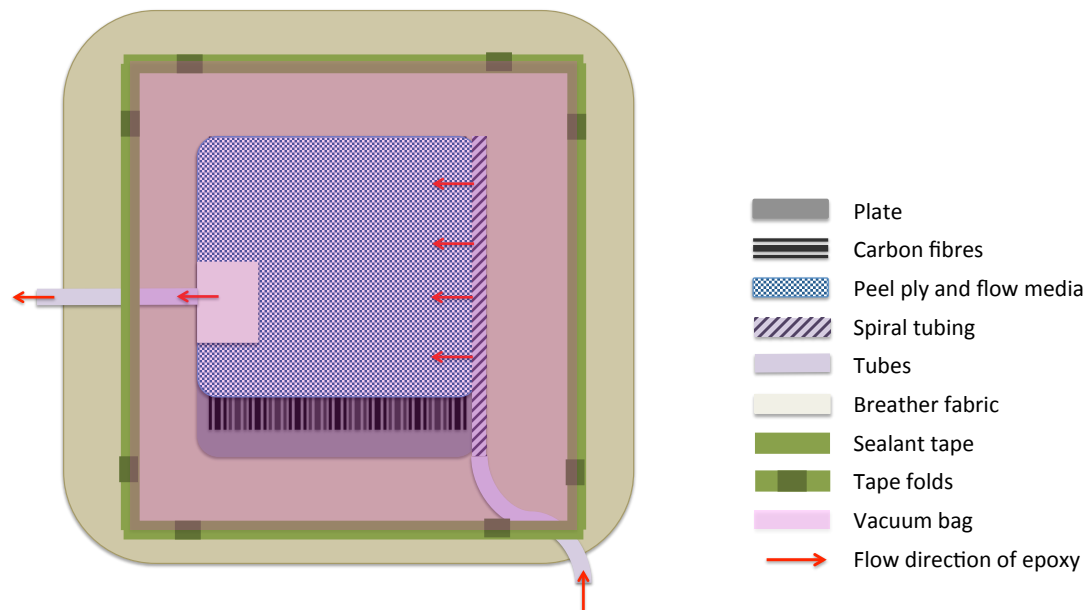


Figure 10 Schematic set-up for the vacuum-bagging. As the vacuum is applied on the left side the epoxy resin flows through the inlet on the lower right side, infuses the fibres from the spiral tubing until the flow line reaches the left side.

Table 6 Process parameters for the vacuum-bagging.

	Infusion pressure	Cure pressure	Resin temp.	Tool temp. filling	Tool temp. cure	Curing time	Postcure
Epoxy 1	100 mbar	600 mbar	40°C	40°C	80°C	15 h	4h at 140°C
Epoxy 2	100 mbar	600 mbar	40°C	40°C	80°C	15 h	-

Different resins were tested to achieve a complete wetting of the fibres and minimize pore volume. The resins tested are listed in Table 7. The glass transition temperatures mentioned therein are derived from product data sheets according to the applied curing procedure. However, additional testing has been conducted to determine a more exact glass transition temperature and the stiffness-reduction at T_g (see 3.5.2 DMTA). Cross-sections of the composites were evaluated using an optical microscope to estimate the pore volume and the distribution of fibres within the matrix. Prior to testing the composites were machine-cut and polished to reduce roughness and remove matrix-rich regions on the surface.

Table 7 Components used for the two epoxy resins which were tested and their respective weight ratios. Values for the T_g are derived from product data sheets.

	Base	Hardener	Accelerator	Weight ratio	T_g DSC [°C]
Epoxy1	Araldite LY 556	HY 917	DY 070	100/90/0,5	145 - 150
Epoxy2	Araldite LY 5052	Aradur 5052	-	100/38	114 - 122

3.5 Mechanical characterisation of composites

3.5.1 Three-point bending

Three-point bending tests under current were performed to determine the stiffness-reduction in relation to applied current thus increased temperature. It was further investigated if the deformation of the samples was reversible.

Prior to the three-point bending tests the samples had to be prepared specifically as during testing a current was applied. For preparation the specimens were machine-cut to a size of 80 x 10 mm and polished as described in the previous chapter. The height varied depending on if the composite was made with coated fibres (2.6 - 3.2 mm) or non-coated fibres (1.8 – 2.1 mm). After polishing the surface both ends of the specimen were grinded at the corners so that pointy ends were created. Next a double layer of silver conductive paint (Electrolube) was spread onto the grinded ends and they then were wrapped up in aluminium foil. This preparation was done to allow contacting of as many fibres as possible. For testing the specimen contacted with crocodile clamps at the aluminium foil ends.

The three-point bending test could not be performed according to standard because the rig had to be adjusted to ensure safe handling even if high potential or current is used. The testing was therefore done using the custom made rig presented in Figure 11 (left). The ground plate consisted of an isolating material (Teflon) and the load was applied in form of a weight that exhibits no contact to other parts of the rig. Throughout the experiment the temperature was recorded at the end and in the middle of each specimen (see Figure 11, right).

The specimen was placed on top of the rig and a weight of 6.5 kg was added at room temperature to determine the initial flexural modulus. No current was applied at that point. To heat the specimen an electrical current was applied by a DC Power Supply (TSX1820P from Thurlby Thandar Instruments) with a maximum output of 18V/20A. All tests were performed by applying a constant potential.

After the test, the specimen was cooled down to room temperature and the weight was removed. The specimen was then heated again through application of constant potential to evaluate if the bent specimen recovers its original shape and straightens out.

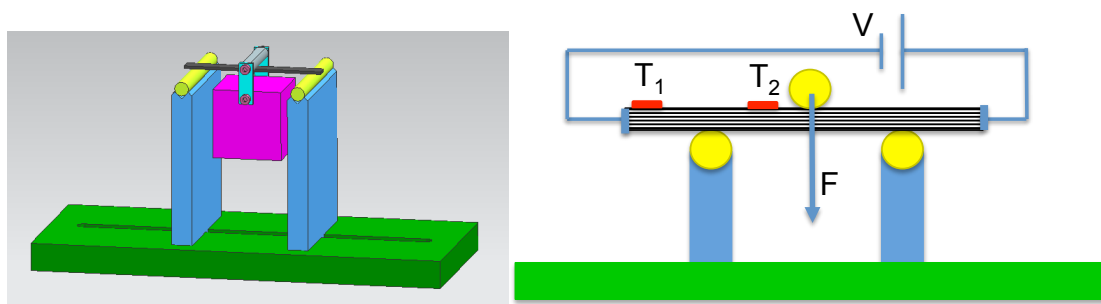


Figure 11 Experimental set-up for the three-point bending test. A specific rig had been built to perform under voltage (left). The specimen was placed on two isolated metal tubes and a weight was added in the middle. During testing a voltage was applied and the temperature was measured at two different positions (T1 at the end, T2 near to the middle; right).

3.5.2 DMTA

Dynamic Mechanical Thermal Analysis was carried out to determine the glass transition temperature of the composites and to further evaluate the possibility of the materials to reduce their stiffness upon heating. For the analysis a DMTA IV Rheometric Scientific (Swerea IVF,

Mölnidal) was used in single cantilever bending mode. The specimens had a dimension of 30 x 10 x 1.4 mm and were clamped to the frame with a torque of 30 cNm. The analysis was performed in dynamic strain-controlled mode with a maximum strain of 0.1% and at a frequency of 1 Hz. The temperature ramp was set to 5°C/min starting at an initial temperature of 25°C and the test finished at 155°C.

4 Results

4.1 Electrocoating

In this chapter observations and voltammograms from the electrocoating process are presented. During all experiments a change in colour of the electrolyte was observed from transparent to yellow-green and the electrolyte became more viscous. This was on the one hand assigned to a polymerization in solution. On the other hand did the screws used to fixate the stainless steel tube react during the application of current as they were not stainless. Hence, over the experimental time rust seemed to appear and dissolve into the electrolyte. Additionally, depositions of polymer formed in solution were visible at the end of the steel tube in form of a stream or small particles. MMA was also polymerized on the edge of the tube and these depositions became loose over the course of the experiments especially for the continuous coating.

Furthermore, with the help of an infrared camera, it was observed that the fibre temperature increased locally at the connection between the carbon fibres and the working electrode during the electrocoating experiments depending on the potential or current applied. The maximal temperature observed was 43°C.

4.1.1 Cyclic voltammetry

A general observation from the linear potential sweeps was that for each experimental series the curves varied significantly from experiment to experiment even if the main conditions stayed the same and if the voltammograms were achieved right after each other as can be seen from Figure 12 (1st and 2nd sweep, 5 M). No distinct and stable peaks could be identified for any of the experiments, except for the electropolymerization performed without the inhibitor MEHQ (see Figure 12 in comparison to Figure 13). However, it could be observed that the current needed to achieve the reduction potential decreased with increasing molar concentration of MMA (Figure 12). Additionally, if two cycles were performed the current decreased from the first to the second cycle (Figure 12; 1st and 2nd cycle, 10 M). Hence, for coating experiments at constant potential a value was chosen where the potential sweep underwent some kind of change. For example, 1.6 V was chosen for the 5 M experimental series because the curve of the first sweep evened out a bit at that point (see Figure 12; 1st sweep, 5 M). In case of the 7 M experimental series (S) no change in the curves could be detected and the potential was therefore set to a relatively high potential of 5 V.

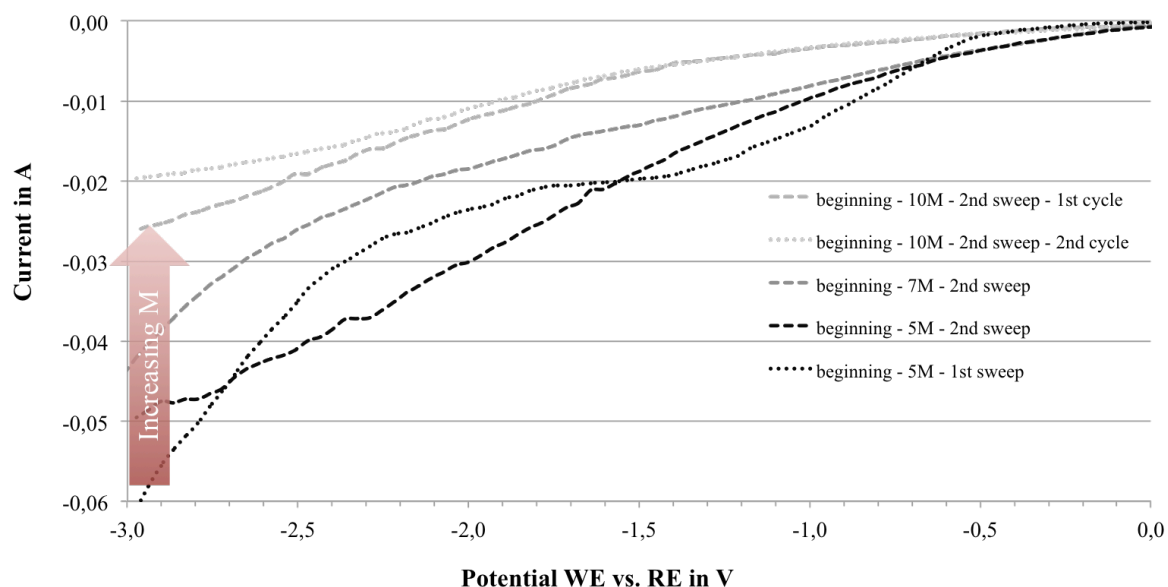


Figure 12 Cyclic voltammetry with varying molar concentrations of MMA (scan rate: 20 mV/s). An increase in current is observable with the increase of the concentration. A decreased slope is observed if the sample is run for two cycles: 1st sweep and 2nd sweep for the 5 M experiments.

In case of the series where the inhibitor had been removed from the monomer slight signals could be identified (Figure 13). These signals occurred at different positions at the beginning of an experimental series and stabilized at the end after some experiments had been conducted with the same electrolyte. With increasing experimental time the position of the identified peaks moved to a higher potential and it stabilized at a potential of about -0.9 V.

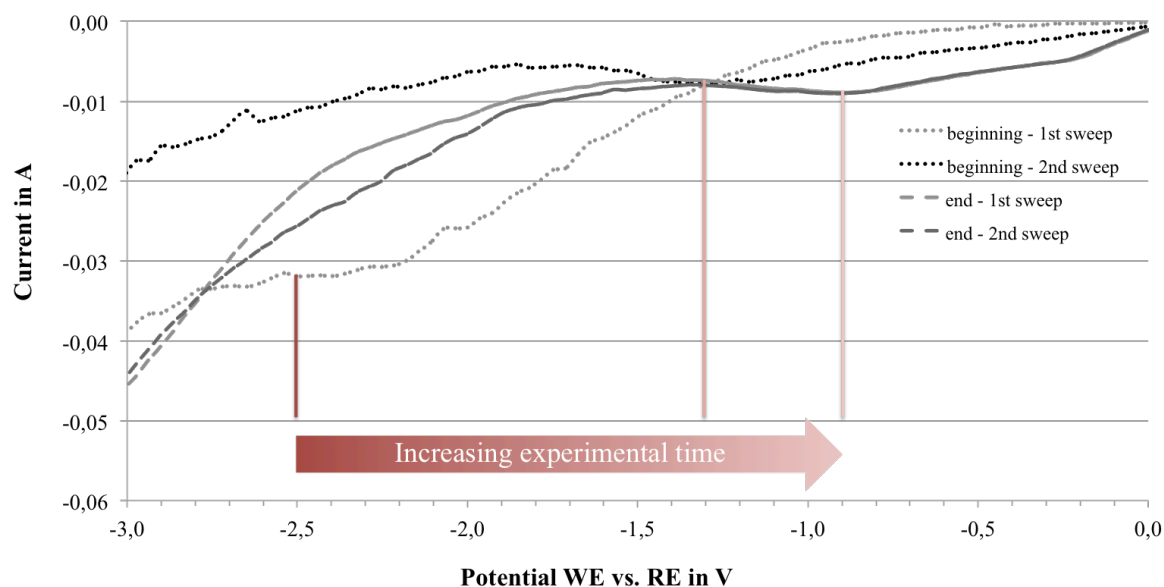


Figure 13 The cyclic voltammetry of the experiment where the inhibitor was removed exhibited more clear peaks. In one experimental series with the same solution the peak moved to higher potentials with an increasing experimental time. The repetition of sweeps even if new fibres were used did not change the position of the peak.

For the experiments under inert conditions no peaks or signals were observable at any of the scan rates tested. The curve progression was consistent with observations from the experiments under ambient conditions (see Figure 12).

4.1.2 Batch electrocoating

The currents recorded for the batch electrocoating at constant potentials showed a peak at the beginning of the experiment and further decreased in a steeper slope (Figure 14). The current stabilized after 10 seconds and only decreased slightly until the end of the experimental time. The highest current achieved was at the second linear potential sweep for the 7 M experimental series (S6) with approximately -0.25 A. For this curve a more distinct decrease in current was observed until the end of the experiment.

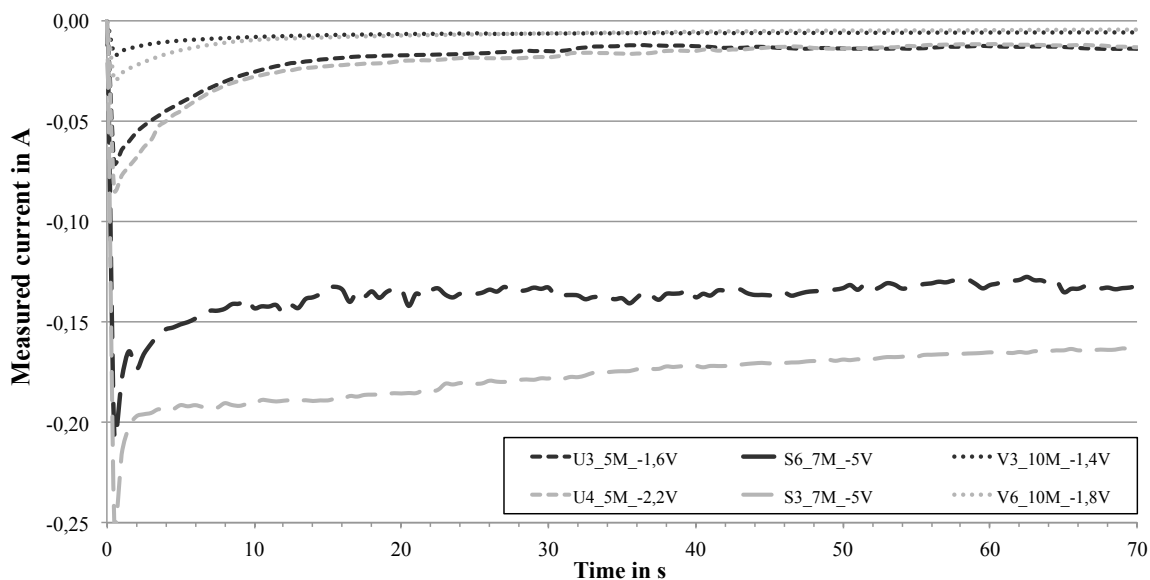


Figure 14 Measured current values for the experiments at constant potential.

The measured potential at the working electrode against the reference electrode increased slightly over the coating time for all experiments (Figure 15). For equal current densities an increase in molar concentration led to a decrease of the potential. In case of a current density of 0.79 mA/cm^2 the potential for 5 M, 7 M and 10 M reached 7.5, 8 and 12 V at the end, respectively. The latter represented the maximal reachable potential of the potentiostat. The maximum was also reached at a current density of 1.19 mA/cm^2 for the 7M series (S5) and at 1.58 mA/cm^2 for the 5M series (U7).

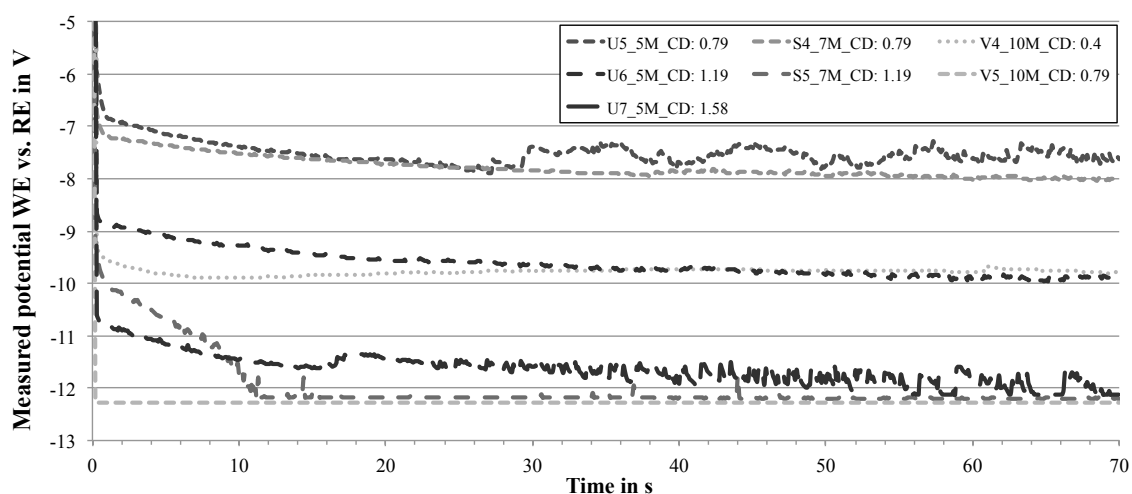


Figure 15 Measured potential WE vs. RE for the experiments at constant current densities and different molar concentrations.

For the experiments under inert conditions the electrolyte evaporated to a level under the fibre tow. This was detected, after T5 and T6 had been tested. The electrolyte was completely refilled for T7 and T8.

4.1.3 Continuous electrocoating

An excerpt of the measured potential from one continuous coating experiment at constant current can be seen in Figure 16. Periodic fluctuation occurred over the whole length of the experiments. Larger peaks in potential (Figure 16, at ~1950 s) could through observation be related to deposits around or inside the tube, which built up and later loosened at the potential peak and fell off during the experiments. The sharp peak in the middle results from the start of a new experiment as the continuous coating was interrupted every 1200 s to slue the basin and to refill MMA if necessary.

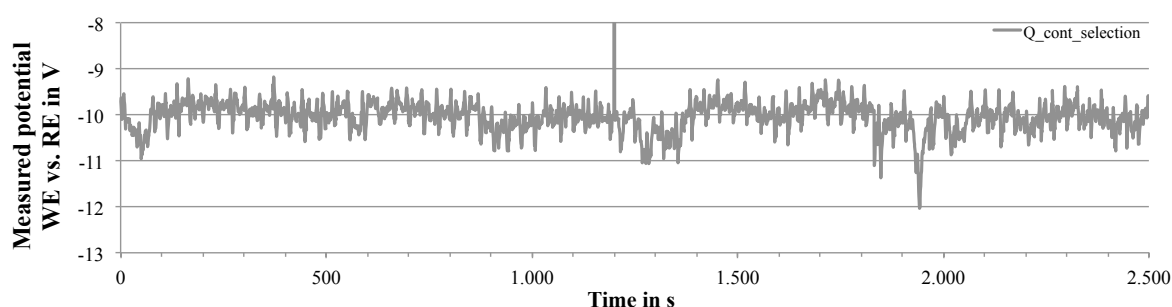


Figure 16 Measured potential WE vs. RE for a section of a continuous coating experiment. The experiment was interrupted and restarted at 1200 s.

4.1.4 Mechanism

As all experiments on the mechanism contained 5 M MMA the results will be compared to the 5 M series (U-series) for each experimental series.

Removal of inhibitor

The curve progression for the experiments with removed inhibitor MEHQ looked similar to the initial experiments with inhibitor (Figure 17). A slight decrease in potential was visible for no inhibitor (O-series) and this difference was most distinct for the electrocoating at the highest current density of 1.58 mA/cm^2 where the potential for the removed inhibitor (O5) stayed very stable at approximately 10 V in comparison to U7 which reached the maximal achievable potential at the end.

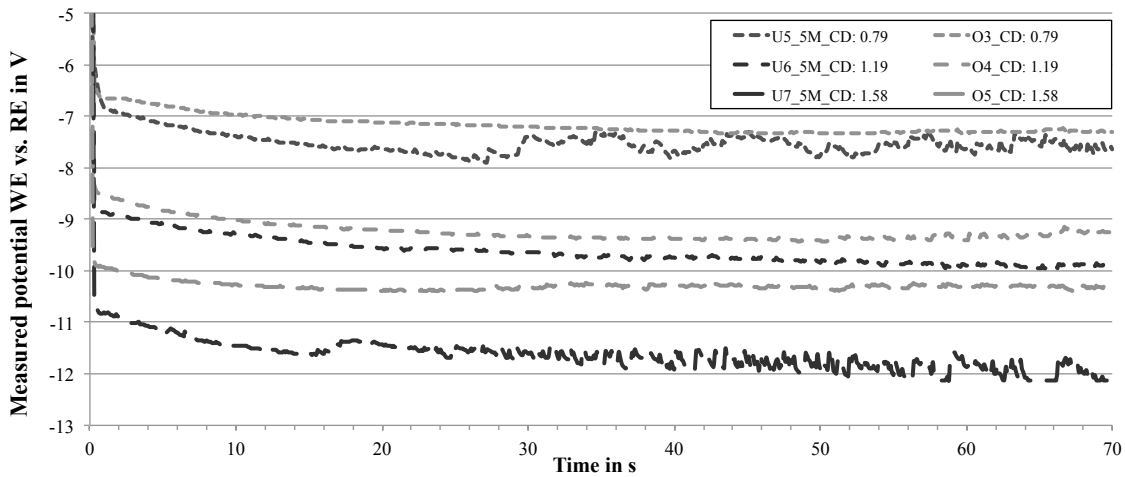


Figure 17 Measured potential WE vs. RE for the experiments with removed inhibitor MEHQ at constant current densities in comparison to experiments with inhibitor.

Addition of water

The addition of 1.1 M H₂O led to potential curves, which decreased over the course of the experiment (Figure 18, K-series). The initial potential was thereby slightly lower than the potential for the experiments where no water was added (U). However, at the end of the experiments the difference was approximately one volt for a current density of 0.79 mA/cm² and two volts for 1.19 mA/cm² towards a more negative potential for the experiments with water.

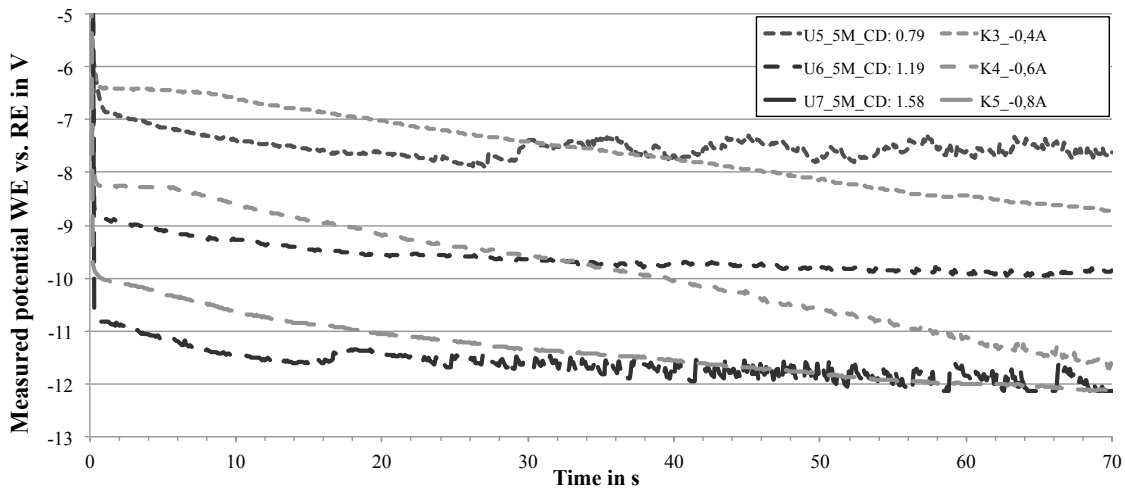


Figure 18 Measured potential WE vs. RE for the experiments with 1.1M H₂O at constant current densities in comparison to experiments without added water.

Room temperature

The curve progressions for the experiments at room temperature looked similar to the initial experiments at elevated temperatures (Figure 19). The experiment at the lowest current density of 0.79 mA/cm² seemed disturbed and it is assumed that this was caused by small short-circuits between emerging fibres and the steel tube. A slightly decreased potential for the series at RT (J-series) was visible for all other current densities and the maximal negative potential was not reached for the highest current density of 1.58 mA/cm² (J7).

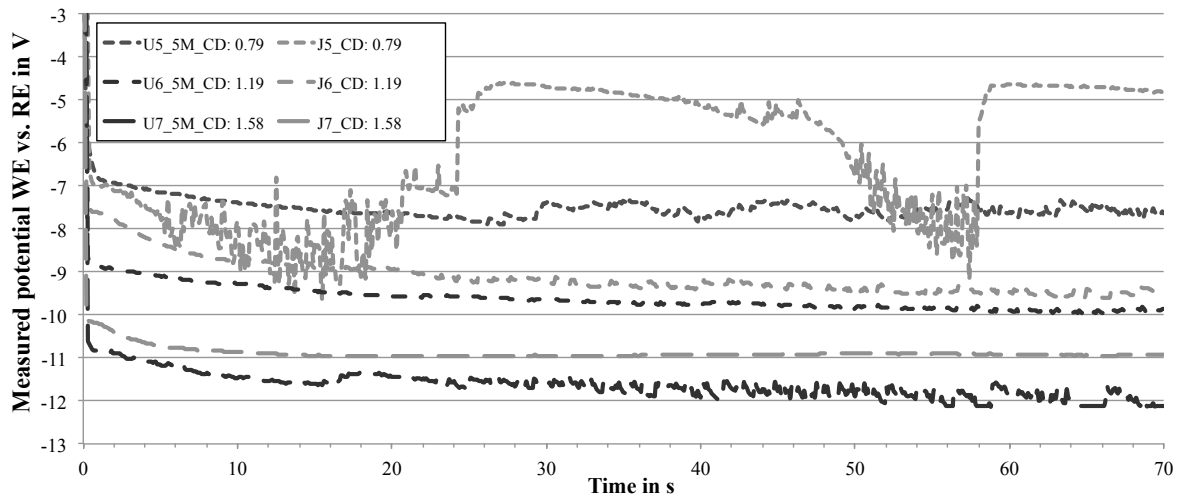


Figure 19 Measured potential WE vs. RE for the experiments under room temperature at constant current densities in comparison to experiments at elevated temperatures.

Ultrasonication and bending

Coated fibre samples were stored in transparent plastic bags. It was observed that a white powder residue became visible on the inside of the bags when the coated fibres were unintentionally moved or bent (Figure 20, left). The amount of observed powder increased when the fibres were vigorously bent for the sample J7 (Figure 20, right). During the ultrasonication of the fibre tow defibration occurred so that the fibre tow disintegrated into smaller parts. No powder was observed after ultrasonication, but the fibres obtained were also too short and small to be bent.



Figure 20 Powder residue visible in storing bags after the fibres have been moved or bend (left). The amount of powder increased with a vigorously bending of the fibres (right, J7).

4.2 Characterisation of coated fibres

The results from the characterisation methods used are summarized in Table 8 and are described in more detail in the following chapters.

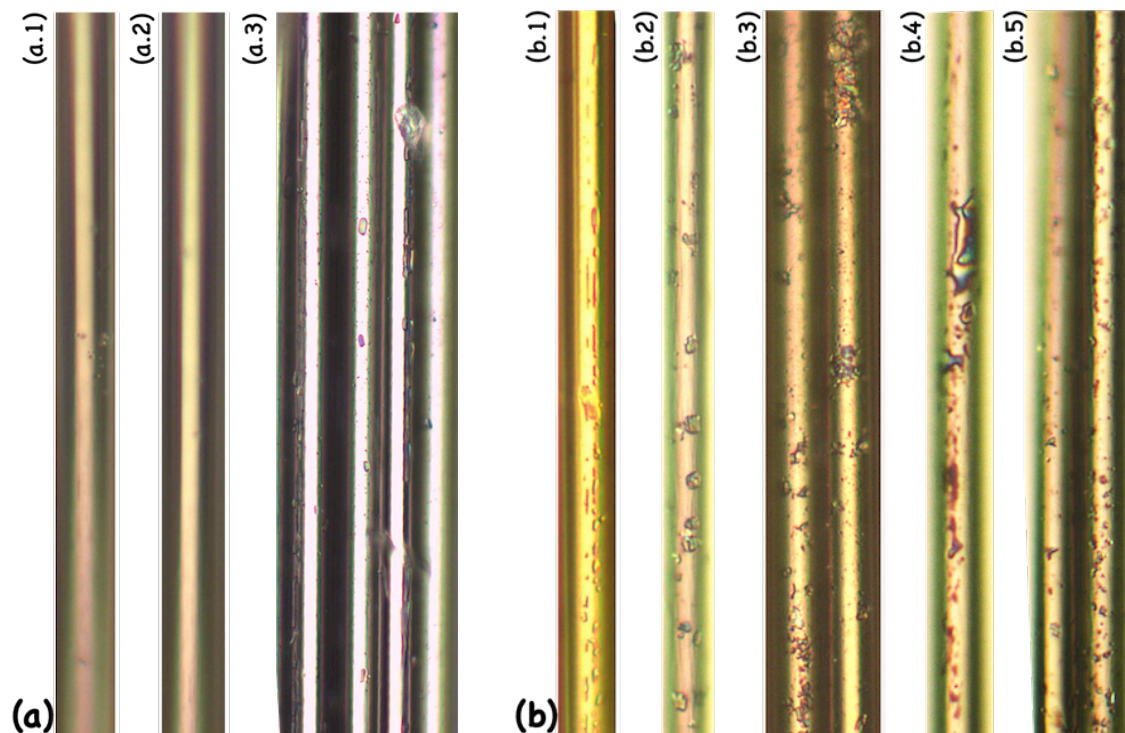
Table 8 Summary of the results from the optical microscopy, TGA, weight measurements and SEM (all coating thicknesses and particle heights are measured from KTH picture; CH = Chalmers SEM). From the tensile testing of the fibres a 256 nm coating thickness was determined (RT = room temperature).

Exp.	Treatment	Optical microscopy [a,b,c,d]	Coating thickness from TGA [nm]	Coating thickness from weight [nm]	SEM	Notes
V3	CA	a	5	-		
V4	CP	c	12 ± 8	-	49 nm, 67 nm particles	
V5	CP	c	8 ± 2	-		
V6	CA	a	4	-	0 nm	
U3	CA	a	13 ± 1	-		
U4	CA	a	12	-		
U5	CP	c	15 ± 7	-		
U6	CP	d	79 ± 74	-		
U7	CP	d	41 ± 21	-		
U8	CP	c	41	-		cont.
T4	CP	c	113	-	123 nm, 215 nm particles	
T5	CP	c	82	-	0 nm	glove box
T6	CA	b	45	-	54 nm	
T7	CP	c	77	-	68 nm	
T8	CP	d	231	-	159 nm	layer
S3	CA	a		38	CH, small drop-like particles	
S4	CP	c	27 ± 38	238	CH, fibres glued together - residues	
S5	CP	c	93 ± 96	287	CH, dirt/dust-like particles, sharper	
S6	CA	a	12	3	CH, nothing visible	
S7	CP	c	41 ± 41	18	CH, fibres glued together - residues, coating visible	cont.
R	CP	d		-		layer?, cont.
Q	CP		45 ± 17	-		cont.
P	CP	d		-		layer?, cont.
O2	CA	-		34		
O3	CP	c		109		
O4	CP	c		203		removed
O5	CP	d, rainbow!	35 ± 19	198		MEHQ
O7	CA	b	13 ± 6	7		
N	CP					cont.
M	CP					cont.
L	CP					cont.
K3	CP	c		222		
K4	CP	d	22 ± 2	251		
K5	CP	b - d	5	284		
K6	CP	c		165		1.1M H ₂ O
K7	CP	d		236		

J2	CA	a		108	
J5	CP	d		189	
J6	CP	d		222	RT
J7	CP	d	6 ± 4	239	(~23°C)
J10	CA	a		112	
J11	CP	c		227	

4.2.1 Optical microscopy

From optical microscopy it was in general possible to assign different types of fibre coating according to the classification in Table 4 as can be seen in Figure 21. No or only a few small particles are visible for mark **a** and the surface of the fibres appears evenly coloured. Both mark **b** and **c** vary in the characteristics of the coating formation. Depositions with a needle-shaped appearance can be seen that follow the fibre direction (Figure 21 **b.1**, **c.2**, **c.3**), small particles that show a large variation in size and shape (Figure 21 **b.2** – **b.5**) and even splash-like depositions (Figure 21 **b.4**). In agglomeration these particles seem to form partly continuous layers (Figure 21 **c.3**), but a continuous layer can even consist of a very even distribution of droplet-like particles (Figure 21 **c.5**). An increase in degree of continuous coating seems to correlate with a change in colour as the partly coated fibres and the fully coated fibres appear rainbow-coloured (Figure 21 **c.4**, **c.5**, **d.1** – **d.3**). The fully coated fibres exhibit a rough surface (Figure 21 **d.1** – **d.3**). However, this classification was in some cases difficult to apply to each sample or coating procedure as the distribution of the different types varied within one sample (Figure 22). Partly coated fibres appear right beside fully coated fibres and the variation in coating characteristics can be large. The resulting characterisation in Table 8 is therefore a qualitative proposition of the general mean appearance of one sample done by manual screening of the samples.



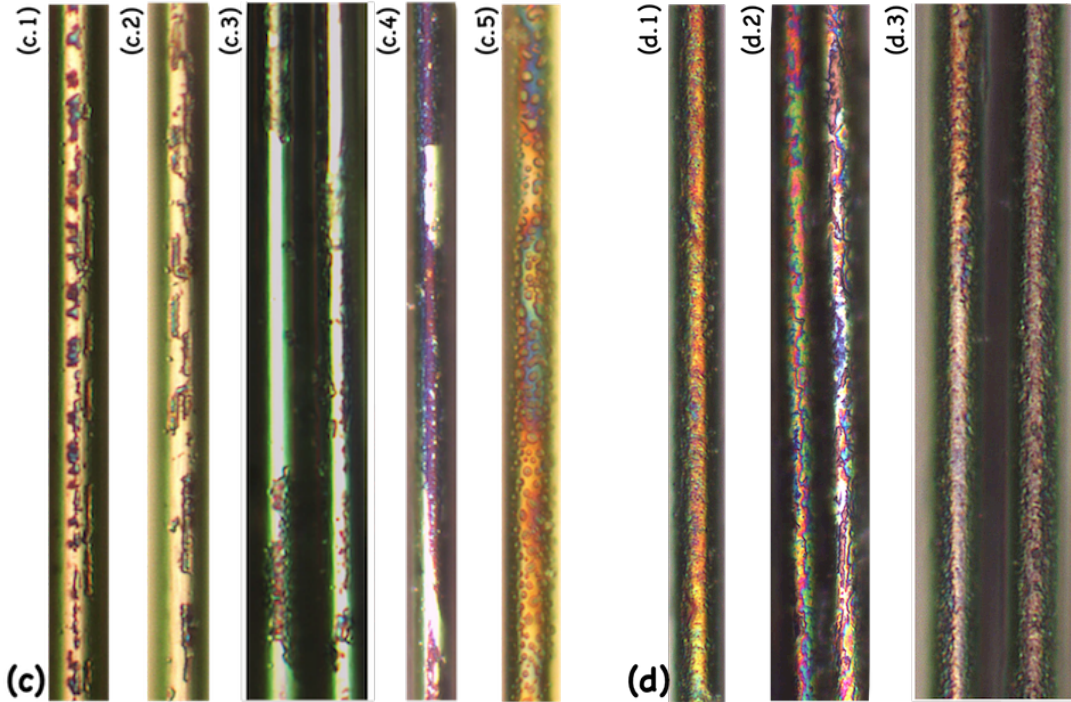


Figure 21 Fibres seen in the optical microscopy according to the classification described in **Table 4**. No or only a few small particles are visible for mark **a**. Both mark **b** and **c** vary in the characteristics of the coating formation: Depositions that follow the fibre directions with a needle-shaped appearance (**b.1**, **c.2**, **c.3**); small particles that show a large variation in size and shape (**b.2** – **b.5**) and even splash-like depositions (**b.4**); in agglomeration these particles seem to form partly continuous layers (**c.3**), but a continuous layer can even consist of a very even distribution of droplet-like particles (**c.5**). An increase in continuous coating seems to correlate with a change in colour as the partly coated fibres and the fully coated fibres appear rainbow-coloured (**c.4**, **c.5**, **d.1** – **d.3**). The fully coated fibres exhibit a rough surface (**d.1** – **d.3**). The pictures are enhanced to highlight the different characteristics and the fibres are therefore not shown to scale.

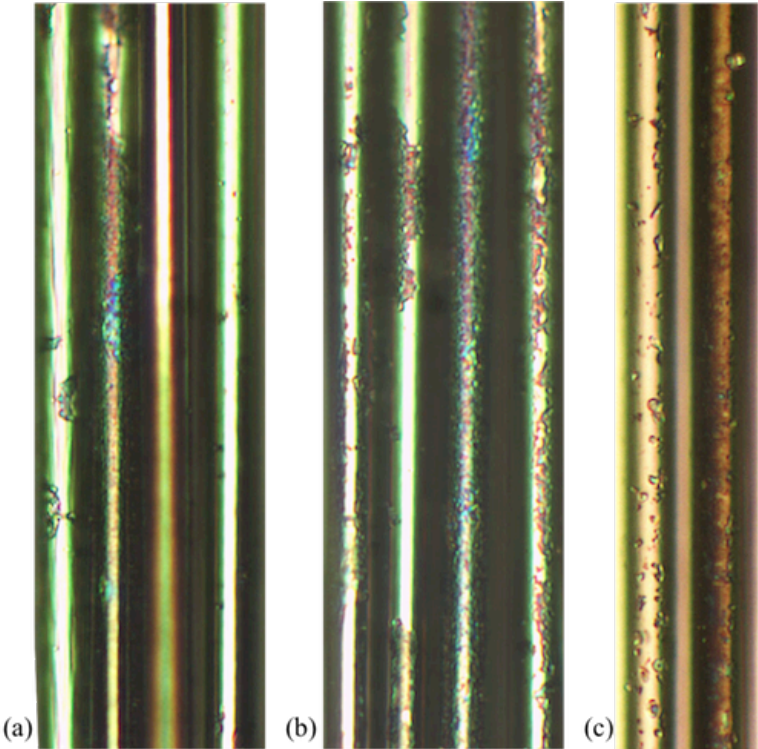


Figure 22 Variation of coating characteristics over the filaments within one sample. While the third fibre looks completely covered by a continuous coating the fibres besides are only partly coated (b).

With two exceptions (T6 and O7) all experiments performed at constant potential led to very poor or no fibre coating. Some coating was observed only for the experiment performed under inert conditions and for one experiment where the inhibitor had been removed. With a constant current density of 0.79 mA/cm^2 it was for some specimens possible to achieve an even, all-covering coating (J5). Consistent covering coatings were achieved with current densities $\geq 1.19 \text{ mA/cm}^2$. In the following paragraphs important observations from the mechanism experiments are presented in short.

Removal of inhibitor

For the high current density of 1.58 mA/cm^2 a very intensive rainbow colour was observed, which indicates a thick and even coating (Figure 23). The other coatings were similar to the ones achieved with inhibitor.

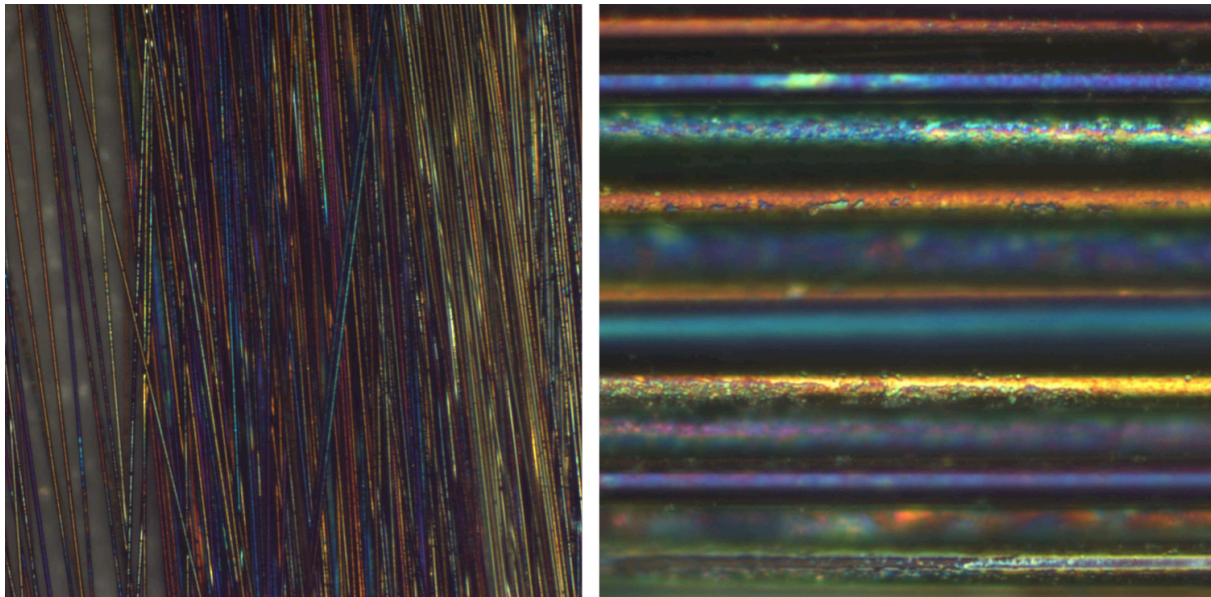


Figure 23 Experiment number O5. Electrolyte with removed inhibitor and 5 M MMA. The current density was 1.58 mA/cm^2 , the optical microscope grade is d and the fibres appear strongly rainbow coloured.

Addition of water

A major number of the experiments with 1.1 M H_2O led to even and fully coated fibres, especially at higher current densities (Figure 24). In the case of K5 a big difference in coating quality between various parts of the fibre tow was observed. While one side seemed to be covered by a thick coating, the other side appeared almost un-coated and only a few particles were visible on the fibre surfaces (Figure 25).

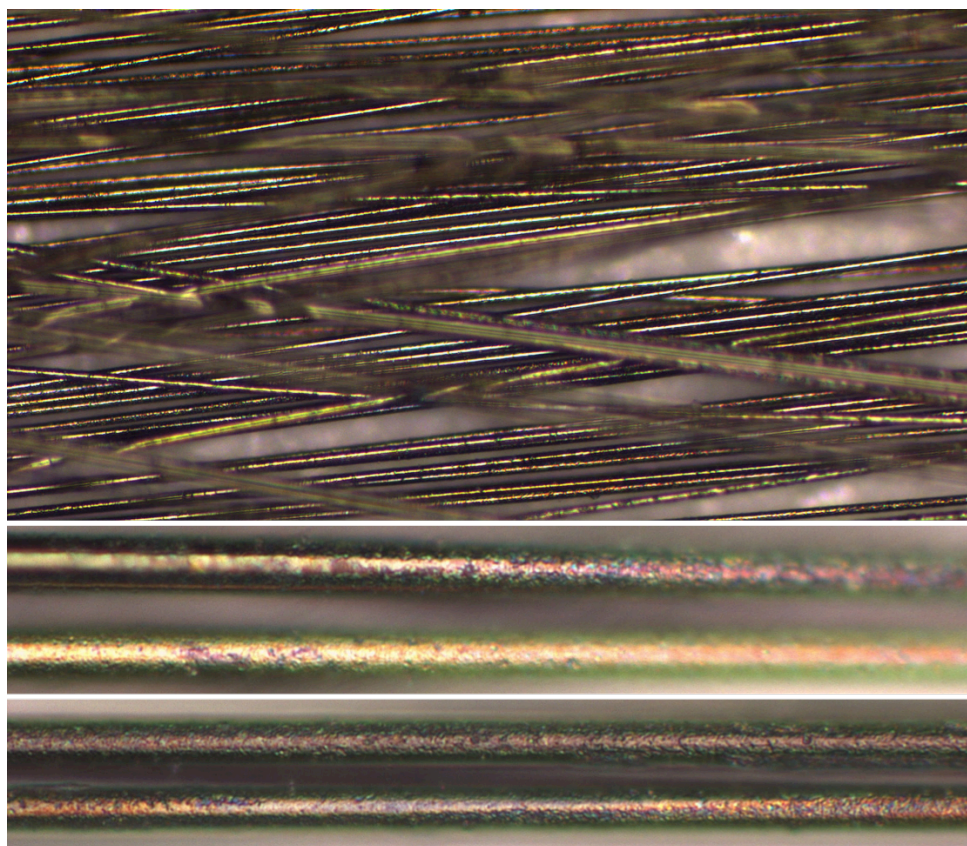


Figure 24 Experiment number K4. Electrolyte with 1.1 M H₂O and 5 M MMA. The current density was 1.19 mA/cm², the optical microscope grade is d.

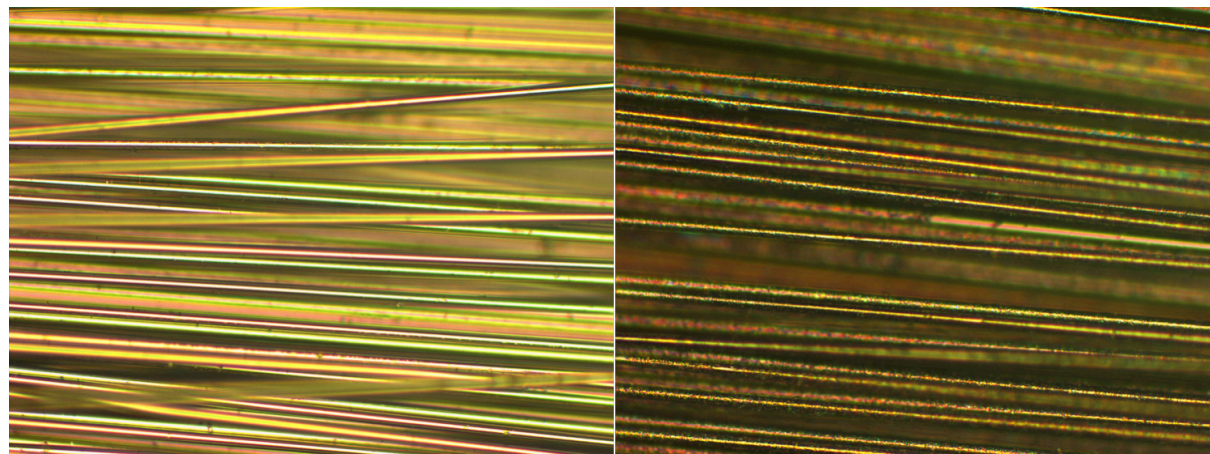


Figure 25 Experiment number K5. Electrolyte with 1.1 M H₂O and 5 M MMA. The current density was 1.58 mA/cm², the optical microscope grade is b - d. A variation of coating quality over the fibre tow length is observed from almost no coating at all (left) to fully covered fibre surface (right)

Room temperature

All experiments performed at a constant current at room temperature led to even and fully coated fibres, both at lower and higher current densities (Figure 26, Figure 27).

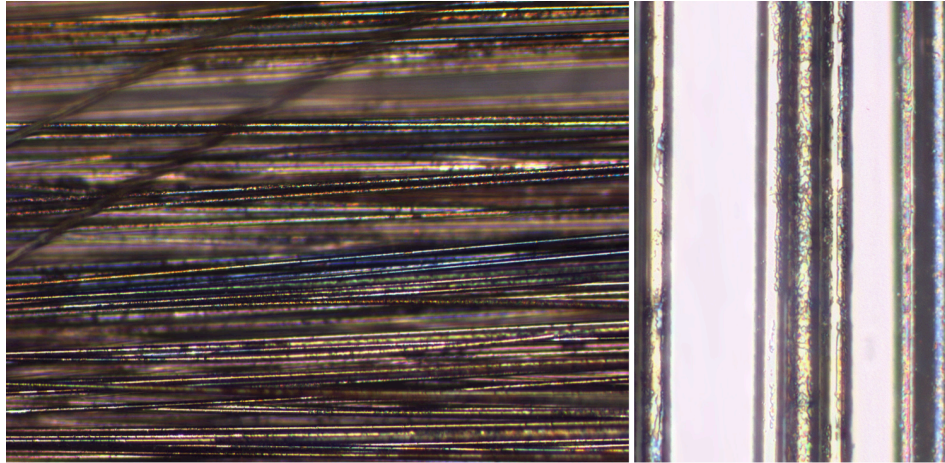


Figure 26 Experiment number J6. The experiment is conducted at room temperature and the electrolyte contains 5 M MMA. The current density was 1.19 mA/cm^2 , the optical microscope grade is d.

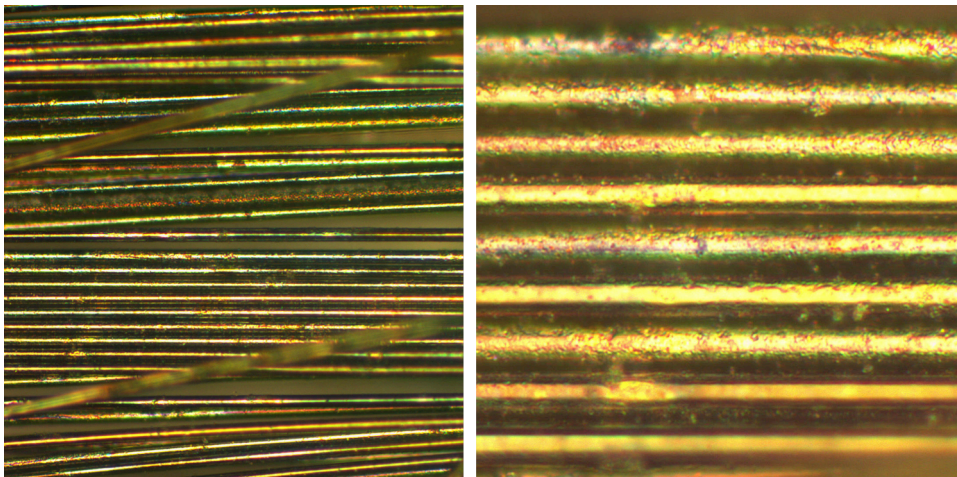


Figure 27 Experiment number J7. The experiment is conducted at room temperature and the electrolyte contains 5 M MMA. The current density was 1.58 mA/cm^2 , the optical microscope grade is d.

Ultrasonication and bending

After ultrasonication a continuous coating of the fibres was still observable. Only some areas appeared blanker than before (Figure 28). In contrast to this, if the fibres were manually bent in the dry state the quality of the fibre coating decreased (Figure 29). The fibres appeared less coated and only particles instead of a continuous coating were attached to the fibre surface (Figure 30).

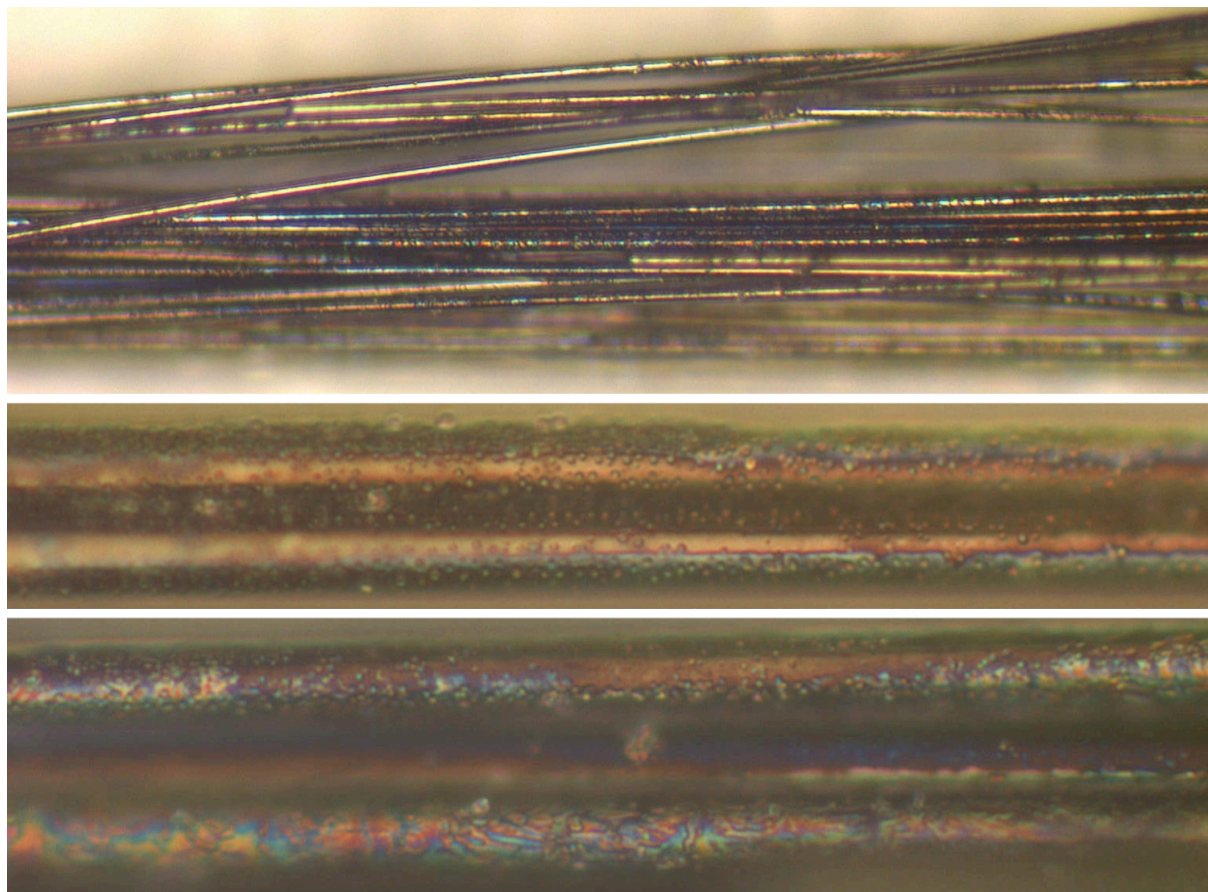


Figure 28 Appearance of fibre coating after ultrasonication. Continuous coating is observed.

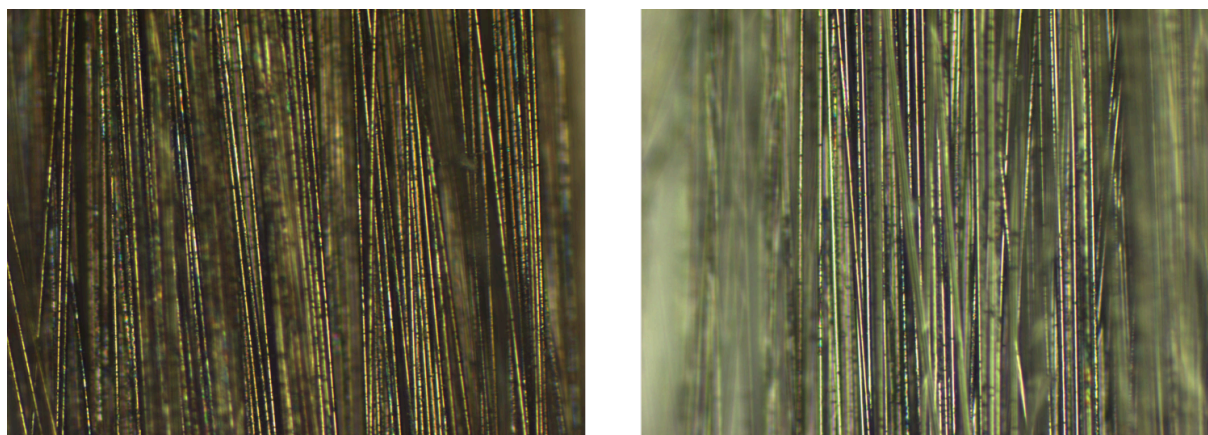


Figure 29 Experiment number S7 under continuous coating. The electrolyte contains 7 M MMA. The current density was 0.79 mA/cm^2 , the optical microscope grade is c (left). On the right side, the same sample is shown but the fibres had been bend and vigorously moved against each other.

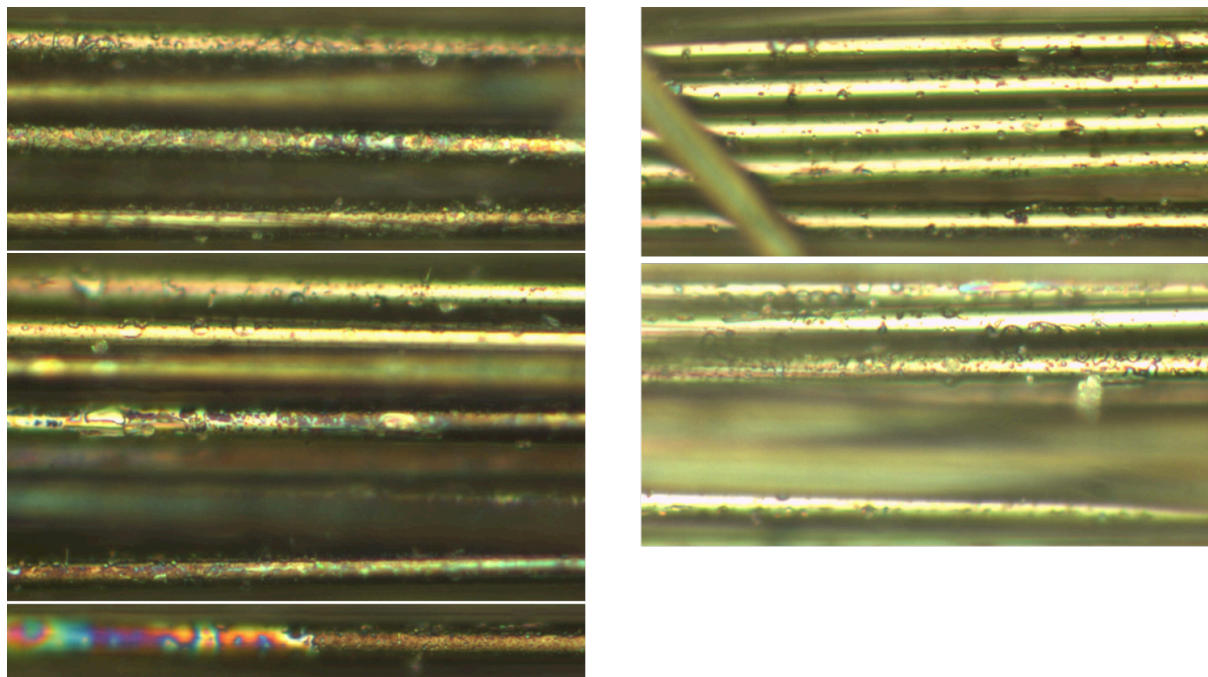


Figure 30 Closer view of the fibre surface. Experiment number S7 under continuous coating. The electrolyte contains 7 M MMA. The current density was 0.79 mA/cm^2 . The optical microscope grade is c (left). On the right side, the same sample is shown but the fibres had been bend and vigorously moved against each other.

4.2.2 TGA and weight measurement

Variation

By analysing several sections of a fibre tow using TGA it was observed that the measured weight loss for the coating and therefore the coating thickness varied extensively as can be seen from the values and standard deviations in Table 8. In the case of S5 for example, the calculated coating thickness within three tested samples was in the range of 16 to 220 nm.

Comparing TGA values to the coating thickness determined by weight measurement, large differences were seen. The results from weight measurement were in general lower for chronoamperometry experiments (min. 3 – max. 112 nm) and higher for chronopotentiometry (min. 18 – max. 287 nm). For the experiments at constant potential, TGA and weight measurement results are similar except for sample K5, where a huge variation of coating quality over the length of the fibre tow was observed. For the experiments at constant current, the coating thickness from weight measurement was always higher than the coating thickness calculated from TGA.

Current vs. Potential

In accordance to the observations in the optical microscope the TGA of the fibres produced at constant potential gave poor results. It can be seen from Figure 31 that only with constant current thick coatings could be achieved as all samples achieved at constant potentials lie in the lower part of the diagram.

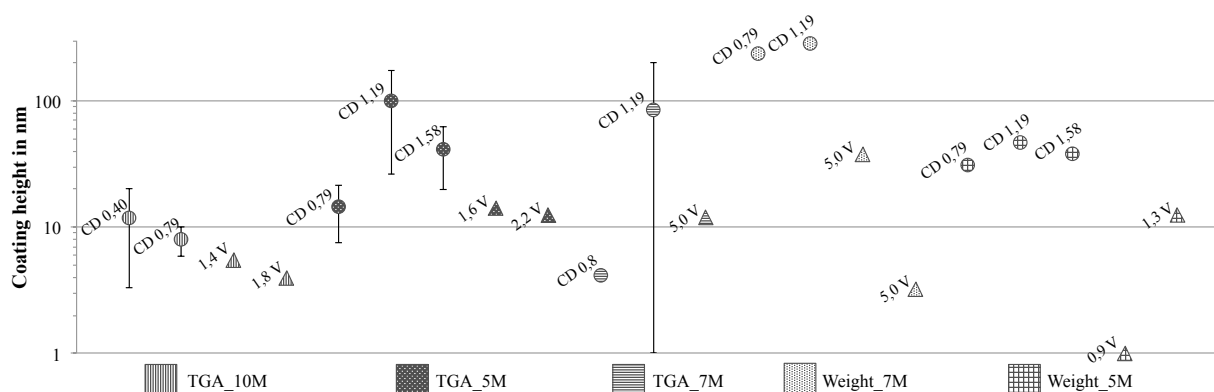


Figure 31 Comparison of coating thickness measured with TGA and through weight for different experimental series emphasizing the difference of coating at constant potential (triangles) and constant current (circles; CD = current density).

Influence of molar concentration

For a current density of 0.79 mA/cm^2 the coating thickness for different molar concentration of MMA was compared (Figure 32). At 5 M the coating thickness was 15 nm with a standard deviation of 7 nm, half of the measured value. The coating thickness increased for 7 M to 27 nm, but a very high standard deviation of 38 nm was calculated. For 10 M the coating thickness decreased again to $8 \pm 2 \text{ nm}$, which represented the lowest value.

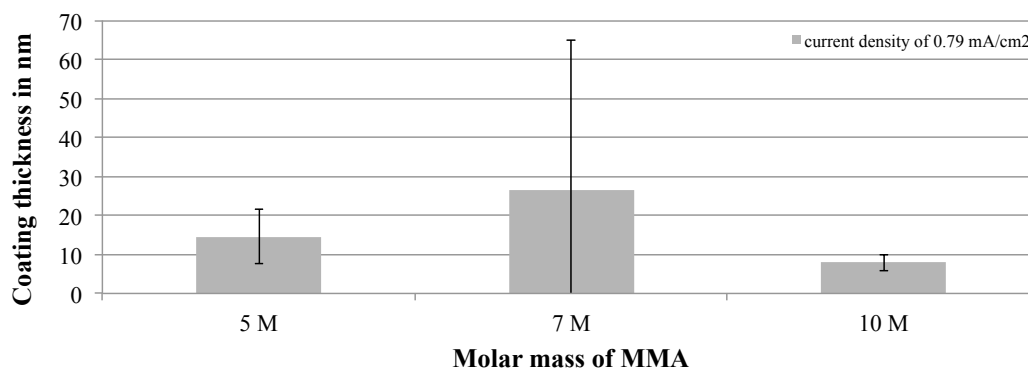


Figure 32 Comparison of coating thickness for the same current density at different molar concentrations of MMA.

Influence of current density

As the applicable potential became restricted at higher molar concentration due to a higher electrical resistance of the electrolyte and due to the limited potential output of the potentiostat used, the number of current densities investigated was limited. For experiments at 10 M the current densities applied were 0.4 and 0.79 mA/cm^2 . For both densities the coating thickness achieved was similar with $12 \pm 8 \text{ nm}$ and $8 \pm 2 \text{ nm}$, respectively. The results from the 7 M experiments showed a high standard deviation for both experiments with $27 \pm 38 \text{ nm}$ and $93 \pm 96 \text{ nm}$. However, the coating thickness increased with increasing current density. The same applied for the 5 M experiments from 0.79 to 1.19 mA/cm^2 , where the maximum coating thickness of $79 \pm 74 \text{ nm}$ was reached. The thickness decreased again if the current density was increased further to a maximum of 1.58 mA/cm^2 . Again the standard deviation was high especially for the coating at 1.19 mA/cm^2 .

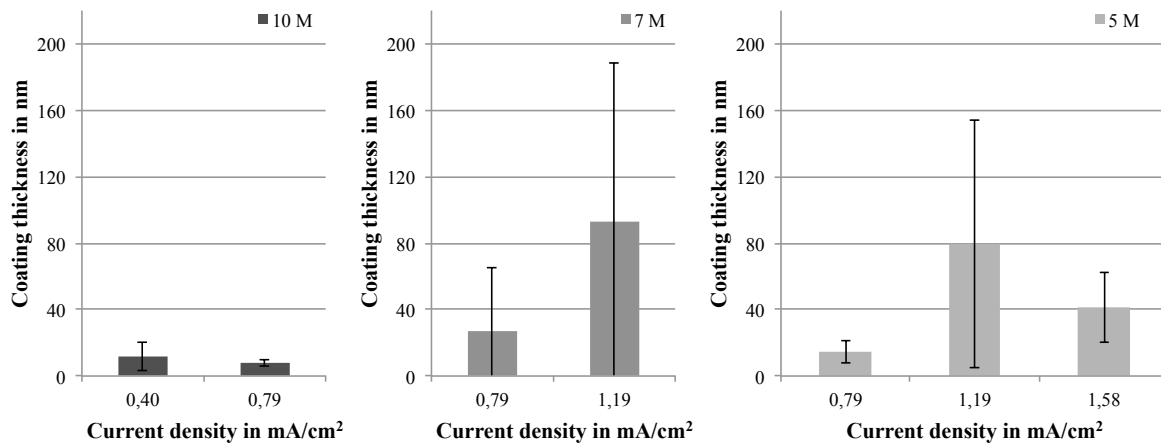


Figure 33 Coating thickness in dependence of the current density at different molar concentrations of MMA.

4.2.1 SEM

The SEM images provided a very detailed insight into the structure of the coatings from different experiments. For the high resolution SEM at KTH it was possible to determine the fibre diameter and thus the coating thickness (see Table 8: V4, V6, T4 – T8) and for some coatings the height of observed particles was measured (Figure 34; Table 8: V4, T4).

Depending on the SEM used, different details of the coating were observed. For the experiment at 10 M and at a current density of 0.40 mA/cm² (V4, Figure 34) the surface is evenly covered with small particles. Some of these particles seem to have grown together so that broader particles were formed. On areas, where fewer particles had formed, the striations of the original carbon fibre surface are visible. Experiment U6 – 5 M, 1.19 mA/cm² – was observed with the SEM from Chalmers. A coating with a cauliflower-like appearance is visible. It is not clear, if some of the structure could be related to striations from the original carbon fibre (Figure 35, upper left). For the continuous coating experiment U8 a continuous coating was achieved and several layers of coating are visible. Larger particles loosely attached to the fibre could be identified, which might be attributed to residues from the non-deposited polymer. (Figure 36) Under inert conditions the experiment at 5 M and 1.58 mA/cm² led to a very homogenous, thick coating that seems to exhibit several layer (Figure 37, upper left). The surface structure appears fine and evenly rough (Figure 37, upper right). For some of the experiments it also occurred that the fibres seem to be glued together by the polymer coating (Figure 38). A more uneven coating was observed for the experiment at 1.19 mA/cm² and 7 M (S5). Here, the dust-like particles are attached to the fibre surface and parts of the area are covered by a cauliflower-like coating (Figure 39).

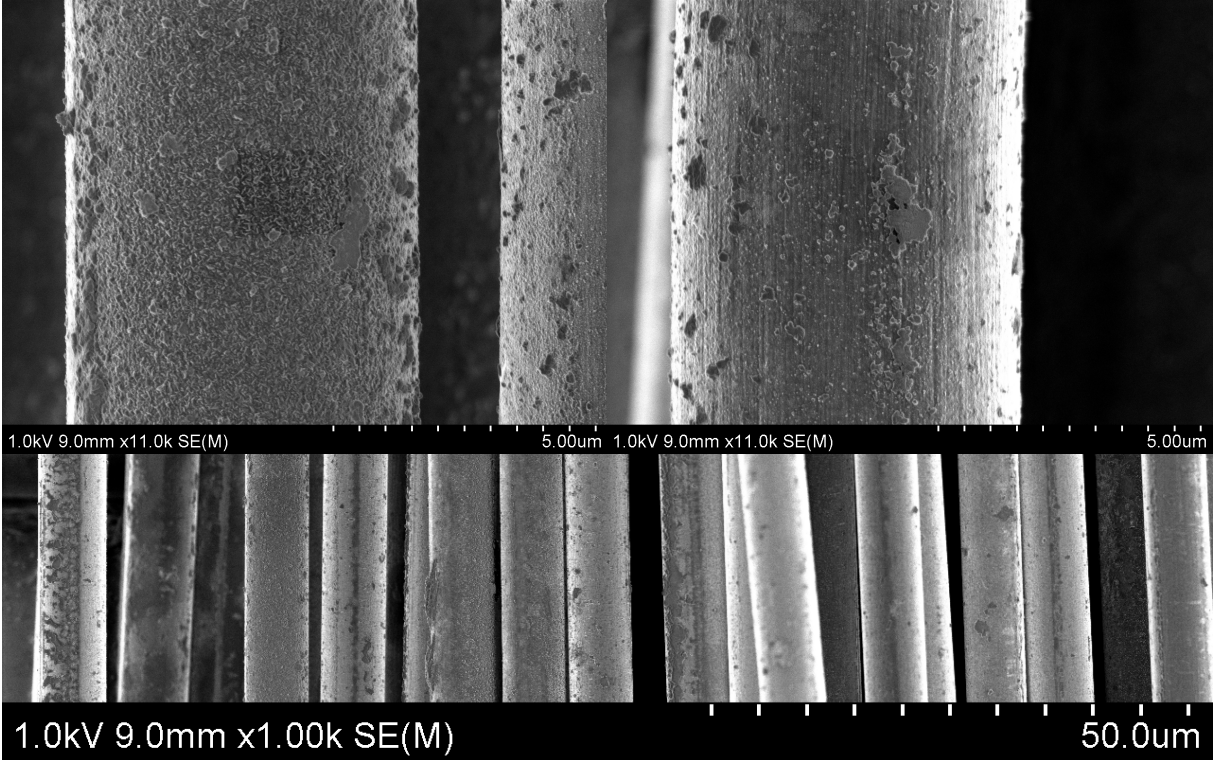


Figure 34 Experiment number V4. The electrolyte contained 10 M MMA. The current density was 0.40 mA/cm². Powder-like particles are visible on the fibre surface. Striations from the original fibre shine through.

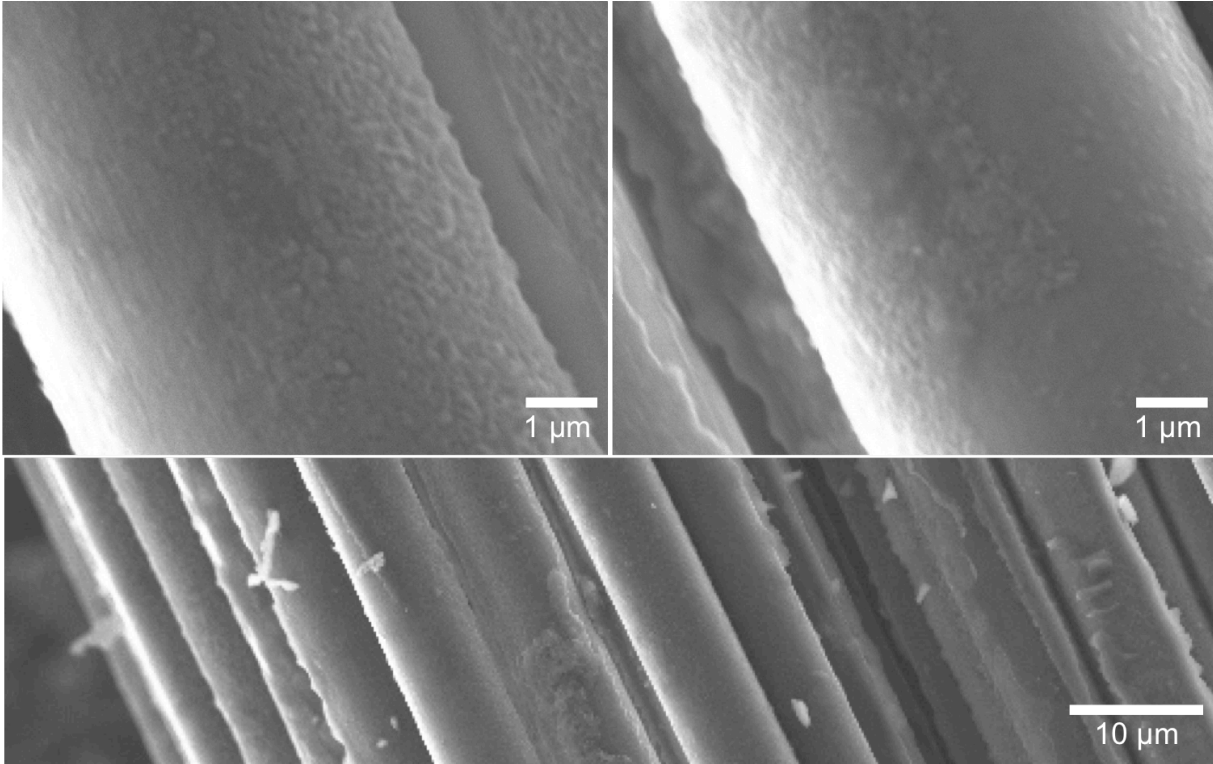


Figure 35 Experiment number U6. The electrolyte contained 5 M MMA. The current density was 1.19 mA/cm². A continuous coating is visible.

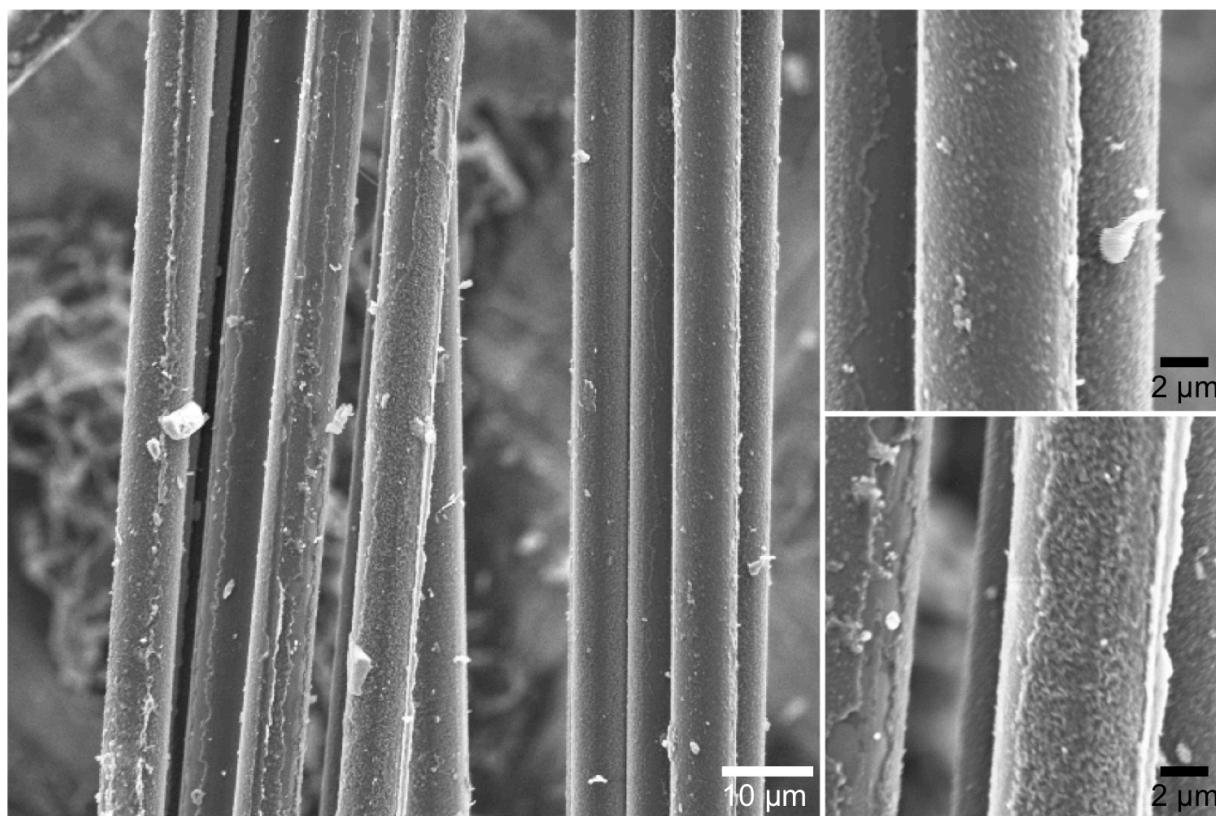


Figure 36 Experiment number U8 for continuous coating. The electrolyte contained 5 M MMA. The current density was 1.19 mA/cm^2 . A continuous coating with a cauliflower-like structure is visible. Some bigger particles or residues seem loosely attached to the fibres.

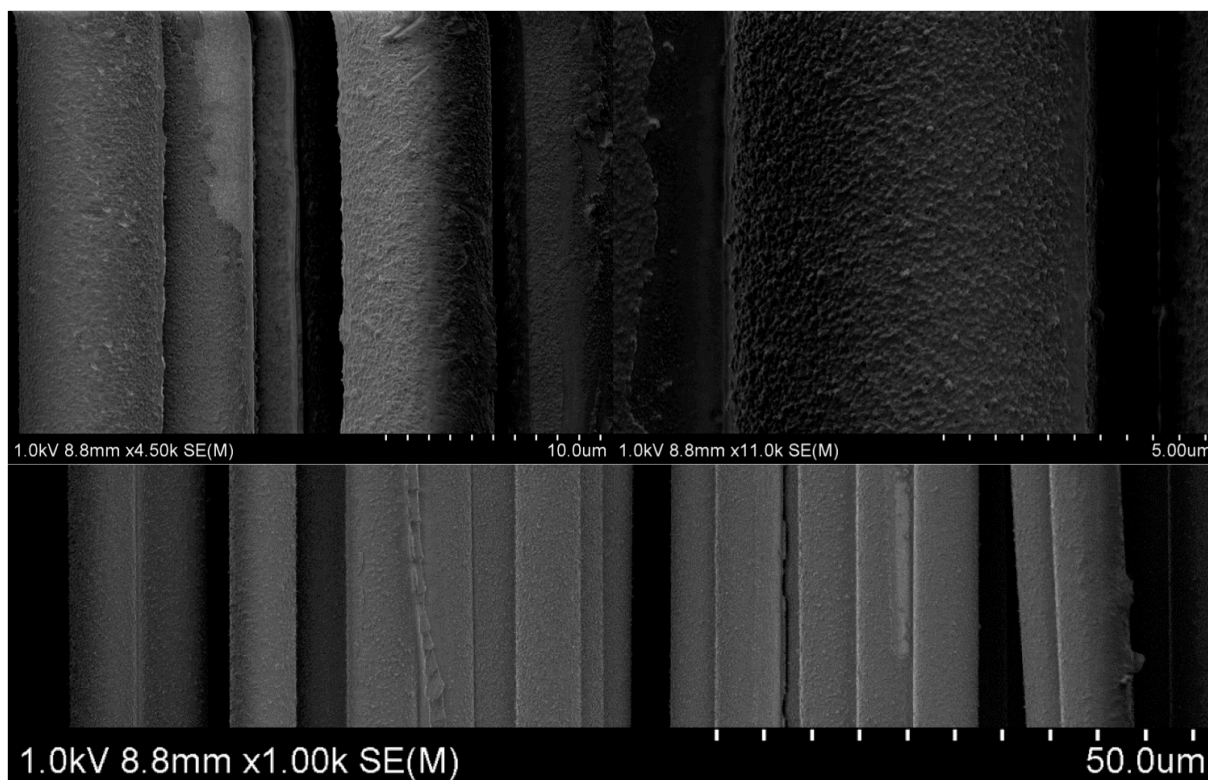


Figure 37 Experiment number T8 performed under inert conditions. The electrolyte contained 5 M MMA. The current density was 1.58 mA/cm^2 . A very homogenous continuous coating is visible. Several layers of coating are possible (upper left).

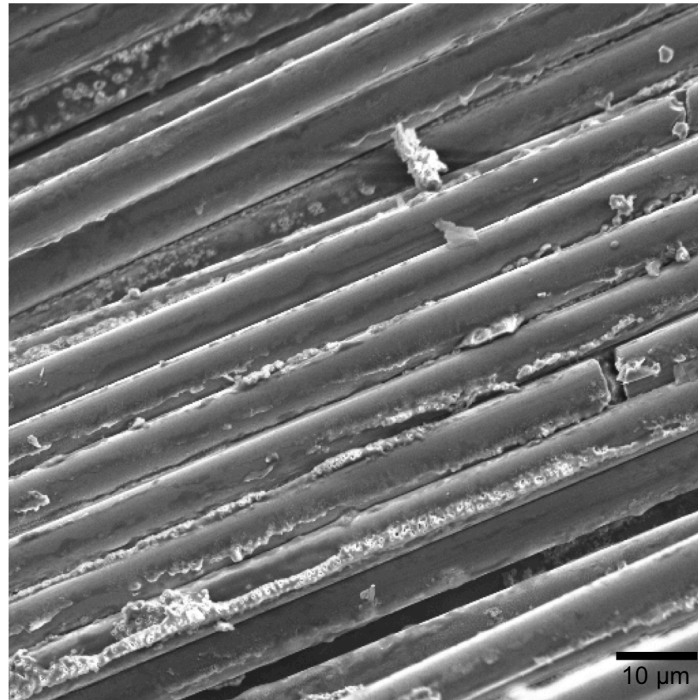


Figure 38 Experiment number S4. The electrolyte contained 7 M MMA. The current density was 0.79 mA/cm². The fibres appear glued together through the polymer coating.

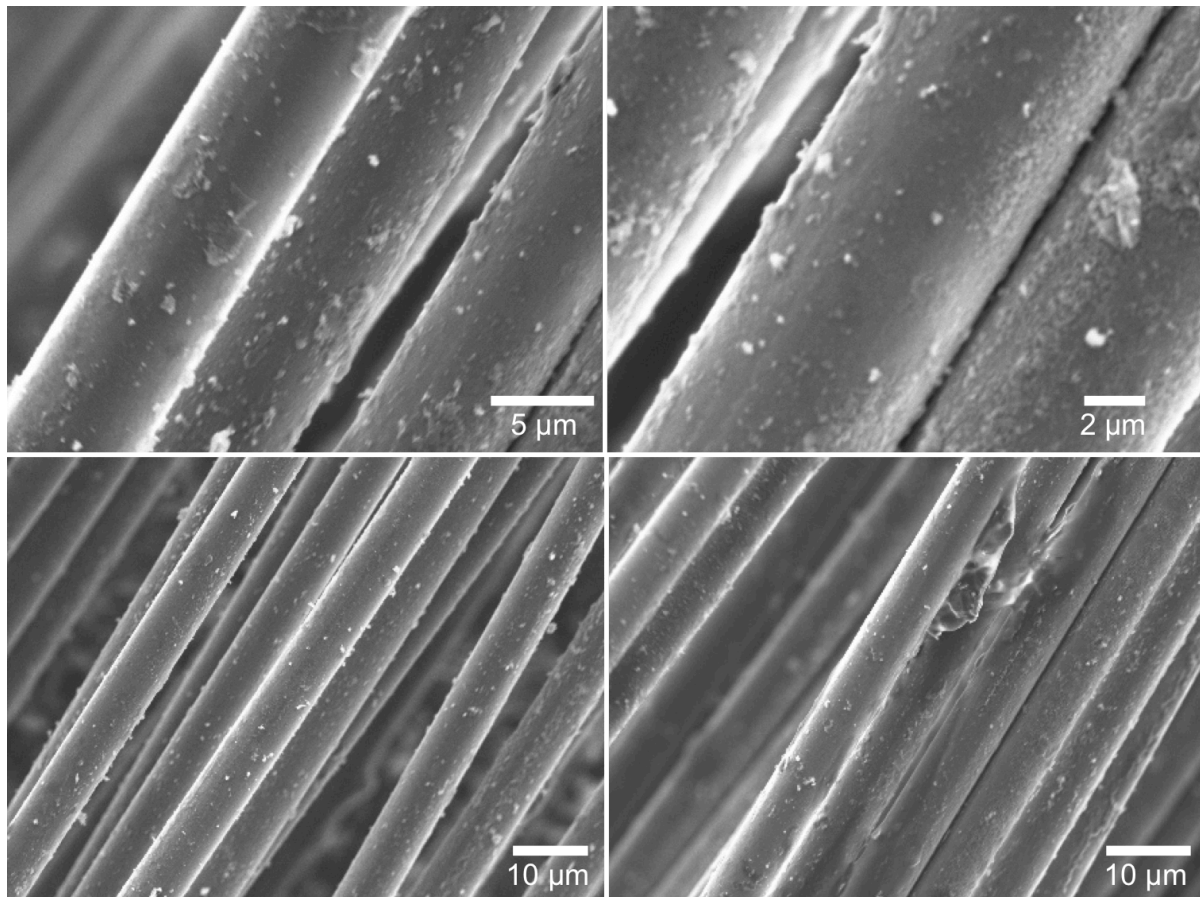


Figure 39 Experiment number S5. The electrolyte contained 7 M MMA. The current density was 1.19 mA/cm². The coating seems patchy and dust-like particles are attached to the surface.

4.2.2 Tensile testing

The tensile testing revealed a change in properties for the fibres that had been continuously coated at a current density of 1.19 mA/cm² and with a speed of 3.4 mm/s in comparison to sized, non-coated fibres (Table 9). With the tensile testing machine it was possible to determine the titer of every fibre and from this the diameter was calculated. According to this measurement the coated fibres exhibited a 0.5 µm larger diameter in average, which would in turn correlate to a coating thickness of 0.25 µm. The elongation at failure was similar for the reference samples and the coated fibres being around 1.5% and is comparable to the value given in the product sheet of 1.8%. The values for both the tenacity and the Young's modulus showed a strong fluctuation. The reference fibres exhibited an average tenacity of around 2000 MPa while the continuously coated fibres had 1400 MPa. The standard deviation for both fibre categories was slightly above 1000 MPa. Both tenacity values were lower than the 4750 MPa stated in the product sheet with 60% and 70% respectively. The result was similar for the Young's modulus even though the difference between the measured values and the product sheet is smaller with a 30% and 50% lower value for the reference and the coated fibres respectively. By comparing the reference fibres to the coated fibres, the coated fibres showed a decrease of approximately 25% in Young's modulus with 120 GPa in relation to 164 GPa.

Table 9 Results from the tensile test comparing sized, non-coated fibres (reference) and electrocoated fibres (continuous coating). Furthermore, the values from the product sheet of the used fibres are listed (product sheet). For each fibre category 20 fibres had been tested and the standard deviation is given.

	Titer [dtex]	Diameter [µm]	Elongation at failure [%]	Tenacity [MPa]	Young's modulus [GPa]
Reference	0,68 ± 0,05	6,95 ± 1,82	1,59 ± 0,42	1956 ± 1040	164 ± 23
Continuous coating	0,78 ± 0,06	7,46 ± 2,11	1,49 ± 0,17	1401 ± 1080	120 ± 26
Product sheet	0,63	6,69	1,8	4750	245

4.2.3 Resistivity

The non-coated fibre tow had a resistivity of $1.8 \times 10^{-5} \Omega\text{m}$ and the continuously coated fibre tow had a resistivity of $3.0 \times 10^{-5} \Omega\text{m}$.

4.3 Manufacturing of composites

Differences between the manufacturing of composites containing coated fibres and sized fibres were observed. In vacuum-bagging it was possible to wet the fibres of Epoxy1 + CF and Epoxy2 + CF over the whole length of the prepared sample. For Epoxy1 + CF + PMMA the wetting of the fibres proceeded very slowly and it was not possible to complete the wetting over the whole length of the composite with the applied pressure. The process was improved for Epoxy2 + CF + PMMA but the wetting was still partly incomplete. These difficulties during the vacuum-bagging process led to a poor quality of the Epoxy1 + CF + PMMA composites. Grooves are visible on the surface of the composite whereas Epoxy1 + CF has a smooth surface appearance (Figure 41).

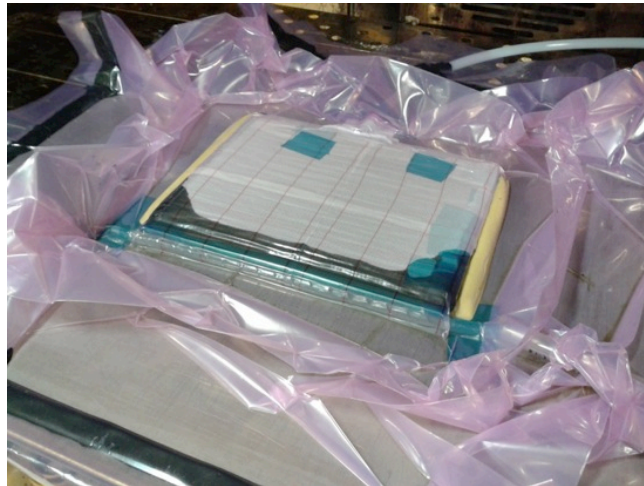


Figure 40 Vacuum-bagging at the beginning of the infusion. The wetted fibres can be seen as the black part. The infusion was very slow and was later not completed on the upper side.

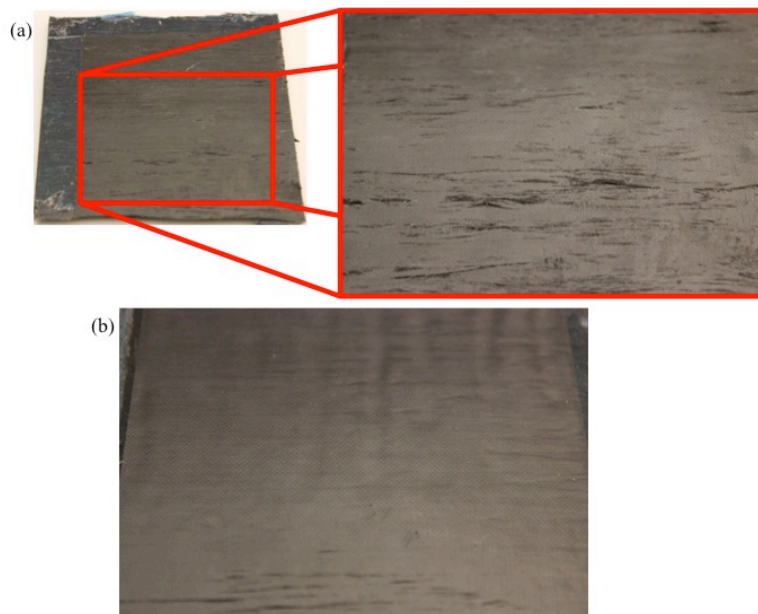


Figure 41 Photographs, that show the appearance of Epoxy1 + CF + PMMA (a) and Epoxy1 + CF (b).

Cross-sectional optical microscope images of Epoxy1 + CF + PMMA showed large amounts of voids of different sizes (Figure 42). From this the void volume fraction was calculated to be 20%. Additionally an uneven distribution of the fibres in the matrix was observed which led to matrix-rich regions within the composite. The overall fibre volume fraction for these composites was 45%. In contrast to this, Epoxy1 + CF showed a very even distribution of the carbon fibres, no pores or voids were visible and the fibre volume fraction was calculated to be 60% (Figure 43). The quality of the composites with coated fibres could be improved with the use of Epoxy2 (Figure 44). Voids were only visible on the edge of the composite (Figure 44, right). The distribution of the fibres within the matrix was more even and the volume fraction was increased (Figure 45 ,left). However, some fibre bundles and matrix-rich regions could still be observed (Figure 45 ,right). Epoxy2 + CF had the same appearance as Epoxy1 + CF.

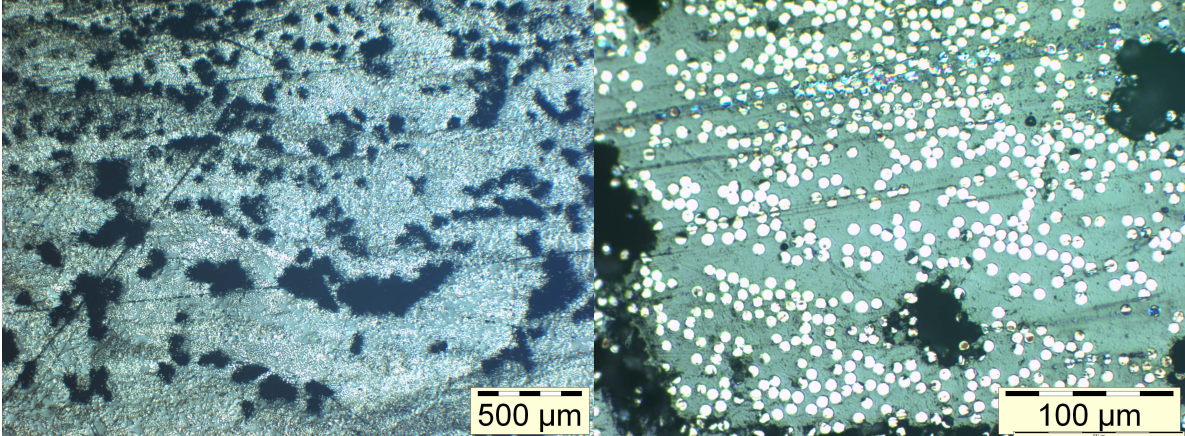


Figure 42 Optical microscopy images of the cross-section of Epoxy1 + CF + PMMA composites. The dark areas represent voids or pores, the white dots represent the carbon fibres and the grey area is the thermoset matrix. The fibres are unevenly distributed and matrix-rich regions are visible ($V_f = 0.45$).

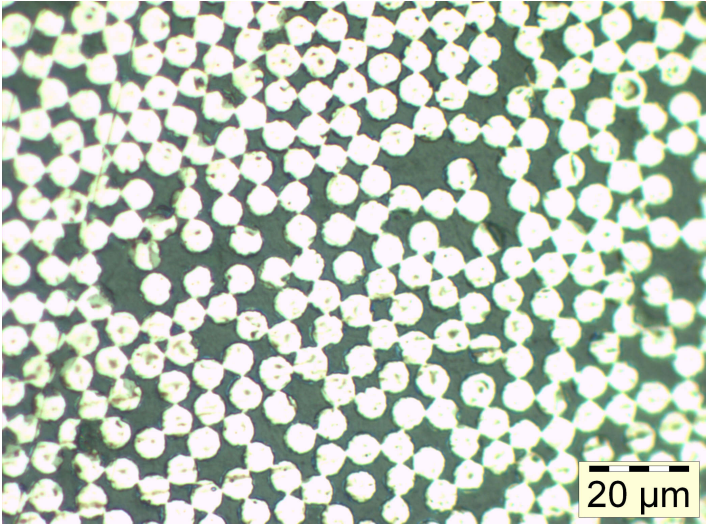


Figure 43 Optical microscopy images of the cross-section of Epoxy1 + CF. The matrix is packed with carbon fibres ($V_f = 0.6$).

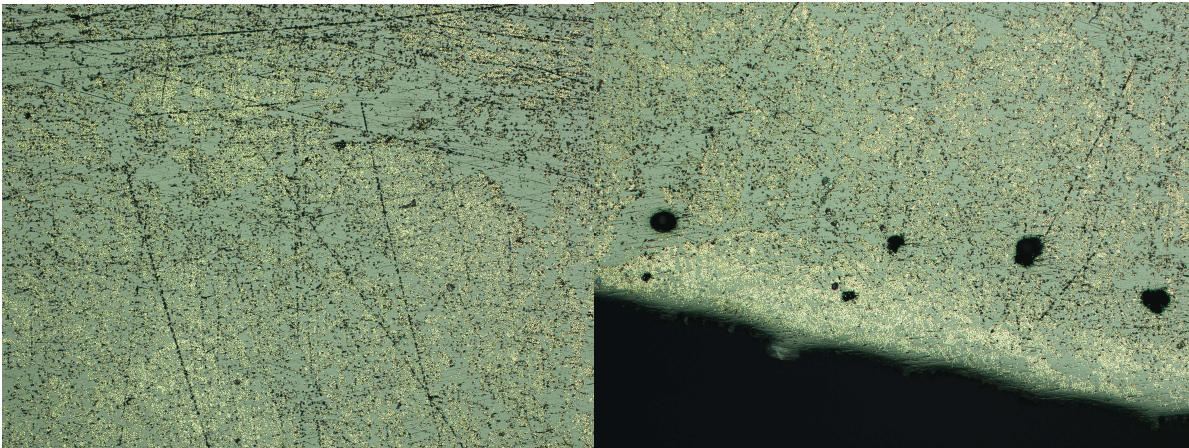


Figure 44 Optical microscopy images of the cross-section of Epoxy2 + CF + PMMA composites. The dark areas represent voids or pores at the edge of the composite, the white dots represent carbon fibres and the grey area is the thermoset matrix. Long black lines come from the polishing process.

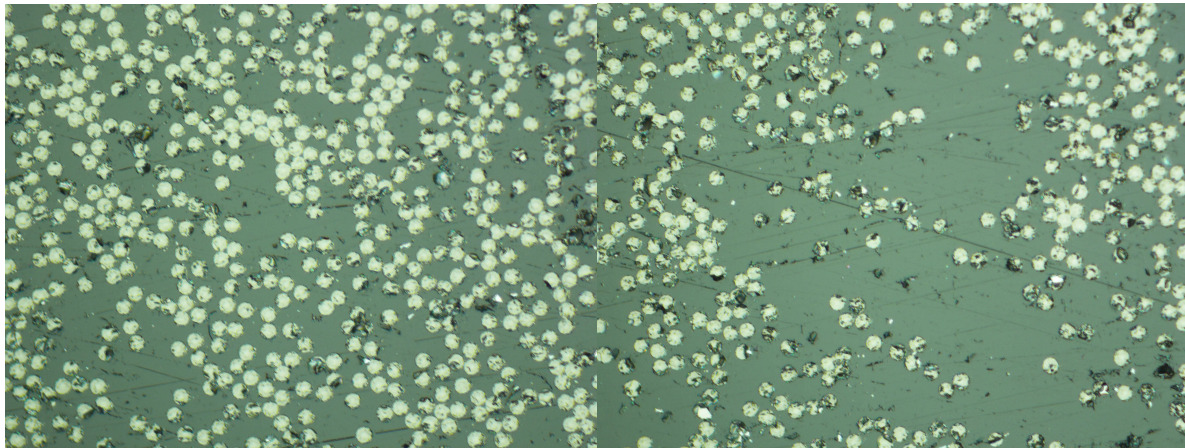


Figure 45 Optical microscopy images of the cross-section of Epoxy2 + CF + PMMA composites. The fibres are partly unevenly distributed and matrix-rich regions are visible (right).

4.4 Electrical properties

The resistance and resistivity was directly calculated from the recordings of the three-point-bending tests. For all temperatures the Epoxy + CF systems showed considerable lower values of resistance and resistivity (Figure 46, Figure 47). At 50°C the Epoxy2 + CF systems had the lowest resistivities with values between 6.9 and 8.1 x 10⁻⁵ Ωm. Epoxy1 + CF had slightly higher values of 8.2 to 9.9 x 10⁻⁵ Ωm. The resistivity increased for Epoxy + CF + PMMA and two outliers were observed for these systems. While for Epoxy1 + CF + PMMA the resistivity was 2.9 x 10⁻⁴ Ωm, one specimen had 5.9 x 10⁻⁴ Ωm. Epoxy2 + CF + PMMA showed a wider variation with resistivities ranging from 1.9 to 2.9 x 10⁻⁴ Ωm and an outlier at 5.6 x 10⁻⁴ Ωm. These outliers could be associated with a bad connection between the clamps and the specimen.

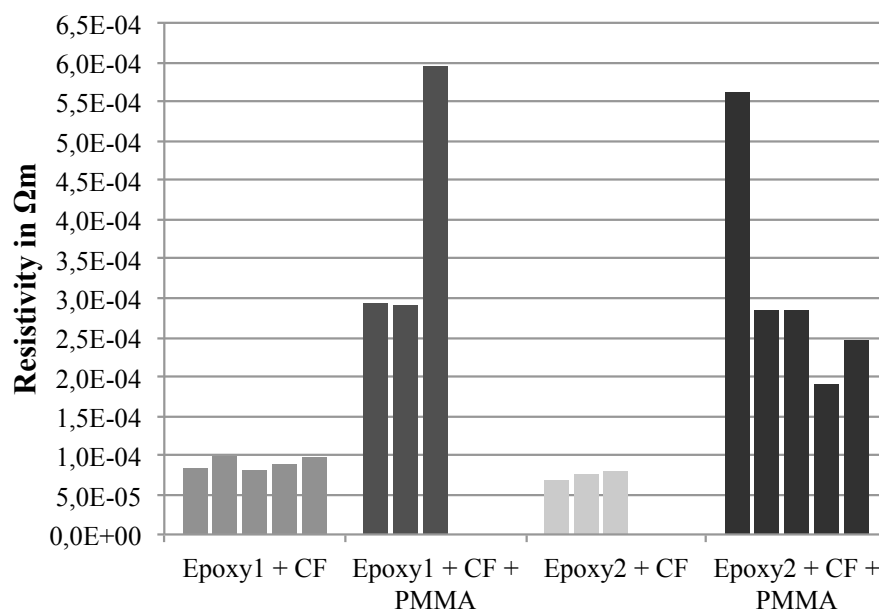


Figure 46 Resistivity values for all epoxy systems at 50°C. Values of each specimen tested are shown.

With increasing temperature no significant change was visible for the Epoxy1 + CF system, whereas a decrease in resistivity was observed for the Epoxy1 + CF + PMMA system (Figure 47).

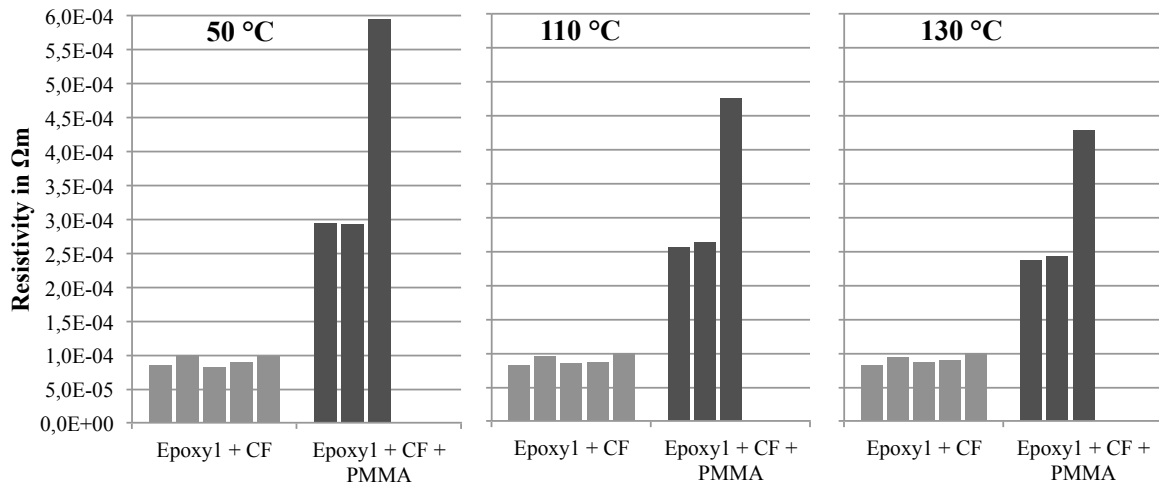


Figure 47 Development of the resistivity with increasing temperature for the Epoxy1 systems. Values of each specimen tested are shown.

Figure 48 depicts representative curves for the development of the resistance in relation to the potential and the temperature. The resistance of the Epoxy2 + CF specimens decreased at the beginning and then stayed relatively constant even if the temperature increased further. In contrast to this all Epoxy2 + CF + PMMA systems decreased in resistance as the temperature increased. One exception for this was the last specimen tested, where the resistance increased constantly with increasing temperature.

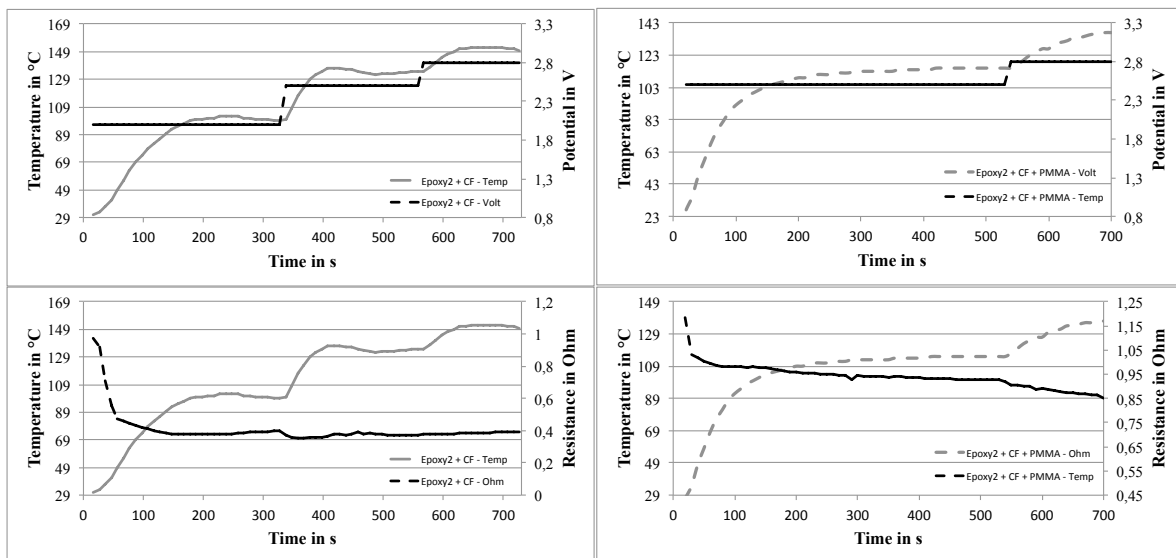


Figure 48 Curves showing the temperature in relation to the potential (upper diagrams) and to the resistance over the course of a three-point bending experiment for Epoxy2 + CF (left) and Epoxy2 + CF + PMMA (right).

4.5 Mechanical characterisation of composites

4.5.1 Three-point bending

An overview of the flexural moduli at different temperatures and the relative change in stiffness for heated composites in comparison to the initial value is given in Table 10. For both epoxy systems the initial flexural modulus was lower for the composites with coated fibres in comparison to the composites containing sized fibres with 46 ± 13 GPa to 91 ± 5 GPa for Epoxy1 + CF + PMMA to Epoxy1 + CF and 59 ± 8 GPa to 124 ± 7 GPa for Epoxy2 + CF + PMMA to Epoxy2 + CF, respectively. The Epoxy2 system showed higher values in comparison to the Epoxy1 system. The stiffness was reduced as the composites were heated through applying a current. At the maximum temperature Epoxy1 + CF showed the lowest stiffness reduction of 31 % of all epoxy systems. Epoxy1 + CF + PMMA and Epoxy2 + CF + PMMA had similar values for the maximum relative change of approximately 70 %. Epoxy1 + CF showed a maximum reduction in stiffness of 50 %.

Table 10 Initial flexural modulus, flexural moduli at different elevated temperatures and the relative change of stiffness in comparison to the initial value are shown for all epoxy systems.

	Flexural modulus [GPa]	Flexural modulus [GPa]	Relative change	Flexural modulus [GPa]	Relative change	Flexural modulus [GPa]	Relative change
	at RT	at 125°C		at 138°C		at max temp*	
Epoxy1 + CF	91 ± 5	82 ± 7	10 %	74 ± 4	18 %	66 ± 5	31 %
Epoxy1 + CF + PMMA	46 ± 13	25 ± 8	46 %	18 ± 2	60 %	13 ± 2	70 %
	at RT	at 80°C		at 100°C		at max temp**	
Epoxy2 + CF	124 ± 7	93 ± 16	25 %	74 ± 3	41 %	62 ± 3	50 %
Epoxy2 + CF + PMMA	59 ± 8	37 ± 7	37 %	20 ± 7	66 %	16 ± 7	72 %

* maximal measured temperature for Epoxy1 + CF samples: 181, 175, 180, 124°C; for Epoxy1 + CF + PMMA samples: 165, 141, 161°C

** maximal measured temperature for Epoxy2 + CF samples: 114, 123, 152°C; for Epoxy2 + CF + PMMA samples: 103, 118, 137, 147, 124°C

Considering the relative bending over the temperature increase of a three-point bending test, characteristics of the curve progression for each system were identified (Figure 49). The curves of the Epoxy1 systems show a separate increase of bending, where Epoxy1 + CF started to increase slightly from 110°C whereas Epoxy1 + CF + PMMA already increased at 90°C. This increase was shallow until approximately 110°C and increased sharply after that. In contrast to this, the Epoxy2 systems started to bend slightly above 60°C and showed the same bending behaviour up until 80°C. After that, Epoxy2 + CF + PMMA increased more linearly while Epoxy2 + CF increased at a lower rate and flattened around 100°C. If the

temperature for Epoxy2 + CF + PMMA was further increased other specimens showed a further linear increase in bending.

The bending of the specimen depended on the increase in temperature and this in turn was related to the applied potential. It can be seen from Figure 50 that the adjustment of the potential allowed for a gradual control of the temperature especially for the Epoxy + CF systems. The Epoxy + CF + PMMA systems were less prone to control as the potentials needed to achieve a certain temperature varied extensively among the specimens.

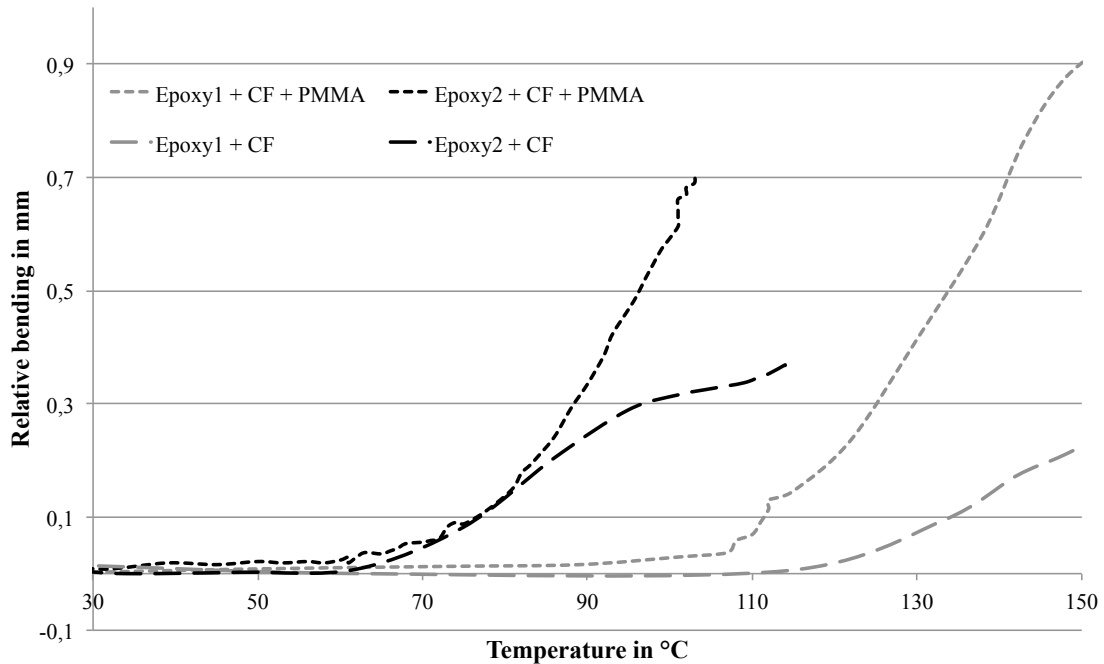


Figure 49 Representative curves that show the relative bending of the composites in relation to temperature change. The base line presents the position after the weight was added and before voltage was applied. The temperature increased as a constant voltage was applied.

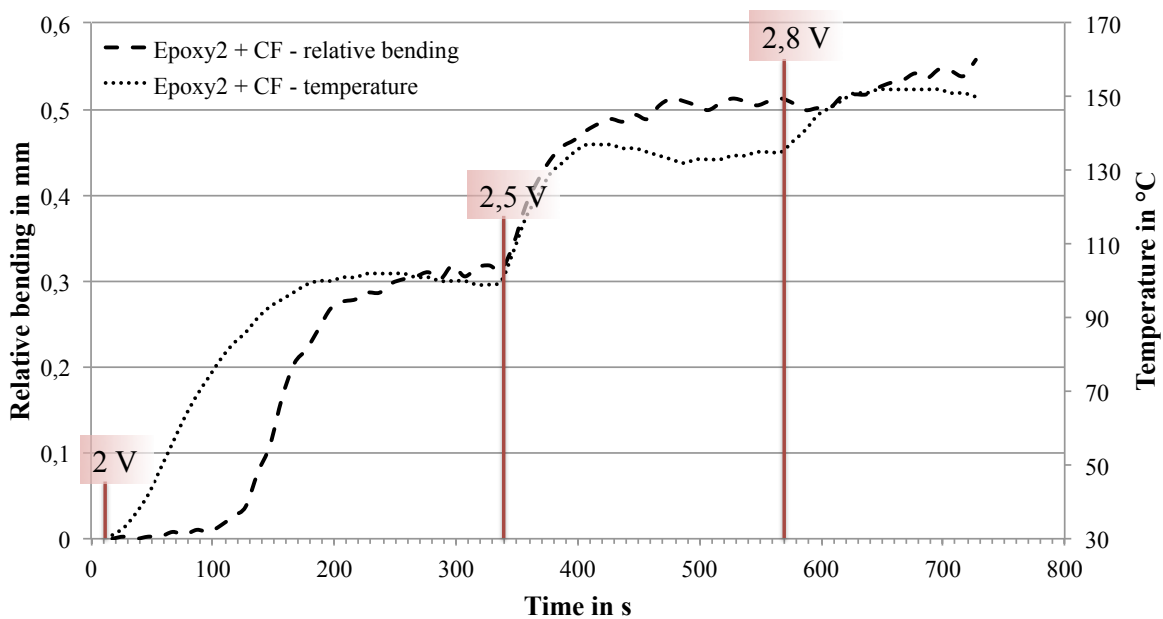


Figure 50 Relative bending of an Epoxy2 + CF specimen and temperature over the course of the three-point bending experiment. The initial applied voltage and increases in voltage are plotted.

4.5.2 DMTA

The DMTA results showed differences in the glass transition temperature between composites that contained sized carbon fibres and those that contained PMMA-coated carbon fibres. Furthermore, Epoxy1 had a higher T_g than Epoxy2 (Table 11). In case of Epoxy1 + CF the glass transition temperature determined by the onset of the storage modulus curve (T_g onset) was 133°C and the T_g determined by the tan delta curve peak (T_g peak) was 150°C. The T_g was decreased if PMMA-coated fibres were used to 118°C and 135°C, respectively. Epoxy2 + CF had a T_g onset of 90°C which was increased for Epoxy2 + CF + PMMA to 101°C. The same trend applied for T_g peak with 111°C and 123°C, respectively. It can be seen from the progression of the normalised modulus (Figure 51) that the main drop in the storage modulus for all composite systems took place in a temperature range of about 20°C. The composites reinforced with PMMA-coated fibres showed a more immediate decrease in modulus than the corresponding composites with sized CF. The main drop in modulus was shifted to a lower temperature with 16°C for Epoxy1 + CF + PMMA in comparison to Epoxy1 + CF and the curves were clearly separated, whereas Epoxy2 + CF and Epoxy2 + CF + PMMA overlapped. The main drop of Epoxy2 + CF + PMMA showed a slight shift of about five degrees to higher temperatures. The total decrease in modulus was higher for the composites reinforced with PMMA-coated fibres than for the composites with sized CF.

Table 11 Glass transition temperatures obtained from DMTA for both epoxy composites.

	Epoxy1 + CF	Epoxy1 + CF + PMMA	Epoxy2 + CF	Epoxy2 + CF + PMMA
T_g onset [°C]	133	118	90	101
T_g peak [°C]	150	135	111	123

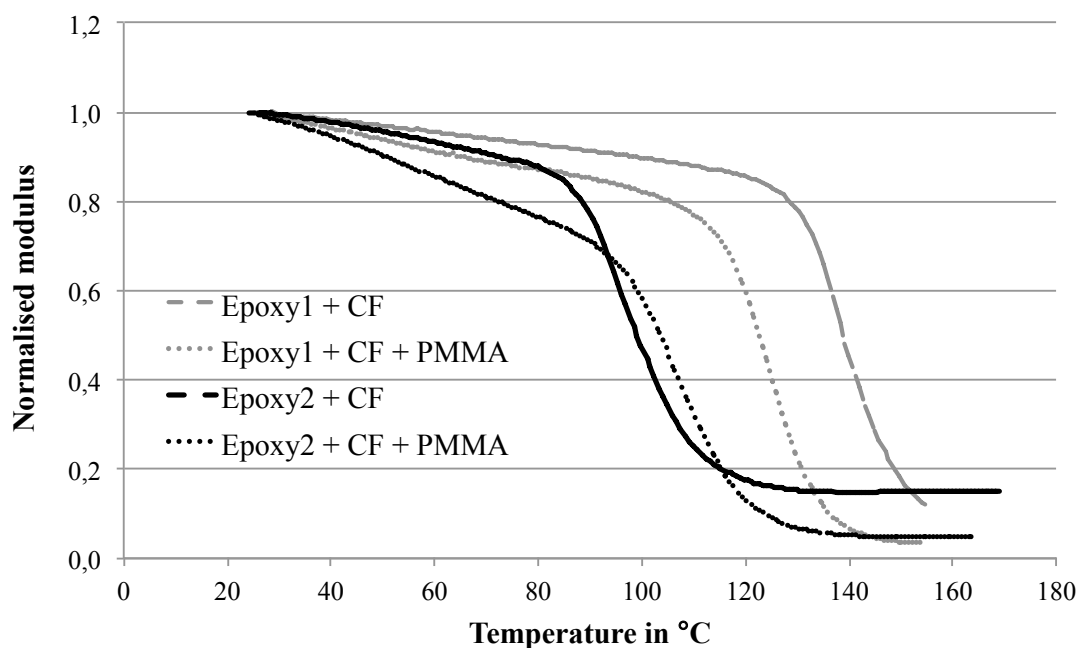


Figure 51 Progression of the normalised modulus over the temperature for all composite systems.

5 Discussion

5.1 Characterisation of coating quality

5.1.1 Cyclic voltammetry

For all experiments except for the series performed without the inhibitor, no significant peaks or signals could be observed. As stated by Bureau (1999) and Bureau et al. (1997) this does not necessarily need to be the case to prove that an electropolymerization at the surface took place. In fact, a signal would only be detected if the charge transfer from the electrode to the monomer depicts the slowest step involved in all reactions that take place in the solution. By the coating of the electrode surface, the charge transfer is slowed down and therefore a peak is often observed for the electropolymerization processes. In the presented experiments it is possible that other steps are rate-limiting for the reaction and no signal is detected. In the present case a possible explanation is that due to high temperatures in the solution and around the carbon fibres the main reaction is radical polymerization. This uncoordinated reaction would create a noise that influences the curve progression and overlaps all possible signals from any anionic polymerization reaction.

However, if two consecutive cycles were performed the slope of the curve decreases after the first cycle and a lower current is achieved. This indicates that a coating reaction took place leading to a passivation of the carbon fibre surface, which increased the resistance. The decrease in current was previously also connected to a reduced availability of the monomer near the electrode surface (Bachinger 2014), but this possibility can be excluded in this case as the solvent only contained MMA.

With increasing molar concentration of MMA the currents that are achieved become lower and it can be assumed that the monomer exhibits a higher resistance than DMF. For the experiments where the inhibitor was removed signals were observed and with increasing experimental time these signals moved to lower potentials. A possible reason for the observation of signals is the following: The radical polymerization exhibits less side reactions (termination, chain transfer) as it is not hindered by the contained inhibitor and exhibits thus a more constant progression. This polymerization influenced the voltamogram more evenly over the range of potentials and underlying reactions became visible. The shift to lower potentials presumes that lower energy was needed to perform the reaction. This might be caused through an increase in temperature around the fibres or in solution. Indeed the recorded temperature for these experiments was slightly increased from 59°C to 63°C.

5.1.2 Batch electrocoating

Variation and quality measures

Using quantitative experiments to determine the coating thickness, large variations in the coating thickness were detected by both, TGA and weighing of fibres. Possible explanations are:

- (1) The grafting thickness varies over the length and thickness of the fibre tow.

- (2) The washing process is not sufficient and polymers formed in solution stay deposited on parts of the fibre surface.
- (3) The coated polymer is very brittle and due to the handling of the fibres parts of the polymer can break off.
- (4) The methods used to determine the coating thickness are less reliable.

As can be seen from the qualitative analysis of the coating by microscopy and the SEM a completely covering layer could be achieved (see 4.2.1). However, this layer seems to vary slightly in its thickness as it exhibits a rough, cauliflower-like appearance. Additionally, in some cases the coating is not covering the whole surface but is instead spread out over the surface in the form of splashes or dots (see 4.2.1). Most of these observable variations appeared in a consistent structure over the length of the fibres but the coating between single fibres could vary extensively. Furthermore, for experiment K5 (1.58 mA/cm², 5 M MMA, 1.1 M H₂O) a strong variation in coating quality was observed over the length of a fibre tow (Figure 25). In batch electrocoating the parameters applied are kept constant. However, as the current tends to take the pathway of the lowest resistance it is not certain that the current passes through the whole length of the fibre tow before it goes through the electrolyte to the steel tube. The possibility needs to be taken into account that the current directly passes through the electrolyte at the beginning where the fibres are led into the steel tube. For batch electrocoating this would support explanation (1). If the continuous coating is taken into account this explanation is no longer valid, as every part of the fibre tow passes the beginning of the steel tube and conditions stay the same over the fibre tow length. Thus, varying coating conditions can only partly cause the registered variation in coating thickness. Another possibility represents the poor spreading of the fibres during the electrocoating experiment. Here, the current might not go through all fibres but instead pass across the fibres which creates an inconsistent coating of fibres next to each other.

During handling of the fibres it appears that a white powder can fall off if the fibres are bent. The powder was also observed in the form of residues in storage bags (Figure 20) or as dust scattering from the fibres. This would support explanation (3) as it implies brittle behaviour of the polymer. However, it remains unclear whether the observed powder is bound coating breaking off the fibres, or rather deposited polymer as described in explanation (2).

Bismarck et al. (2005) observed a similar behaviour evidenced by the fact that they easily could shake off a polymer powder from the coated fibres. Bismarck and colleagues explain this observation with the discontinuity of the PMMA film. In their experiments SEM images show aggregated, nodular polymer structures that seem not fully attached to the fibre surface. (Bismarck et al. 2005) This observation would in fact mostly agree with explanation (2) as the described powder can be found only loosely connected to the fibres in the SEM. It is possible that the washing process, which in Bismarck's study did not include a good solvent for PMMA, was not sufficient to remove deposited polymer. Palacin et al. (2004) emphasize the importance of washing the electrocoated surface with a good solvent for the polymer to remove deposited polymers. Fibres in this work have been washed with the solvent DMF and

additional ultrasonication experiments show a stable coating even under extensive washing. Thus, explanation (2) is unlikely to cause the high variations.

The last possible explanation concerns the reliability of the methods used. Preparation of the TGA samples required strong bending and compacting of the fibres. As indicated above during this handling coating could break off and a lower weight step would be sensed in the TGA. Furthermore, it is possible that the polymer was not fully decomposed due to a rather fast heating rate. This agrees with the observations that the weight measurements consistently give higher values for the coating thickness. However, also for this method a certain error existed as the weight percentage of the coating in comparison to the total weight of the fibres is very small. The values obtained from the high-resolution SEM pictures might be considered as most accurate because even the height of particles could be considered. However, SEM analysis can only show a small part of the sample. Other methods used in the literature include the modified Wilhelmy technique and laser diffraction (Bismarck et al. 2005; Tridech and Maples 2013; Tridech 2010). These methods were either not applicable or not available for this thesis. In earlier experiments the Wilhelmy method showed a standard deviation of $\pm 0.16 \mu\text{m}$, which lies in the range of the coating thickness. Laser diffraction represents a very fast method, but is considered to be as accurate as SEM measurements (Meretz et al. 1992).

To summarize the aspects on the variation of the coating a combination of both quantitative and qualitative methods is needed to evaluate the coating quality. Microscopy images seem to be suitable to rate the overall coating quality in terms of continuity, whereas SEM images give a more detailed impression of the structure of the coating and coating height. TGA and weight measurements can be used to roughly estimate the coating thickness. From this, it is concluded that the maximum achievable coating thickness in this thesis lies in the range of $0.2 \mu\text{m}$.

Influence of washing process

In earlier studies performed at Swerea SICOMP Bachinger (2014) has shown that the washing process plays an important role for the quality of the coating. It was observed that washing with acetone and water led to the detachment of the coating by breaking and falling off. By experiments and theoretical analysis Jing et al. (2010) arrive at the following explanation for this observation: When a thin film of PMMA comes in contact with water the surface of the polymer absorbs some of the water. This results in a very thin swollen top layer while the water does not affect the interior layer. The swollen top layer expands and causes a misfit strain between the two layers within the PMMA film. As a consequence an equibiaxial compressive stress is induced, which in turn leads to the bending of the whole polymer film. If this induced bending passes the binding strength between the polymer and the substrate, the film will peel away. (Jing et al. 2010) In the case for the electrocoated PMMA films on the carbon fibres this would mean that washing with water is not recommendable. For this reason, DMF was used as a solvent to wash the coated fibres in this work.

Glove-box vs. air

The coating achieved under inert conditions exhibited similar coating quality and structural features as the equivalent coatings produced under ambient conditions. It was therefore

assumed, that traces of water and oxygen do not influence the coating process conducted in this thesis. These results could also be seen as first hints for the electrochemical mechanism as the classical cathodic electropolymerization under the assumption of anionic polymerization requires strictly anhydrous conditions (Mouanda et al. 2009).

Influence of coating parameters

For none of the experimental series an even and all-covering coating could be achieved under constant potential. It therefore seems not possible to use this approach for the continuous coating process. In contrast to this, the use of constant current led to good results. The drawback of constant current is, that it makes the process less controllable. Side-reactions can take place, the current leads to higher temperature, which increases the likelihood for radical polymerization. However, radical polymerization in itself might not represent a problem. Even if the polymers are not grafted to the surface or only some of them are, entanglement can lead to a strongly attached and consistent coating (see 5.1.4). The current densities examined showed no sufficient coating at a very low current density and the coating quality increased with increasing current density. Above a current density of 1.19 mA/cm^2 no significant improvement of the coating quality was registered. This value was therefore used for the continuous coating. This current density is lower than the ones used in the literature previously published, where current densities of 2.38 mA/cm^2 (Tridech 2010) and 1.56 mA/cm^2 (Bismarck et al. 2005) were used.

5.1.3 Continuous coating

Continuous electrocoating of carbon fibres was successfully performed. To avoid errors due to varying coating speed and to assure constant coating quality the samples were continuously analysed by optical microscopy and for the most part exhibited an even and consistent coating. The handling for washing and drying was difficult and time-consuming and it is assumed that through this damages can be introduced to the fibre structure and the fibre surfaces. Washing seemed to be more crucial in comparison to batch electrocoating as over the long experimental time the amount of polymer in solution increased and residues could be left on the fibre surface. However, a physisorption of polymer chains is in general limited as the electrolyte consists partly of a good solvent of the polymer (Palacin et al. 2004).

The minimum coating speed applied was 2.9 mm/s and the maximum was 4.2 mm/s . In all cases the velocity was thereby increased from the coating speed used by (Tridech and Maples 2013) of 1.9 mm/s . However, no accurate values for the speed could be given, as the adjustment was too coarse and varied. To avoid errors due to too high speed and assure constant coating quality the samples were therefore continuously analysed by optical microscopy.

5.1.4 Mechanism

The experiments under the section 'mechanism' were performed to get further insights into the electrochemical mechanism during electrocoating. This mechanism covers aspects about the initiation of the polymerization – anionic or radical – and the polymer chain growth,

which can be anionic or radical as well. The voltamograms were not suitable to determine if the reactions were radical or anionic.

The removal of the inhibitor would allow radical polymerization more easily because the inhibitor would not need to be consumed in the beginning. The nice and more intensive looking coating achieved in these experiments suggests that radical polymerization is active. The addition of a high amount of water is supposed to suppress any anionic reaction. According to Mouanda et al. (2009) anionic polymerization is in general not possible under ambient conditions and can only be achieved if water is excluded. Under ambient conditions traces of water might already be included under 'normal' coating conditions. However, if water is added a sufficient coating can still be achieved. This supports the assumption that both initiation and polymerization are radical.

Low temperature would inhibit or hinder radical polymerization to a certain amount as it is thermally induced and the speed of the radical polymerization increases with increasing temperature. High temperatures led to radical polymerization in solution, which was visible as the solution became more viscous over the experimental time and the resistance of the electrolyte increased. Therefore, it was expected that less radical polymerization takes place at room temperature in comparison to elevated temperatures of about 60°C. It was observed that the polymerization in solution indeed decreased for the experiments conducted at room temperature. The colouring of the electrolyte during the experiments was less distinct and the resistance of the electrolyte was lower and more constant in comparison to experiments at elevated temperatures. However, as the fibres become heated through the applied current and high temperatures of the fibres itself were observed, this does not eliminate the possibility for radical polymerization in the close vicinity of the fibres. Thus, for the electrocoating at room temperature the reactions take place mostly in the vicinity of the working electrode and both anionic and radical initiation and polymerization remain possible.

To identify the type of interaction of the polymer with the carbon fibre surface, ultrasonication and bending of the coated fibres were performed. As mentioned previously, a physisorption of the polymer on the surface is very limited especially for the batch electrocoating as a good solvent for the polymer was used in the electrolyte and the fibres were washed with this solvent after the electrocoating. This leaves polymers that are grafted to the surface or a combination of grafted polymer and entangled polymer chains. After three minutes of ultrasonication in DMF a continuous coating can still be observed which highly supports a grafting of the polymer or very strong entangling. Bending of the fibres led to a significant decrease of the coating quality, which supports the existence of a grafted and strongly entangled coating and the assumption of a brittle behaviour of the PMMA coating.

5.2 Characterisation of fibres

5.2.1 Tensile testing

With the tensile testing machine it was possible to determine the titer of every fibre and from this the diameter was calculated. According to this measurement the coated fibres in average exhibited a 0.5 μm larger diameter, which would in turn give a coating thickness of 0.25 μm . However, this value cannot be fully trusted due to the different nature of the coating

compared to the carbon fibre, resulting in different vibrational properties. All fibre properties measured were substantially lower than stated in the product sheet. This difference could be caused by the limited possibility to apply the standard test procedure. A main aspect would be, that no cardboard frame was used for fibre fixation and it could not be made sure, if the fibres broke at the fixation or in the middle. Considering the fibre properties comparing the non-coated reference fibres with the continuous coated fibres both stiffness and strength seem to be affected. The strength is decreased from 1956 ± 1040 MPa for the reference fibres to 1401 ± 1080 MPa for the coated fibres, the stiffness is decreased from 164 ± 23 GPa to 120 ± 26 GPa, respectively. The tensile strength can be drastically influenced by surface defects, whereas the stiffness is influenced by changes of the internal and surface fibre structure (Ehlert, Lin, and Sodano 2011). One suggestion for the observed decrease in properties would therefore be that the structural integrity of the fibres was somehow decreased due to the electrocoating treatment. Several handling steps for the continuously coated fibres could furthermore introduce more defects in the fibre surface. Furthermore, Bismarck et al. (1999) stated that minor differences in tensile strength are common when this testing method is used. They detected a decrease in tensile strength for carbon fibres of up to 600 MPa and considered this to be only a slight decrease. They also obtained similar high standard deviations of up to ± 850 MPa. However, due to possible errors caused by the used method the fibre properties for coated fibres need further evaluation. For this, it is advised to use a tensile test machine suitable for carbon fibres as the machine used was more matched to textile fibres and the values had to be calculated based on the unit titer.

5.2.2 Resistivity

Abry et al. (1999) conducted electrical resistance measurements on CFRP laminates for in situ detection of damage processes. From their experiments with the composites they assessed the fibre resistivity to be in the range of 1.6×10^{-5} to 1.9×10^{-5} Ωm , which corresponds well to the range observed in their considered literature of 1.2×10^{-5} to 3×10^{-5} Ωm . The results obtained in the present work fall in fact also within this range, the un-coated fibres in the middle with 1.8×10^{-5} Ωm and the coated fibres at the upper end of this range with 3×10^{-5} Ωm .

To explain the clear shift in resistance for the un-coated fibres compared to the coated ones several suggestions can be made: (a) The deposited coating can inhibit or hinder the current transfer between the fibres. (b) Fibres within the fibre bundle can be broken due to various handling step before and during the coating process. (c) Structural changes of the fibre structure can occur due to the high current applied. To evaluate these possible explanations further testing that has been already suggested in the previous chapter (5.2.1) is needed and the electrical properties of the coating need to be evaluated.

5.3 Manufacturing of composites

Regarding manufacturing of the composites the most significant problem was the poor through-wetting of the coated fibre bundles within the composite. In a first step this behaviour had been improved through the use of a second epoxy that exhibited a lower viscosity during the impregnation. One option to improve the wetting behaviour further would be a more careful separation of the fibres within the fibre tow as fibres tend to stick together. First

follow-up experiments with fibre coating at room temperature indicate that the fibres tend to stick less to each other and that they are easier to separate.

5.4 Electrical properties

As already mentioned in a previous section (5.2.2), Abry et al. (1999) conducted electrical resistance measurements on CFRP laminates for in situ detection of damage processes. They produced unidirectional epoxy composites reinforced with high-strength carbon fibres. The resistance measurements were carried out first by polishing the desired locations on the specimen surface and then by electroplating copper electrodes on these locations. To measure the longitudinal resistance the electrodes were placed on both ends of the specimen. As for the longitudinal direction the composite behaves like an electrical circuit of resistances in parallel being the carbon fibres. Therefore, they express the resistance of the composite R_c as follows:

$$R_c = \frac{\rho_f}{A_c V_f} l + R_e,$$

where R_e is the resistance of the connection to the electrodes and the resistance of the wires.

In general, the longitudinal resistance changes linearly with the length of the specimen and the value for R_e can be determined by extrapolating this line to $l=0$. They observed a very low value for R_e of around 0.04 Ω , which can be explained by the high efficiency of the copper connection. The observed longitudinal resistivity is 4.72×10^{-5} , 3.71×10^{-5} and 2.93×10^{-5} Ωm for a fibre volume fraction of 0.43, 0.49 and 0.58 respectively. (Abry et al. 1999) These values are slightly lower than the ones obtained from 3-point bending tests for uncoated fibre composites in the present work ($V_f = 0.6$). The increased resistance might be caused by a higher value of R_e as the contact through silver paint and aluminium foil is less effective. However, for the coated fibre composites the resistivity is increased by an order of magnitude ranging between 1.9×10^{-4} and 2.9×10^{-4} Ωm (excluding the two extreme cases). The lower volume fraction of fibres ($V_f = 0.45$) is not sufficient to explain these values. As Abry et al. (1999) have observed an increase in resistance in case of both macroscopic (ply failure) and microscopic (fibre breaks and fibre elongation) damage, the increased resistance for coated fibre composites is assigned to a larger amount of broken fibres. Such fibre damage is likely to occur during the additional steps of fibre coating or washing. Moreover, the polymer coating present on the fibres inhibits contact between the fibres and therefore decreases electrical conductivity in transverse direction. According to Abry et al. (1999), this is an important factor, if not all fibres are connected to the electrodes at the ends of a specimen.

Tridech and Maples (2013) used the same base epoxy as used in Epoxy1 and applied a voltage to heat their specimens. Their given applied voltage and current for composite temperatures of 110°C and 130°C (see chapter 2.1.3) correspond to a resistivity of 1.25×10^{-2} and 1.43×10^{-2} Ωm , which is extremely high. Additionally, the applied potential of 15 and 20 V is very high. A reason for these high values can be found in the preparation method for the contact between specimens and cables described in (Tridech 2010). Hence, tightly clamped stainless steel plates were used at the end of the specimens to transfer the potential. No further preparation of the specimen ends is documented. This probably leads to poor contact properties. Also, the resistance and the resistivity seem to increase with increasing temperature from the information given in the short publication, but this is not true if one

looks at the table in the thesis of (Tridech 2010), where composite temperature, voltage and current are depicted (see Appendix 8.1). The resistance is high around room temperature, decreases to approximately 25Ω between 50 and 100°C and increases again up to the maximum temperature of 140°C . These values are presented as being representative for all composites containing both coated carbon fibres and unsized carbon fibres.

In the present work the resistivity varied between systems with coated carbon fibres and for sized carbon fibres. The resistivity did not change with increasing temperature for Epoxy1 + CF and even decreased for Epoxy1 + CF + PMMA.

5.5 Mechanical characterisation of composites

5.5.1 Three-point bending

For all epoxy systems a lower flexural modulus for the coated-fibre composites was observed. This can be explained by the poor wetting with epoxy of the coated fibre bundles through the composite thickness. Through this, voids were introduced into the composite, which was especially pronounced for Epoxy1 + CF + PMMA. Liu et al. (2006) investigated the influence of voids on the flexural properties of carbon/epoxy laminates. They found that both flexural modulus and strength were decreased with increasing void content. They observed a reduction in modulus of 18% for a void content of 3.2%. Considering a void content of up to 20% for Epoxy1 + CF + PMMA the decrease in flexural modulus appears reasonable.

Other possibilities to explain the differences are: (i) the thickness of the interface thermoplast layer influences the properties, (ii) the Epoxy + CF + PMMA specimens were thicker, which alters the behaviour in the three-point bending and (iii) as indicated by the tensile test results of the fibres the modulus of the coated fibres is decreased and therefore influences the performance of the composite. However, possibility (i) is not likely, as the thermoplast interface layer would have a very low influence on the initial flexural modulus in fibre direction (as indicated by theoretical calculations performed at Swerea SICOMP).

To validate the reliability of the custom-made rig, reference three-point bending tests were performed at room temperature at Swerea SICOMP. They gave a flexural modulus of 105 GPa for Epoxy2 + CF and 60 GPa for Epoxy2 + CF + PMMA, which is in good agreement with the obtained results from the rig used in this thesis.

The high standard deviation for Epoxy2 + CF at 80°C can be explained by the much slower heating of one specimen in comparison to the other two samples since a lower voltage was used.

Tridech and Maples (2013) achieved a flexural modulus that was higher for the PMMA coated composites in comparison to the uncoated fibre composites. However, they used unsized fibres in the reference specimens, which results in poor fibre-matrix interaction. Optical micrographes of the cross section of the composites given in (Tridech 2010) suggests the existence of pores, which might explain that they still achieve a lower modulus of approximately 90 GPa than the theoretical modulus of around 127 GPa (estimated in theoretical calculations performed at Swerea SICOMP).

Furthermore, Tridech and Maples (2013) observed that the flexural strength was much lower for the coated composites (Table 1). As an explanation they proposed that many fibres stuck

together by the coating and therefore both the impregnation and the distribution of the fibres by or within the matrix was poor. Poor washing of the fibres after the coating process or a thick coating can give poor spreadability of the fibre tow as a consequence. Even though the flexural strength was not measured in the present work, a similar behaviour was observed, especially for composites with LY556 epoxy matrix. For these materials, an uneven distribution of the fibres and a large amount of pores was visible. However, also in the optimized composites with LY5052 epoxy matrix, fibre agglomerations were observed and the fibre distribution remained unsatisfying. During handling of the fibres it was indeed noticed that it was in some cases difficult to separate them and the microscopy images confirmed that the polymer coating held some fibres together.

5.5.2 DMTA

Comparing the range of T_g given in the datasheet for Epoxy1 (130 – 150°C, see Table 7) the values of 133°C and 150°C obtained from the DMTA agree very well. For Epoxy2 slightly lower values of 90 and 111°C were obtained in comparison to the T_g range stated in the datasheet (112 – 122°C, see Table 7). However, no pre-cure was applied for the Epoxy2 composites and for this type of epoxy the glass transition temperature can be significantly increased (up to 130°C) if it is post-cured at elevated temperatures. This is applicable even after the material has been stored at ambient temperatures for a long period. By DSC Saraç, Bismarck, and Springer (2006) have observed that PMMA has a T_g of about 120°C obtained from the electrocoating carbon fibres. Therefore the glass transition temperature is increased for Epoxy2 + CF + PMMA in comparison to Epoxy2 + CF.

The curve progressions of the Epoxy2 systems were close to each other because of a similar T_g for the Epoxy and PMMA. This made the systems more easily comparable. The influence of the PMMA coating on the T_g was more distinct for the Epoxy1 systems as the T_g differs more between PMMA and Epoxy1. Thus, the coating had more influence in that case.

The steep change in modulus over a small temperature range is desired and this can be seen for all composite systems. This indicates the possibility to also use the epoxy systems without coating in a stiffness-modifiable composite. This indication is backed by the results from the three-point bending tests as a stiffness reduction was possible for all systems. However, this reduction was more immediate and more distinct for systems that contained coated fibres.

5.6 Scale-up possibilities for industrial application

Based on the experimental set-up used in this thesis and in similar laboratory-scale coating methods (Varelidis, McCullough, and Papaspyrides 1999), a possible route for industrial processing is presented in Figure 52. A spreading of the fibres at the beginning and at the end is suggested to possibly increase the uniformity of the coating as differences in the coating quality were observed that might be caused by a poor spread. The electrocoating process itself is performed similar to the experimental set-up but with an increased amount of fibre tows. To minimize the use of chemicals, some improvements can be proposed: (i) the electrocoating section should be sealed so that the evaporation of MMA is minimized and (ii) recovery of DMF and salt from the electrolyte after the polymerization of the monomer in solution. The second proposal is also related to the addition of new electrolyte, which should be pumped in

as a constant flow. A cycle of addition and recovering would be useful. Furthermore, to use a low temperature for the electrolyte during coating seems useful as radical polymerization is decreased at lower temperatures. Washing with DMF and the use of ultrasonication would ascertain that all loosely deposited polymer will be removed. However, the use of DMF should be limited and another additional washing step is optional. Acetone might be suitable to remove remaining DMF without influencing the coating but has not been tested in the current work. As a last step the continuous heating and drying of the fibres is proposed. This step could be easily implemented if the fibres are washed with acetone. Then, the drying would be fast as acetone exhibits a much lower boiling point of 56°C compared to DMF (153°C).

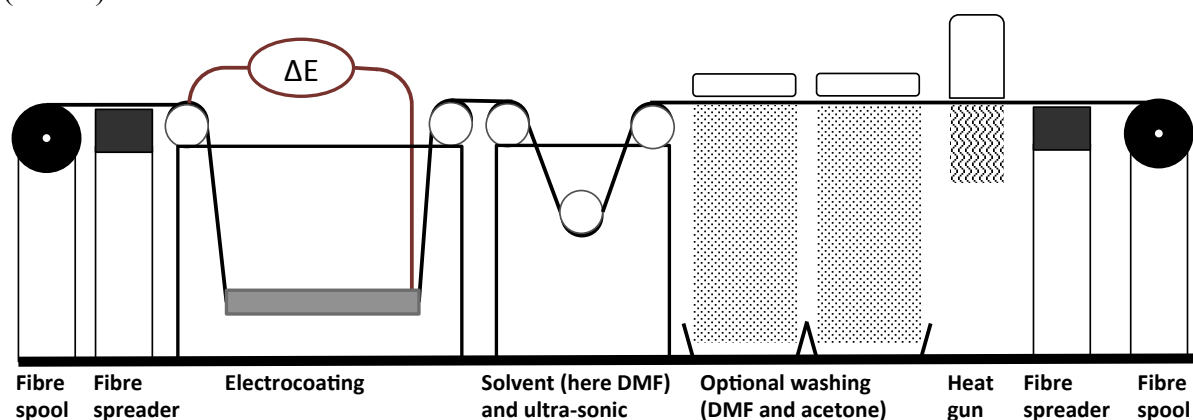


Figure 52 Possible route for the continuous industrial production of electrocoated carbon fibres.

6 Conclusions and Outlook

The aim of the thesis to develop a first prototype of a stiffness-variable composite was achieved. Upon external stimulation a stiffness reduction of up to 72 % was achieved for the composites containing coated fibres. As different epoxy systems have been evaluated, the amount and rate of stiffness change seem to be adjustable over various temperature ranges. In fact, it was found that even the reference material (a commercial sized carbon fibre reinforced epoxy composite) can reduce its stiffness of up to 50% and that the extent of stiffness-reduction of such a composite can be adjusted by choosing matrix (epoxy system) and temperature. Hence, two different concepts for stiffness-modifiable materials have been developed in the present work offering a range of different properties depending not only on the concept, but also on the chosen thermoset matrix. The adjustment of these properties might offer different possibilities for future applications. For the use within automotive applications as proposed in the introduction a material including electrocoated carbon fibres might not be competitive with a regular epoxy composite, due to required production at high volumes. However, it needs to be assessed if the achievable stiffness-reduction with a regular epoxy composite is sufficient to decrease injury risks for pedestrians hitting the hood.

As a first subsidiary aim the fibre coating process was considered. This process was optimized and a continuous production of completely coated carbon fibres could be realized on a small scale. The process has the potential to be implemented for industrial production as discussed in section 5.6. Continuous coating could be achieved by optimizing a range of process parameters. Therefore, the process is rather robust to different environmental conditions, which is an advantage in future industrial application. Even if some variation in the coating quality over the fibre tow length and between neighbouring fibres occurred, the functionality of the resulting material was satisfactory. Comparing the present experiments and optimizations made to similar research studies presented in literature, the coating process could be improved. The current density was decreased at the same time as the coating speed was increased. The first aspect already leads to a decreased energy consumption, which might even be further reduced, as first experiments performed to evaluate the mechanism indicate that the continuous coating can be performed at room temperature. The use of DMF could not be avoided even if steps towards a limited use of this mutagenic solvent are proposed in section 5.6.

The second subsidiary aim concerned the production and characterisation of composites containing coated carbon fibres. Process parameters for the vacuum infusion were optimised and the suitability of different epoxy resins was evaluated. The reduction in stiffness at increased temperatures was detected by DMTA, whereas the ability of the material to be activated by application of current was verified by flexural bending tests.

6.1 Further experiments

For the future, desired application of this material as a passive crash system the evaluation of both time- and temperature-dependent properties would be important. To transfer the electrical energy more efficiently and thus heat the material as fast as possible it seems most crucial to decrease the resistivity of the material through an improvement of the manufacturing process and a better contact between the fibres and the electric device.

Several experiments regarding the optimization and evaluation of the coating process can be proposed:

- (i) Tests at room temperature indicated that the amount of radical polymerization in solution decreases and the fibres are prevented from sticking together. This would in turn lead to a better processability of the fibres. Room temperature should therefore be applied for the continuous coating.
- (ii) Spreading of the fibres during the experiments should be tested to evaluate if the coating quality becomes more even between individual fibres.
- (iii) A characterisation of the fibre surface using AFM (Atomic force microscopy) might give additional information about the coating structure. According to Saraç, Tofail, et al. (2004) with this method it is possible to even measure layers of coating and the variation in height.
- (iv) While the handling of the fibres might influence the TGA because parts of the coating fall off, TGA of composite samples might reveal a more accurate amount of the coating applied on the surface of the fibres used in the functional composites.
- (v) For the continuous coating process a continuous washing and drying process should be included as the handling procedure increases the risk for fibre damage.

For the composites time-depending three-point bending tests are proposed to evaluate the use for the specific application in car crash. The material needs soften very fast, the time span being a few hundredth of a second. This reaction time is also highly dependent on a good contact between the specimen and the electrical input device. Thus, an aim for further research would be to improve this contact at specimens to decrease the resistivity of the material. Besides an improved separability of the fibres the manufacturing process of the composites generally needs to be improved to achieve higher initial moduli. Therefore, different process parameters such as impregnation speed and pressure should be evaluated with regard to the desired performance.

7 References

- Abry, J C, S Bochart, A Chateauinois, M Salvia, and G Giraud. 1999. "In Situ Detection of Damage in CFRP Laminates by Electrical Resistance Measurements." *Composites Science and Technology* 59(6): 925–35.
<http://www.sciencedirect.com/science/article/pii/S0266353898001328>.
- Bachinger, Angelika. 2014. "Deliverable 3.5. Coated Carbon Fibres for Stiffness-Modifiable Composites." *ENLIGHT (EU-FP7-Grant agreement no 314567)*.
- Baute, Noëlle, Cédric Calberg, Philippe Dubois, Christine Jérôme, Robert Jérôme, Lucien Martinot, Marc Mertens, and Philippe Teyssié. 1998. "„Bonding” Electropolymerization: A New Electron-Transfer Strategy for the Tailoring of Performant Polymer-Based Composites." *Macromolecular Symposia* 134(1): 157–66.
<http://dx.doi.org/10.1002/masy.19981340115>.
- Bismarck, Alexander, M.E. Kumru, B. Song, J. Springer, E. Moos, and J. Karger-Kocsis. 1999. "Study on Surface and Mechanical Fiber Characteristics and Their Effect on the Adhesion Properties to a Polycarbonate Matrix Tuned by Anodic Carbon Fiber Oxidation." *Composites Part A: Applied Science and Manufacturing* 30(12): 1351–66.
<http://www.sciencedirect.com/science/article/pii/S1359835X99000482> (March 6, 2014).
- Bismarck, Alexander, Adam F. Lee, a. Sezai Saraç, Eckhard Schulz, and Karen Wilson. 2005. "Electrocoating of Carbon Fibres: A Route for Interface Control in Carbon Fibre Reinforced Poly Methylmethacrylate?" *Composites Science and Technology* 65(10): 1564–73. <http://linkinghub.elsevier.com/retrieve/pii/S0266353805000357> (January 8, 2014).
- Bureau, Christophe. 1999. "Polymerization Reaction Coupled to Charge Transfer: Propagation versus Termination as a Source of Permanent Travelling Waves and Multi-Peak Voltammograms." *Journal of Electroanalytical Chemistry* 479(1): 43–56.
<http://www.sciencedirect.com/science/article/pii/S0022072899004295> (March 10, 2014).
- Bureau, Christophe, Guy Deniau, Pascal Viel, and Gérard Lecayon. 1997. "Comments on 'The Electroreduction of Acrylonitrile: A New Insight into the Mechanism' by Mertens et Al." *Macromolecules* 30(2): 333–36. <http://dx.doi.org/10.1021/ma961333c>.
- Calberg, C., M. Mertens, R. Jérôme, X. Arys, A.M. Jonas, and R. Legras. 1997. "Characterization of Polyacrylonitrile Films Grafted onto Nickel by Ellipsometry, Atomic Force Microscopy and X-Ray Reflectivity." *Thin Solid Films* 310(1-2): 148–55.
<http://www.sciencedirect.com/science/article/pii/S0040609097004069> (March 5, 2014).

- Carter, E L, C E Neal-Sturgess, and R N Hardy. 2008. "APROSYS in-Depth Database of Serious Pedestrian and Cyclist Impacts with Vehicles." *International Journal of Crashworthiness* 13(6): 629–42. <http://dx.doi.org/10.1080/13588260802411457>.
- Chopra, Inderjit. 2002. "Review of State of Art of Smart Structures and Integrated Systems." *AIAA Journal* 40(11): 2145–87. <http://arc.aiaa.org/doi/abs/10.2514/2.1561>.
- Ehlert, Gregory J, Yirong Lin, and Henry A Sodano. 2011. "Carboxyl Functionalization of Carbon Fibers through a Grafting Reaction That Preserves Fiber Tensile Strength." *Carbon* 49(13): 4246–55.
<http://www.sciencedirect.com/science/article/pii/S0008622311004337>.
- ENLIGHT Consortium. 2014. "ENLIGHT - Enhanced Lightweight Design." <http://www.project-enlight.eu/> (November 6, 2013).
- Euro NCAP. 2014. "Our Tests." <http://www.euroncap.com/tests.aspx> (May 7, 2014).
- Farshad, M, and Andre Benine. 2004. "Magnetoactive Elastomer Composites." *Polymer Testing* 23(3): 347–53.
<http://www.sciencedirect.com/science/article/pii/S014294180300103X>.
- Fredriksson, Rikard, and Erik Rosén. 2012. "Integrated Pedestrian Countermeasures – Potential of Head Injury Reduction Combining Passive and Active Countermeasures." *Safety Science* 50(3): 400–407.
<http://www.sciencedirect.com/science/article/pii/S0925753511002645>.
- Gabriel, Sabine, Robert Jérôme, and Christine Jérôme. 2010. "Cathodic Electrografting of Acrylics: From Fundamentals to Functional Coatings." *Progress in Polymer Science* 35(1-2): 113–40. <http://linkinghub.elsevier.com/retrieve/pii/S0079670009001099> (January 22, 2014).
- Holland, B.J, and J.N Hay. 2002. "The Effect of Polymerisation Conditions on the Kinetics and Mechanisms of Thermal Degradation of PMMA." *Polymer Degradation and Stability* 77(3): 435–39.
<http://www.sciencedirect.com/science/article/pii/S0141391002001003> (March 10, 2014).
- Huang, Sunan, and Jikuang Yang. 2010. "Optimization of a Reversible Hood for Protecting a Pedestrian's Head during Car Collisions." *Accident Analysis & Prevention* 42(4): 1136–43. <http://www.sciencedirect.com/science/article/pii/S000145750900342X>.
- Jérôme, C. 2012. "Electroinitiated Polymerization." In *Polymer Science: A Comprehensive Reference*, Elsevier B.V., 903–18. <http://dx.doi.org/10.1016/B978-0-444-53349-4.00122-9>.

- Jing, Benxin, Jiang Zhao, Yan Wang, Xin Yi, and Huiling Duan. 2010. "Water-Swelling-Induced Morphological Instability of a Supported Polymethyl Methacrylate Thin Film." *Langmuir : the ACS journal of surfaces and colloids* 26(11): 7651–55.
<http://pubs.acs.org.proxy.lib.chalmers.se/doi/abs/10.1021/la1004566> (May 19, 2014).
- Kasem, Kasem K., and Stephanie Jones. 2008. "Platinum as a Reference Electrode in Electrochemical Measurements." *Platinum Metals Review* 52(2): 100–106.
<http://openurl.ingenta.com/content/xref?genre=article&issn=0032-1400&volume=52&issue=2&spage=100> (January 20, 2014).
- Kumru, M.Emin, Jürgen Springer, A.Sezai Saraç, and Alexander Bismarck. 2001. "Electrografting of Thiophene, Carbazole, Pyrrole and Their Copolymers onto Carbon Fibers: Electrokinetic Measurements, Surface Composition and Morphology." *Synthetic Metals* 123(3): 391–401.
<http://www.sciencedirect.com/science/article/pii/S0379677901003381>.
- Leijonmarck, S., T. Carlson, G. Lindbergh, L.E. Asp, H. Maples, and a. Bismarck. 2013. "Solid Polymer Electrolyte-Coated Carbon Fibres for Structural and Novel Micro Batteries." *Composites Science and Technology* 89: 149–57.
<http://linkinghub.elsevier.com/retrieve/pii/S0266353813003898> (January 22, 2014).
- Liu, Ling, Bo-Ming Zhang, Dian-Fu Wang, and Zhan-Jun Wu. 2006. "Effects of Cure Cycles on Void Content and Mechanical Properties of Composite Laminates." *Composite Structures* 73(3): 303–9. <http://linkinghub.elsevier.com/retrieve/pii/S0263822305000437> (August 18, 2014).
- Manz, Holger, and Elmar J Breitbach. 2001. "Application of Smart Materials in Automotive Structures." In *SPIE's 8th Annual International Symposium on Smart Structures and Materials*, International Society for Optics and Photonics, 197–204.
- Meretz, S, T Linke, E Schulz, A Hampe, and M Hentschel. 1992. "Diameter Measurement of Small Fibres : Laser Diffraction and Scanning Electron Microscopy Technique Results Do Not Differ Systematically X .. L _ J Laser R ' Y Ph °~ E °." *Journal of Materials Science Letters* 11: 1471–72.
- Mertens, M, C Calberg, L Martinot, and R Jérôme. 1996. "The Electroreduction of Acrylonitrile: A New Insight into the Mechanism." *Macromolecules* 29(14): 4910–18.
<http://dx.doi.org/10.1021/ma946442a>.
- Mertens, M, L Martinot, and R Jerome. 2001. "Method for Making Composites." <http://www.google.nl/patents/US6325911>.

- Michaud, V. 2004. "Can Shape Memory Alloy Composites Be Smart?" *Scripta Materialia* 50(2): 249–53. <http://www.sciencedirect.com/science/article/pii/S135964620300575X>.
- Mouanda, Brigitte, Esmeeless Bassa, Guy Deniau, Pascale Jegou, Pascal Viel, and Serge Palacin. 2009. "Comparison of Two 'grafting From' Techniques for Surface Functionalization: Cathodic Electrografting and Surface-Initiated Atom Transfer Radical Polymerization." *Journal of Electroanalytical Chemistry* 629(1–2): 102–9. <http://www.sciencedirect.com/science/article/pii/S0022072809000448>.
- Naarmann, H. 1988. "Electrochemical Coating of Carbon Fibers." <http://www.google.com/patents/US4749451> (May 11, 2014).
- Oh, Cheol, Youn-soo Kang, and Wonkyu Kim. 2008. "Assessing the Safety Benefits of an Advanced Vehicular Technology for Protecting Pedestrians." *Accident Analysis & Prevention* 40(3): 935–42. <http://www.sciencedirect.com/science/article/pii/S0001457507001947>.
- Palacin, Serge, Christophe Bureau, Julienne Charlier, Guy Deniau, Brigitte Mouanda, and Pascal Viel. 2004. "Molecule-to-Metal Bonds: Electrografting Polymers on Conducting Surfaces." *Chemphyschem : a European journal of chemical physics and physical chemistry* 5(10): 1468–81. <http://www.ncbi.nlm.nih.gov/pubmed/15535544> (February 21, 2014).
- Peelamedu, Saravanan M, Nagi G Naganathan, and Steve Buckley. 1999. "Impact Analysis of Automotive Structures with Distributed Smart Material Systems." In *Proc. SPIE*, , 813–24.
- Poleunis, Claude, Patrick Bertrand, C Calberg, M. Mertens, and R. Jérôme. 1998. "ToF-SIMS Analyses of Polyacrylonitrile Films Electrografted onto Nickel in the Presence of CDCl₃ as Radical Transfer Agent." <http://dial.academielouvain.be/handle/boreal:83732> (March 10, 2014).
- Rasmussen, Winola Lenore. 2002. "Novel Carbazole Based Methacrylates, Acrylates, and Dimethacrylates to Produce High Refractive Index Polymers." <http://scholar.lib.vt.edu/theses/available/etd-12202001-135708/> (May 9, 2014).
- Saraç, A. Sezai, Alexander Bismarck, and Jürgen Springer. 2006. "Reflectance FTIR and SEM Characterization of poly[N-Vinylcarbazole-Co-Methylmethacrylate] Electrografted Carbon Fiber Surface: Current Density Effect." *Journal of Materials Science* 41(2): 389–98. <http://link.springer.com/10.1007/s10853-005-2275-2> (May 11, 2014).
- Saraç, A. Sezai, Una Evans, Marina Serantoni, Jason Clohessy, and Vincent J Cunnane. 2004. "Electrochemical and Morphological Study of the Effect of Polymerization Conditions

on Poly(terthiophene).” *Surface and Coatings Technology* 182(1): 7–13.
<http://www.sciencedirect.com/science/article/pii/S0257897203008892>.

Saraç, A.Sezai, Syed A M Tofail, Marina Serantoni, John Henry, Vincent J Cunnane, and James B McMonagle. 2004. “Surface Characterisation of Electrografted Random Poly[carbazole-Co-3-Methylthiophene] Copolymers on Carbon Fiber: XPS, AFM and Raman Spectroscopy.” *Applied Surface Science* 222(1–4): 148–65.
<http://www.sciencedirect.com/science/article/pii/S0169433203010018>.

Tridech, Charnwit. 2010. “Smart Fibre Coatings: Stiffness Control in Composite Structures.”
<http://ethos.bl.uk/OrderDetails.do?uin=uk.bl.ethos.529352> (December 10, 2013).

Tridech, Charnwit, and HA Maples. 2013. “High Performance Composites with Active Stiffness Control.” *ACS applied materials and interfaces* 5: 9111 – 9119.
<http://pubs.acs.org/doi/abs/10.1021/am402495n> (December 10, 2013).

Varelidis, P C, R L McCullough, and C D Papaspyrides. 1999. “The Effect on the Mechanical Properties of Carbon/epoxy Composites of Polyamide Coatings on the Fibers.” *Composites Science and Technology* 59(12): 1813–23.
<http://www.sciencedirect.com/science/article/pii/S0266353899000391>.

Yang, Dazhi. 2000. “Shape Memory Alloy and Smart Hybrid Composites — Advanced Materials for the 21st Century.” *Materials & Design* 21(6): 503–5.
<http://www.sciencedirect.com/science/article/pii/S026130690000008X>.

Yao, Jianfeng, Jikuang Yang, and Dietmar Otte. 2007. “Head Injuries in Child Pedestrian Accidents—In-Depth Case Analysis and Reconstructions.” *Traffic Injury Prevention* 8(1): 94–100. <http://dx.doi.org/10.1080/15389580600944243>.

8 Appendix

8.1 Information from (Tridech 2010)

Table 12 Coating thicknesses calculated from different characterisation methods used in (Tridech 2010).

Values given in Tridech		Values calculated from Tridech	
Weight gained	12.9 ± 5.0	Coating thickness from weight [μm]	0.3
Coating content %wt	3	Coating thickness from TGA [μm]	0.1
Fibre diameter unsized vs. PMMA coated from SEM [μm]	7.3 vs. 8.1	Coating thickness from SEM [μm]	0.8
Fibre diameter unsized vs. PMMA coated from Wilhelmy [μm]	7.3 ± 0.1 vs. 7.5 ± 0.3	Coating thickness from Wilhelmy [μm]	0.2

Table 13 Values for electrical properties for the specimens tested by (Tridech 2010).

Resistance [Ω]**	Voltage [V]*	Current [A] *	Composite temperature [°C]*
33.3	5	0.15	32 ± 2
26.7	8	0.30	44 ± 1
25	10	0.40	55 ± 4
26	13	0.50	89 ± 2
25	15	0.60	108 ± 6
27.7	18	0.65	120 ± 3
28.6	20	0.70	142 ± 9

* Given in (Tridech 2010)

** Calculated from the values given in (Tridech 2010)